Differential Thermal Isotope Analysis: A Method for the Study of Past Climates

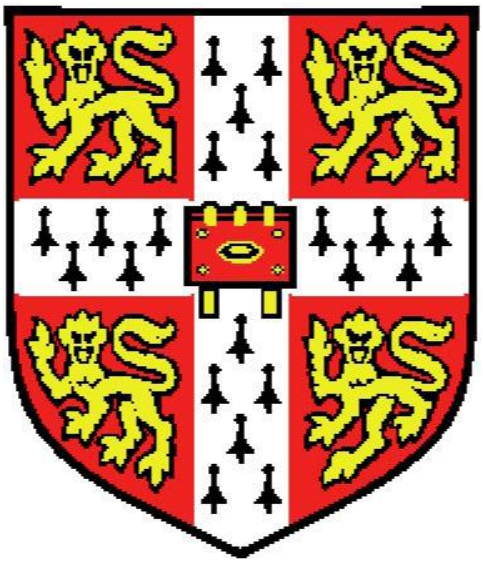

Gregory Lloyd Walters

Department of Earth Sciences

University of Cambridge

Churchill College

A thesis submitted for the degree of

Doctor of Philosophy

October 2023

To my ever patient parents

Acknowledgements

Firstly I would like to thank my supervisors, David Hodell and Simon Redfern; Simon for his help in getting started on my PhD and for his guidance and reviews of work, and David for helping me to carry out my research and set up collaborations, and for his invaluable aid in writing my thesis.

Secondly, I would like to thank everyone else in the department who helped me throughout my PhD. In particular, I would like to thank Thomas Bauska and Fernando Gázquez for sharing their advice and experimental knowledge, and James Rolfe, Ian Mathers and Guilio Lamprotti for helping me run experiments, prepare samples, and helping maintain the equipment required for my research.

Thirdly, I would like to thank Alex Webb for supporting me throughout my final year and helping keep me on track to finish my PhD research.

Finally, I would like to thank my family; my parents for their advice and support when I've struggled, and my brother and sister for keeping an eye out for me. I don't know how they've put up with me for 30 years!

My research was supported by the ERC WIHM Project (#339694) to David Hodell. The bulk oxygen measurements of Chapter 5 were supported by NSF Early-Concept Grants for Exploratory Research (Grant EAR1839341) and American Chemical Society Petroleum Research Fund (Grant 59455-ND2) to both Jordan Hemingway and David Johnston. I am grateful to B.G. Group for initial access to the PETM clay samples.

Declaration

I declare that the contents of this dissertation are original, and have not been submitted for consideration for any other degree or qualification. This dissertation is the result of my own work, including nothing which is the outcome of work done in collaboration except where specifically indicated in the text. This dissertation contains fewer than 275 numbered pages of which not more than 225 pages are text, illustrations and bibliography, and fewer than 80,000 words, as prescribed by the Earth Sciences Degree Committee.

Gregory Walters

Abstract

Online measurements of $\delta^{18}O$ and $\delta^{2}H$ can be used to reveal more information about past climates than current offline methods. In this thesis I present work carried out developing the online Differential Thermal Isotope Analysis (DTIA) method, including demonstrations of the method on gypsum samples and clay samples, and the application of DTIA to the ongoing research into climate conditions during the Paleocene-Eocene Thermal Maximum (PETM).

Measurements of gypsum and clay samples demonstrate the ability of DTIA to separate out different dehydration steps for individual measurement, both for minerals with multiple water environments, and for minerals with multiple-step dehydrations. The gypsum results are also used to examine the dehydration of gypsum to anhydrite, via the intermediate bassanite. I show that this dehydration reaction is highly sensitive to sample grain size and the partial pressure of water, and crucially, that the two-step dehydration of gypsum does not result from the presence of multiple water environments that are preferentially dehydrated at different temperatures, but rather from kinetic factors upon dehydration.

DTIA is also applied to a series of clays buried in the North Sea Basin across the PETM. The results from the hydroxyl isotopic composition of the clays show a trend of slowly decreasing $\delta^{2}H$ prior to the PETM, followed by abrupt decreases in $\delta^{2}H$ at the onset of the PETM, indicating increased precipitation intensity and weathering, and implying an enhanced hydrologic cycle response to global warming, particularly at the early stages of the PETM. These results are consistent with other research indicating higher precipitation rates during the PETM. Our results are presented alongside consistent evidence from the measurements of clay composition and plankton species concentration undertaken by previous researchers at this section, demonstrating how DTIA can be used alongside other methods.

This thesis shows the potential DTIA has to aid palaeoclimate reconstruction in a number of geological settings. DTIA can be applied both to isolated hydrated minerals and to assemblages of hydrated minerals to better understand the formation environments of these minerals, and thus gain insight into the palaeoclimate conditions under which geological deposits form.

Contents

List of Figures

List of Tables

List of Abbreviations

arb. units	Arbitrary units. Where used for time, corresponds to 0.86 seconds.
CIE	Carbon Isotope Excursion
CO_2	Carbon dioxide
CRDS	Cavity Ring-Down Spectrometry
DFT	Density Functional Theory
DSC	Differential Scanning Calorimetry
DTIA	Differential Thermal Isotope Analysis
FTIR	Fourier Transform Infrared
GHW	Gypsum Hydration Water
GISP	Greenland Ice Sheet Precipitation
GMWL	Global Meteoric Water Line
H, D, T	Hydrogen, Deuterium (also referred to as ^2H), Tritium
HCl	Hydrochloric acid
IR	Infrared
IRMS	Isotope Ratio Mass Spectrometry
K-Pg Boundary	Cretaceous–Palaeogene Boundary
Ma	Million years (ago)
OA-ICOS	Off-Axis Integrated Cavity Output Spectroscopy
OH	Hydroxyl
PETM	Paleocene-Eocene Thermal Maximum
PID Controller	Proportional-Integral-Derivative Controller
SLAP	Standard Light Antarctic Precipitation
TCEA-IRMS	High-Temperature Conversion Elemental Analyzer IRMS

TG	Thermal Gravimeter / Thermal Gravimetry
TGA	Thermal Gravimetric Analysis
TOC	Total Organic Carbon
VOC	Volatile Organic Compounds
V-SMOW	Vienna Standard Mean Ocean Water
WASP System	Water Analyzer Sample Preparation System
XRD	X-Ray Diffraction

1 Introduction

1.1 Stable Water Isotopes

Isotopes (forms of an element with different numbers of neutrons, and hence different mass numbers) are broadly speaking chemically identical, possessing the same number of protons and electrons (and the same outer electron configuration), and thus undergoing the same chemical reactions. However, the difference in mass does lead to observable changes to both bonding and reactivity. Heavier atoms will have smaller atomic orbitals, which can affect bond strength (and hence equilibrium processes). Moreover, because of the increased atomic mass (and hence higher reduced mass), bonds to a heavier isotope will have a lower energy vibrational ground state, and will therefore require more energy to excite to the bond to higher vibrational levels (a primary kinetic isotope effect). This can also be seen in bonds adjacent to heavier isotopes (a secondary kinetic isotope effect).

These equilibrium and kinetic effects can lead to the fractionation of isotopes during a reaction. We can more easily quantify this fractionation through the use of delta notation (δ):

$$\delta = \left(\frac{R_{Sample}}{R_{Standard}} - 1 \right) \times 1000$$

which expresses the sample isotope ratio (R_{Sample}) as a value relative to a standard isotope ratio ($R_{Standard}$), in parts per thousand (‰) (Craig, 1961; Dansgaard, 1964). For water stable isotopes (H, D and T for hydrogen and ^{16}O, ^{17}O and ^{18}O for oxygen), Vienna Standard Mean Ocean Water (VSMOW) is the agreed international standard (Coplen, 1995). Fractionation between two substances, A and B, is then defined as:

$$\alpha = \frac{1000 + \delta_A}{1000 + \delta_B} \left(= \frac{R_A}{R_B} \right)$$

though frequently $1000 \ln \alpha$ is used, as otherwise values tend to be very close to one.

Fractionation can occur either as an equilibrium process, or as a kinetically driven process. Equilibrium fractionation is seen when a reaction occurs at equilibrium, such as when water is left to evaporate within a sealed container. Kinetic fractionation occurs for unidirectional processes – water evaporating under a flow of dry nitrogen would be an example of this, as once some water evaporates, the resulting water vapour is removed from the reaction, and is thus unable to reach equilibrium with the liquid water.

1.2 Historical Background and Previous Work

1.2.1 Foundational Work

The first research into stable isotope distribution in nature began in the 1930's (e.g. Dole, 1935), after the discovery of deuterium (Urey *et al.*, 1932) and of oxygen-18 and oxygen-17 (Giauque and Johnston, 1929 a, b respectively). Studies of stable isotopes in minerals also began at around this time, including early measurements of silicate oxygen isotopic ratios using mass spectrometry (Manian *et al.*, 1934). However, the first systemic studies into the isotopic composition of clay minerals did not begin until the 1960's, with the publication of Savin's thesis (Savin, 1967) and subsequent papers (Savin and Epstein, 1970 a, b). This research established the exchangeability of water in clay interlayers and adsorbed water, and measurements of hydrogen isotopic composition were made of water released at temperatures over 250 °C (Savin and Epstein, 1970 a), using modified mass spectrometers which could compensate for the large difference in mass between hydrogen and deuterium (Nier, 1947; Friedman, 1953). It is notable that reproducibility was lower for minerals with interlayer water, thereby establishing the need for the complete removal of interlayer water before analysis. Removal of clay hydroxyl was not possible, however, with this method (Savin, 1967). Although the oxygen isotopic composition of the released water was not measured, measurements of the bulk oxygen isotopic composition of clays and other minerals after drying were made. These measurements required fluorination techniques (e.g. Taylor and Epstein, 1962; Clayton and Mayeda, 1963) that produce total conversion of oxygen within the clay structure to oxygen gas followed by conversion to CO_2. The $^{18}O/^{16}O$ of the resulting CO_2 was measured using mass spectrometry.

1.2.2 Clay Oxygen and Hydrogen Isotopes

Following Savin and Epstein's work, a large number of studies of clay mineral stable isotopes were undertaken. Clay isotopic composition has found use in establishing clay provenance, such as distinguishing between clay formed by weathering versus hydrothermal alteration for British kaolinites (Sheppard, 1977). Isotopes were also used to distinguish detrital from authigenic clay found in marine sediments (e.g. Savin and Epstein, 1970 b; Eslinger and Yeh, 1981). Furthermore, isotopic analysis has been used to estimate the degree

of authigenesis in river sediments (Yeh and Eslinger, 1986), and D/H has been used to distinguish between clay formation in floodplains versus weathering at higher altitudes (Lupker et al., 2012).

In order to accurately use clay oxygen and hydrogen isotopes for determining clay origin and formation conditions, two key questions must be considered. The first is how the measured isotopic composition of the clay relates to the formation environment of the clay. As such, much work has been undertaken to establish the isotopic fractionation factors for a number of clay minerals. These studies can be broadly divided into empirical and theoretical approaches. Empirical approaches include isotopic exchange (O'Neil and Kharaka, 1976; Liu and Epstein, 1984) and synthesis experiments (Vitali *et al.*, 2011; Callabero and Jiménez de Cisneros, 2018). Because of the very slow isotopic exchange rates at low temperatures, leading to incomplete exchange, and difficulty in synthesizing pure samples representative of natural clays (e.g. O'Neil and Taylor, 1969; Torii and Iwasaki, 1987; Klopregge *et al.*, 1994; Caballero and Jiménez de Cisneros, 2018), empirical methods have proven difficult for determining accurate fractionation factors for clay minerals. A number of theoretical approaches have been tried, with very different results for clay fractionation factors – older work includes calculations based on thermodynamic properties (e.g. Kieffer, 1982) and the modified increment method (a method using statistical mechanical theory, but taking into account bond strength, cation mass, low temperature corrections and mineral/water interactions (Zheng, 1993)), while more recent calculations have been made using density functional theory (DFT) (Méheut and Schauble, 2014; Tao Liu, unpublished, based on Liu *et al.*, 2018). As such, some uncertainty still remains about the absolute relationships between clay oxygen and hydrogen isotopes and environmental conditions, but the implications of changing clay oxygen and hydrogen isotopes for changes in environmental conditions are well understood.

The second question to consider for the use of clay oxygen and hydrogen isotopes in establishing past conditions is to what extent the clay stable isotopic composition is preserved over time. Many experiments have been carried out to establish the reliability of clay bulk oxygen and clay hydroxyl hydrogen isotopic compositions as a palaeoproxy. These have primarily focused on investigating the exchangeability of clay stable isotopes over long periods of time and under different pressure and temperature conditions (e.g. O'Neil and Kharaka, 1976; Nolan and Bindeman, 2013). However, due to the very slow isotope

exchange rate for clays, experimental studies carried out under standard conditions have not measured changes in clay oxygen isotope composition, and only rarely measure changes in clay hydroxyl hydrogen composition. As such, many of the studies investigating clay isotopic exchange have focused on comparing natural clay samples. A number of studies have argued that measurements of clay bulk oxygen and clay hydroxyl hydrogen isotopic compositions do not show appreciable signs of exchange. This conclusion has been drawn from measurements of soil profiles across the US (Lawrence and Taylor, 1972) as well as measurements of clay minerals from deep sea sediments of different depths (Yeh and Epstein, 1978). Further evidence for lack of exchange comes from measurements of Cretaceous and Cenozoic kaolinite samples from Georgia, US, which suggest that the kaolinites had preserved formation isotopic composition (Hassanipak and Eslinger, 1985). It has also been reported that terrestrial clays not only do not exchange during sedimentation, but also undergo very little alteration during burial, even over periods of 25 Ma. Furthermore, these terrigenous sediments contain very little in the way of authigenic marine clay formation (Yeh & Eslinger, 1986).

Others have argued that the clay hydroxyl hydrogen is exchangeable independent of oxygen isotope exchange. On the basis of measurements of exposed kaolinites from the western Canada sedimentary basin, Longstaffe and Ayalon (1990) suggested that the hydrogen isotopes were in equilibrium with present day formation waters, while oxygen isotopes of silicate were not (Longstaffe and Ayalon, 1990). Lawrence and Meau (1993) studied ancient kaolinite samples distributed across North America, and found that while some kaolinite samples appeared to preserve formation hydrogen isotopic composition, other kaolinites appeared to have exchanged during the early Cenozoic and preserved this new composition. Some kaolinites also appeared to have undergone partial exchange with more recent meteoric waters – identified by the kaolinite isotopic composition not plotting on the Global Meteoric Water Line. Further evidence for hydroxyl hydrogen exchange has been found by comparison of clay $\delta^{18}O$ to clay $\delta^{2}H$ in illite samples from the Athabasca Basin (Wilson *et al*., 1987), although it is unclear whether this study actually measured illite hydroxyl hydrogen. In summary, it appears likely that, in some circumstances, clay hydrogen can exchange, but it is not entirely clear under what circumstances this occurs – it is possible that mineral alteration can explain some cases of exchange (Savin and Hsieh, 1998).

1.2.3 Other Hydrated Mineral Water Isotopes

Stable isotopes of water have been used in minerals outside of the clay group minerals. Gypsum ($CaSO_4 \cdot 2H_2O$), the hydrated endmember of calcium sulphate, is one such hydrated mineral whose hydration water has been used for palaeoclimatology. As with the clay minerals, much work has focused on establishing the fractionation factors of oxygen and hydrogen isotopes in gypsum hydration water (GHW) (Gonfiantini and Fontes, 1963; Fontes and Gonfiantini, 1967; Hodell *et al.*, 2012; Gázquez *et al.*, 2017; Liu *et al.*, 2018) and the potential for hydration water isotopic exchange (Sofer, 1978; Evans *et al.*, 2015). As gypsum is a precipitate mineral which can very easily be synthesised in laboratory conditions, the isotopic fractionation between GHW and its mother water is far better constrained, and current evidence suggests that isotopic exchange is minimal without reprecipitation (Khademi *et al.*, 1997; Hodell *et al.*, 2012; Grauel *et al.*, 2016). The isotopic composition of GHW has been used to reconstruct environmental conditions in a number of palaeoclimate studies, including the climate of Southwestern Europe during the Messinian Salinity Crisis (Evans *et al.*, 2015), the temperatures across Central America during the last 42 ka (Hodell et al., 2012; Grauel *et al.*, 2016) and the amount of rainfall both during the decline of the Maya civilisation (Evans *et al.*, 2018) and in the western Qaidam Basin in China over the last 2.2 Ma (Li *et al.*, 2017).

All of these experiments have focused on measuring the total hydration water, and the clay experiments focused on measuring clay bulk oxygen, and the total non-interlayer water of clays. Very few previous studies have attempted the separation and measurement of each type of water in a hydrated mineral. One noteworthy exception is the study by Knauth and Epstein (1982), who measured the weight loss and δ^2H of opal ($SiO_2 \cdot nH_2O$) that was released by step-heating. This study is of particular relevance experimentally to clay isotope measurements because opal, like the clay minerals, contains both H_2O and hydroxyl groups bound to silicate. The opal was heated in discreet temperature increments, and released water from each increment cryogenically trapped. The separated water samples were then converted to H_2 by uranium reduction, and measured using traditional Isotope Ratio Mass Spectrometry (IRMS). The study demonstrated that water released at different temperatures had vastly different δ^2H values (from above –40 ‰ to below –110 ‰), meaning that the differences between waters in different mineral environments are significant – information

that is lost when only the total water is measured. However, because the experimental process was highly labour-intensive, there have been very few further studies into this area.

1.2.4 Advances in Experimental Technique

Naturally, the methods used for mineral water stable isotope measurement have improved over time. Early $\delta^{18}O$ measurements required the conversion of bulk clay oxygen, via oxidation with fluorine, to CO_2 (carbon dioxide), which could then be measured using mass spectrometry (e.g. Taylor and Epstein, 1962). Early $\delta^{2}H$ measurements required the trapping of liberated water using dry ice, before conversion of trapped water to hydrogen using hot uranium and measurement by mass spectrometry (e.g. Craig 1961). This precluded the possibility of concurrently measuring the $\delta^{18}O$ of the liberated water, which had to be done separately by isotopic exchange with CO_2. Advances in mass spectrometry mean that these reactions are no longer required for IRMS (Sharp *et al.*, 2001), and precisions have also improved. While mass spectrometry is still common (e.g. Sharp *et al.*, 2001; Eiler and Kitchen, 2001; Playà el al., 2005; Yeh *et al.*, 2014; Bauer *et al.*, 2016), recent advances have seen the use of Cavity Ring-Down Spectrometry (CRDS) as a method to measure $\delta^{18}O$ and $\delta^{2}H$ simultaneously (Hodell *et al.*, 2012; Affolter *et al.*, 2014; Gázquez *et al.*, 2015; Uemura *et al.*, 2016). This allows the simultaneous measurement of both oxygen and hydrogen isotope ratios in real-time, with accuracies comparable to mass spectrometry – with the caveat that generally more sample is required.

When considering the current state of research, there is potential for a continuation of the water-separation methodology devised by Knauth and Epstein (1982), using modern measurement methods which are significantly less labour intensive, and can more accurately measure changes in clay hydration water by combining step heating and CRDS (Bauska *et al.*, 2017).

1.3 Statement of the Problem

Previous research into the use of mineral hydration water isotopic composition has focused almost exclusively on measuring the total hydration water of the mineral. This can potentially cause information stored in the different hydration water types to be lost, as well as make it more difficult to correctly exclude exchangeable water from isotope measurements. Differential Thermal Isotope Analysis (DTIA) therefore has a role in the accurate determination of mineral hydration water isotopes, being capable of both accurately separating different water types from different mineral environments and also capable of measuring the isotopic composition of each water type, without the need for laborious trapping during a step-heating process – especially as DTIA also allows for the simultaneous measurement of both oxygen (^{18}O, ^{16}O) and hydrogen (D, H) isotopes.

As such, DTIA is a powerful method capable of gathering more information from the isotopic composition of hydrated minerals than existing methods. The isotopic composition of mineral hydration water is of interest as oxygen and hydrogen isotopes are highly indicative of formation environments. Potential uses for oxygen and hydrogen isotopes include determining the provenance of a mineral, determining the environmental conditions at time of mineral formation, and determining how hydrated minerals have interacted with fluids after formation, among others. Many of these uses rely on the hydration water signal being preserved over time – here, the ability of DTIA to separate out sample hydration water into different water types offers another advantage, as non-exchangeable water (e.g. hydroxyl water) can easily and accurately be separated from other exchangeable water in a sample.

Mineral hydration water isotope study is a field of great interest; hydrated minerals are common to many different environments and geological periods. In particular, layers of hydrated clays have been deposited globally during significant geological events (e.g. iridium-enriched clay at the Cretaceous–Palaeogene (K-Pg) boundary, and kaolinite in the Paleocene-Eocene Thermal Maximum (PETM)), and clays and other hydrated minerals such as gypsum have also been found on Mars. As such, clay hydration water can provide insight into the nature of palaeoclimate change during geological transitions, and also into the evolution of the Martian climate.

1.4 Thesis outline

This thesis focuses on the development of DTIA and its use to analyse the isotopic composition of water in minerals containing multiple water environments. It is structured as follows:

Chapter 2 presents an overview of the DTIA method. This consists of a description of the experimental setup, the methodological and analytical procedure, as well as a comparison of results of hydration water isotopic composition as measured by DTIA and more traditional offline water extraction techniques. While comparison of gypsum measurements is the main focus for demonstrating the validity of the DTIA method, kaolinite dehydroxylation is also compared. In addition, the separation of water types in the dehydration of minerals with multiple types of water is showcased.

Chapter 3 focuses on the applications of DTIA to the measurement of the gypsum → bassanite and bassanite → anhydrite dehydrations. A number of experiments pertaining to the nature of the two step dehydration are discussed, and it is demonstrated that the two step dehydration does not contain further palaeoclimatic information than the measurement of the total gypsum hydration water. A series of experiments to determine the potential use of bassanite as a palaeoclimatic proxy are also presented, alongside further suggested experiments for finding the oxygen and hydrogen fractionation factors for hydration water in bassanite – of interest because of bassanite deposits found on Mars.

Chapter 4 investigates the application of DTIA to clay minerals, detailing the DTIA method for measuring common clay minerals including kaolinite, beidellite, and both calcium-rich and sodium-rich montmorillonite samples. Further experiments consider the measurement of mixed clays, potential impediments to accurate isotope measurement, and the applicability of clay hydroxyl isotope measurement to palaeoclimatology.

Chapter 5 studies climatic changes around the North Sea Basin during the PETM. Using a well-characterised set of mixed clay samples, trends in clay oxygen and hydrogen isotopes across the PETM as measured by DTIA are compared to clay oxygen isotope measurements by mass spectrometry, as well as other climate proxies such as clay composition, the isotopic

composition of total organic carbon and the count of dinoflagellate cysts. The results, and their implications for DTIA's uses in palaeoclimatology, are discussed in the context of other PETM studies at both local and global scopes.

2 An Experimental Overview of the Online Differential Thermal Isotope Analysis Method

Note on Authorship

This chapter is adapted from the publication 'Online Differential Thermal Isotope Analysis of Hydration Water in Minerals by Cavity Ring-down Laser Spectroscopy' in Analytical Chemistry. I am the second author of this paper; all work reported in this chapter is my own.

Bauska, T. K., Walters, G., Gázquez, F., & Hodell, D. A. (2017). Online Differential Thermal Isotope Analysis of Hydration Water in Minerals by Cavity Ringdown Laser Spectroscopy. Analytical Chemistry, 90(1), 752–759. doi:10.1021/acs.analchem.7b03136

2.1 Abstract

A new method for measuring the isotopic composition ($\delta^{18}O$ and δD) of different types of bonded water (e.g. molecular water, hydroxyl) contained in hydrated minerals has been developed by coupling a thermal gravimeter (TG) and a cavity ringdown laser spectrometer (CRDS). The method involves precisely step-heating a mineral sample, allowing the separation of the different types of waters that are released at different temperatures. The water vapour evolved from the mineral sample is analysed for oxygen and hydrogen isotopes simultaneously by CRDS. Isotopic values for the separate peaks are calculated by integrating the product of the water amounts and its isotopic values, and correcting for background. In this chapter examples are provided of the application of the online differential thermal isotope analysis (DTIA) method to a variety of hydrous minerals including gypsum and clays. The isotopic compositions of the total water evolved from a set of natural gypsum samples as measured by DTIA are compared with the results of a conventional offline water extraction method followed by CRDS analysis. The results from both methods are in excellent agreement and precisions (1σ) for $\delta^{18}O$ (± 0.12 ‰) and δD (± 0.8 ‰) of the total gypsum hydration water from the online DTIA method are comparable to that obtained by the offline water extraction method. The DTIA method has wide ranging application for addressing fundamental problems across many disciplines in Earth and Planetary Sciences, including

palaeoclimatology, sedimentology, volcanology, water exchange between the solid earth and hydrosphere, and water on Mars and other planetary bodies.

2.2 Introduction

Oxygen (^{16}O, ^{17}O, ^{18}O) and hydrogen (H, D) isotopes of hydration water in minerals provide powerful constraints on the conditions under which these minerals formed on Earth and other planetary bodies (e.g. Mars). High-precision measurements of hydrated minerals present three major challenges: (i) hydrated minerals often hold multiple forms of water of variable exchangeability and isotopic composition that require separation prior to analysis; (ii) most natural samples are of mixed mineralogy that are not readily separable by mechanical or chemical means; and (iii) oxygen and hydrogen need to be converted to, or equilibrated with, gaseous species for analysis on gas-source isotope ratio mass spectrometers (typically CO_2 for $\delta^{18}O$, O_2 for ^{17}O-excess, H_2 for δD). In this chapter, I provide an overview of the online DTIA method for measurement of mineral oxygen and hydrogen isotopic composition. This method couples a thermal gravimeter to a cavity ringdown laser spectrometer, which allows for precise thermal separation combined with simultaneous online oxygen and hydrogen isotope analysis, bypassing the need for chemical conversion. The general methodology is described with a focus on gypsum, a relatively well studied hydrated mineral, in order to provide information on protocol, data processing requirements, accuracy and precision. Two clay minerals, kaolinite and montmorillonite, are used to further demonstrate the accuracy and precision of DTIA, as well as its advantages in water type separation during measurement.

Research on the isotopic composition of hydrous minerals progressed rapidly in the 1960s and 1970s following the advent of gas source isotope ratio mass spectrometry (IRMS). Pioneering work was carried out on volcanic glass (Friedman and Smith, 1958), gypsum (Gonfiantini and Fontes, 1963), opal (Knauth and Epstein, 1976), clays (e.g. (Savin and Epstein, 1970 a, b; O'Neil and Kharaka, 1976; Suzuoki and Epstein, 1976; Yeh and Epstein, 1978; Sheppard and Gilg, 1996), hydrous carbonates (Matsuo and Friedman, 1972) and manganese hydroxides (Hariya and Tsutsumi, 1981). Typically, water was extracted by heating in vacuum followed by cryogenic trapping and finally conversion to, or exchange with, H_2 or CO_2 gas (though most early studies focused solely on hydrogen isotopes). In order to separate different types of water within a given mineral, Knauth and Epstein (1982), developed a method whereby a mineral (opal in particular) was progressively heated in vacuum and water was trapped over discrete temperature intervals for later analysis by IRMS

(Knauth and Epstein, 1982). A quartz spring balance within the vacuum system allowed the authors to monitor the mass loss over the course of the experiment. The method was termed "Differential Thermal Isotope Analysis" and has subsequently been adopted for a variety of hydrous mineral studies. The downsides to the method include the laborious nature of the trapping procedure (a typical experiment lasted over 8 hours) and the need for chemical conversion of the water to H_2 or CO_2 gas.

In the 1990s and early 2000s, methods became available for online extraction of water and rapid conversion to gaseous species suitable for continuous-flow mass spectrometry (Brand *et al.*, 1994; Sharp *et al.*, 2001). Using a high-temperature (1450 °C) glassy carbon furnace to simultaneously dehydrate/dehydroxylate minerals and convert H_2O vapour to H_2 and CO gas, Sharp *et al.*, 2001, demonstrated high-precision measurements of δD of ± 2 ‰ (1σ) on a variety of hydrous minerals on samples containing about 0.1 μL of H_2O (Sharp *et al.*, 2001). The method also showed promise for the simultaneous analysis of $\delta^{18}O$ (by peak-jumping the IRMS to CO m/z) with precisions of 0.2 ‰ (1σ), but this aspect of the method has been less widely reported in the literature. Any differential thermal isotope analysis with this method requires pre-heating the samples to remove unwanted water followed by methods to prevent any absorption of atmospheric water vapour prior to analysis (see Bauer and Vennemann, 2014). More specialized systems have also been developed to study the hydrogen isotopes of nominally non-hydrous geological samples (e.g. meteorites) with precisions ranging from ± 1-2 ‰ (1σ) on samples yielding as little as 1×10^{-5} μL of H_2O (Eiler and Kitchen, 2001).

More recently, the development of commercially available laser absorption spectrometers has offered another opportunity for technical advancement. Offline extraction of gypsum hydration water followed by CRDS analysis (Picarro i2140) has yielded high precision measurements of $\delta^{18}O$, $\delta^{17}O$ and δD with 1σ standard deviations of 0.13, 0.07 and 0.5 ‰ respectively for water samples of about 20 μL (200 mg of gypsum) (Gázquez *et al.*, 2015). CRDS instruments have also been used in the measurements of much smaller amounts of water released from fluid inclusions in minerals (~0.1-1.0 μL) with precision better than ~0.5 and 2 ‰ (1σ) for $\delta^{18}O$ and δD, respectively (Arienzo *et al.*, 2013; Affolter *et al.*, 2014; Uemura *et al.*, 2016). An online method using off-axis integrated cavity output spectroscopy (Los Gatos Research model 908-004), which focused on organic materials but reported some gypsum measurements, demonstrated precisions of ± 3-4 ‰ (1σ) for δD (Koehler and

Wassenaar, 2012). This recent advance in laser spectroscopy is used to revisit the "Differential Thermal Isotope Analysis" method described by Knauth and Epstein with state-of-the-art instrumentation allowing for online measurement (Knauth and Epstein, 1982).

2.3 Methods

2.3.1 System Design

An overview schematic of the online-DTIA system is provided in Figure 2.1. Samples are heated in a thermal analysis system (Netzsch STA 449 F3 Jupiter) capable of both thermal gravimetric analysis (TGA) and differential scanning calorimetry (DSC). The furnace can range between ambient temperature and 1600 °C with maximum ramp rates of 40 °C / min and the possibility of precisely controlled plateaus. TGA provides continuous data on changes in the mass of the sample with time and temperature. DSC records small differences in the temperature of the sample and a reference material, thus providing constraints on the enthalpy of a phase transition or chemical reaction (i.e. endothermic or exothermic). TGA and DSC are standard analytical techniques in earth sciences; the thermal reactions are characteristic and used for rapid and inexpensive mineral identification (Földvári, 2011).

A sample is held in a crucible that sits perched on a "carrier" that connects to the balance, which is comprised of an alumina stalk housing the thermocouple and alumina baffle system. For samples smaller than ~20 mg the TGA/DSC carrier can be used, which has a platinum platform that can hold a variety of crucibles (Al for temperatures less than 600 °C, Pt or Al_2O_3 for higher temperatures) and allows for simultaneous measurement of TGA and DSC. Larger samples (up to 5 ml in volume) are analysed solely in TGA mode and are held in an Al_2O_3 crucible that fits directly onto the carrier stalk.

The flow of gas can in theory be precisely manipulated by controllers in the TG system to match the flow required by the Picarro CRDS (~30 ml / min); however, in practice, pressure variations mean that the Picarro CRDS (which uses a diaphragm pump to draw sample into the measurement cavity at a constant pressure) draws a variable flow rate, and over the course of hours or days this leads to slight over- and under-pressures within the balance system. Under-pressures are not problematic as the TG system is designed to operate at pressures as low as 10^{-4} mBar (with an attached turbomolecular pumping system not used in this study), but large overpressures can potentially damage the balance, and pressure inconsistencies will distort TGA results. To work around this, an open-split is used upstream of the TGA in the gas flow to prevent overpressures. Dry N_2 is used as the carrier gas in these experiments as it

is non-hydrous and does not contain oxygen (the presence of oxygen may contribute to oxygen isotopic exchange at high temperatures). Other carrier gasses can be used; in particular, experiments trying to remove volatile organics in the course of DTIA measurement using solid catalysts and oxygen have used dry air as a source of O_2 (Bauska *et al.*, 2017). However, the presence of a solid catalyst between the thermal analysis system and CRDS can have a negative effect on measurement accuracy, so is not used in this study.

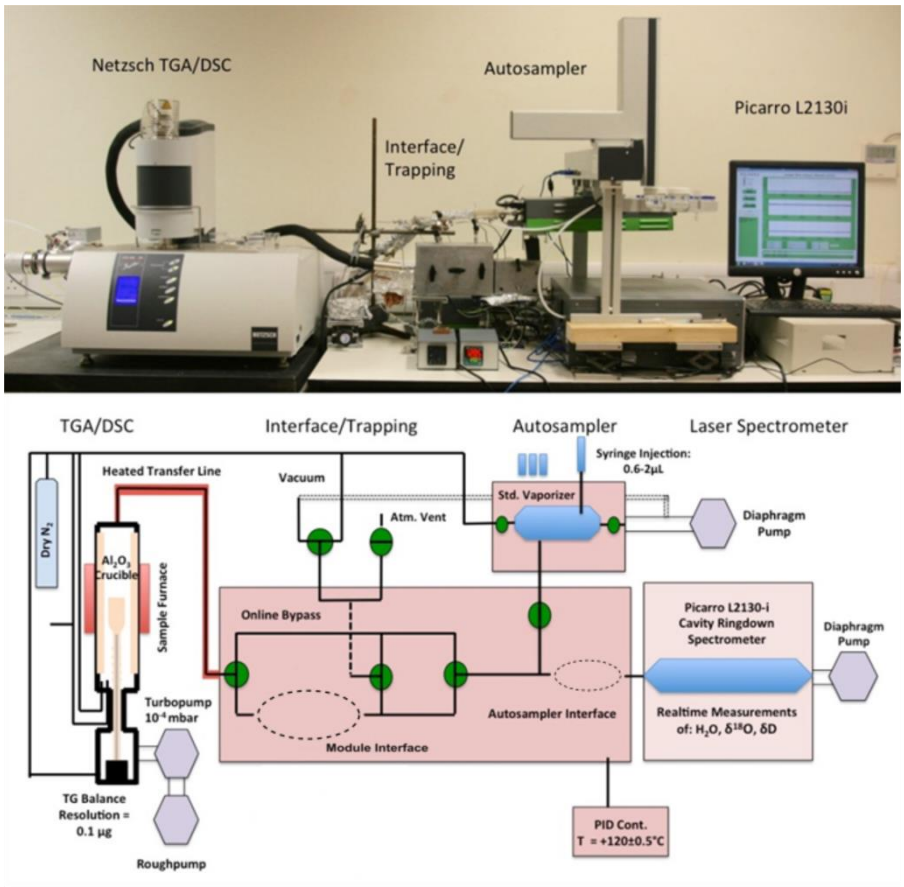

Figure 2.1. An overview of the online-DTIA system. Upper panel: an image of the coupled Netzsch thermal gravimetric analysis (TGA) unit and Picarro L2130i cavity ringdown spectrometer (CRDS). Lower panel: a schematic of the system with an emphasis on the interface box. Solid black lines represent 1/8 stainless steel tubing and green circles represent valves. The module interface dashed circle represents an area where further modules, such as cryogenic trapping, can be added. The autosampler interface dashed circle indicates where a solid catalyst can be inserted to promote the oxidation of volatile organics.

Finally, stock o-rings on many of the seals in the TG system, likely made of silicone and relatively permeable to water, were replaced with Viton, reducing background water amounts and isotopic composition variability.

Downstream of the TGA, water vapour is carried via a heated (120 °C) 1/8 inch stainless steel tube to a heated (120 °C) interface system. The interface box serves multiple purposes. The primary purpose is to enable switching between the autosampler and Netzsch without disrupting the gas flow to the CRDS (the Netzsch and CRDS both require constant gas flow), allowing for the calibration of DTIA measurements using injected water standards, while keeping all tubing heated above 100 °C (preventing water condensation). This could be achieved more simply, but having a heated box enables the easier addition of further function, such as cryogenic trapping, or the insertion of catalysts for the oxidation of volatile organics (Bauska *et al.*, 2017). The gas plumbing is comprised primarily of 1/8 inch stainless steel tubing and Swagelok 3-way ball valves (40G Series).

A Picarro L-2130i provides continuous measurement of the H_2O, $\delta^{18}O$ and δD of the water vapour stream.

2.3.2 Analytical Protocol

A sample is loaded into the TGA system manually and the furnace tube is flushed with dry N_2 (~30 ml / min) for at least 15 minutes, or until water background returns to less than 100 ppm. A temperature program is then started and the TGA/DSC and Picarro water isotopes traces are synchronized. Figure 2.2 shows an example of a gypsum dehydration profile with the coupled TGA/DSC and Picarro data traces. In this case, gypsum was placed in loosely sealed aluminium crucible to produce the two-step dehydration from gypsum ($CaSO_4 \cdot 2H_2O$) to bassanite ($CaSO_4 \cdot 0.5H_2O$) to anhydrite ($CaSO_4$), which illustrates the ability of the system to separate different bonded waters and simultaneously characterise them for their mass loss, enthalpy, H_2O, $\delta^{18}O$ and δD. As the sample is heated (5 °C / min for gypsum two peak dehydration; 40 °C / min for the heating rate of most clay measurements), the mineral dehydrates as evidenced by the mass loss and endothermic reaction. The released water vapour is carried to the CRDS (transit time ~ < 1 minute) where it is measured for H_2O concentration, $\delta^{18}O$, and δD. After analysis, the furnace is cooled to near ambient

temperature and another sample may be loaded immediately. Samples like gypsum, which require relatively low final temperatures (~200 °C), can be measured about every 40 minutes. Samples requiring higher final temperatures (~1000 °C) require at least a 90 minute turn-around period.

2.3.3 Data Processing

Raw data output from the TGA/DSC and Picarro instruments are processed with in-house Mathematica code. Peak shoulders are defined based on the first derivative of the H_2O trace. Theoretical background water amounts and background isotopic values during measurement are calculated by plotting a linear fit between the data before and after the measurement; 200 data points either side of the measurement data is used for this. The linear fit is assumed to represent the background H_2O, $\delta^{18}O$ and δD across the sample peak. Typically, background in the instrument is low (~100 ppm) relative to ideal sample peak heights between 17000 and 23000 ppm (Affolter et al., 2014). The background in the instrument is sourced from lab air with some memory effects from prior samples with $\delta^{18}O$ and δD values of around –20 ‰ and –140 ‰, respectively. The magnitude of the correction can therefore vary depending on both the sample amount and isotopic composition; however, background water amount is so low relative to the measured sample water amount (<1 % of sample water amount) that background correction typically has a negligible effect on final results. Once total background-corrected H_2O, $\delta^{18}O$ and δD values have been calculated, the $\delta^{18}O$ and δD values are then calibrated using at least three working water standards (calibrated against SLAP, GISP and V-SMOW) that are injected multiple times into a vaporizer following the approach outlined in Gázquez *et al.* (2015). Calculation of the background-corrected H_2O, $\delta^{18}O$ and δD values is done following the process outlined in Affolter *et al.* (2014); in short, the measured online sample and calculated background $\delta^{18}O$ and δD signals must be weighted by water amount and integrated over time, so the online measured isotopic compositions must be multiplied by water amount (done for each data point), then integrated against time, and then the total is corrected for total water amount.

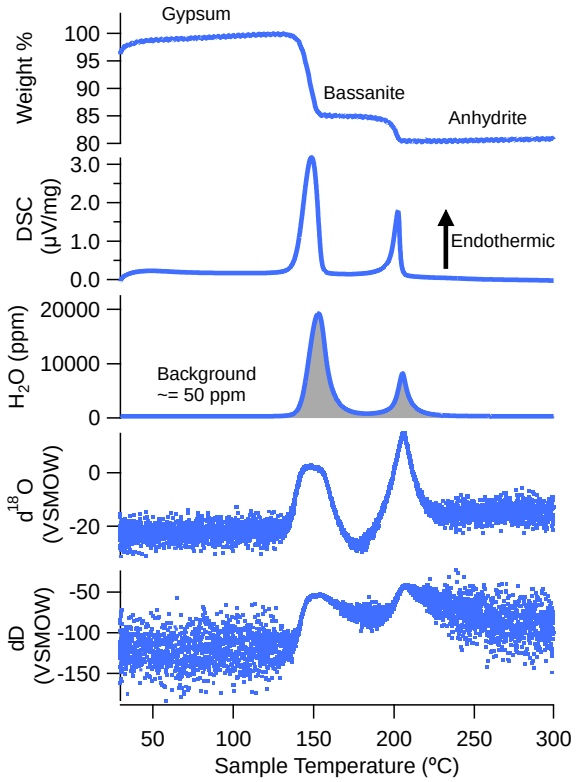

Figure 2.2. An example of a gypsum-bassanite-anhydrite transition with the well-known double release of structural water. The weight % and differential scanning calorimetry (DSC) traces from the Netzsch TGA/DSC are shown in the upper two panels. The lower panels show the H_2O, $\delta^{18}O$ and δD traces from the Picarro CRDS.

2.4 Results and Discussion

2.4.1 Gypsum Results: Precision, Accuracy and Linearity

Gypsum is used as means to characterise the precision, accuracy, and sensitivity of the online-DTIA method. First, measurements were taken of a suite of natural and synthetic gypsum samples with a wide range of isotopic values with an offline, in vacuum total hydration water extraction system (the "WASP") (Hodell *et al.*, 2012; Gázquez *et al.*, 2015). The WASP system requires sample amounts of around 200 mg of gypsum, yielding 40 µl of water or enough to allow 10 syringe injections of 2 µl each into the CRDS. The same samples were then measured with the online-DTIA method. In comparison, the online-DTIA method consumes only ~7 mg of sample per measurement, thus yielding ~1.4 µl of water per measurement. In this instance, each gypsum sample was measured four times using the online DTIA method to establish the possible precision of DTIA, for a total of ~28 mg of sample used – though the required sample amount could likely be further reduced for the DTIA method if not trying to produce a two peak gypsum dehydration following the gypsum-bassanite-anhydrite transition, as if the gypsum hydration water is released in a single peak (and hence over a shorter period of time), the water amount peak height will be higher for the same sample amount.

The results of the comparison are shown in Figure 2.3, where the total gypsum hydration water $\delta^{18}O$ and δD from the "WASP" method are plotted against the results from the online DTIA method. In the $\delta^{18}O$ comparison, a linear regression yielded a slope, intercept and root-mean-square error of 1.03, 0.06, and 0.35 ‰, respectively; the δD comparison (similarly using a linear regression) produces a slope, intercept and root-mean-square error values of 0.96, –2.41, and 1.3 ‰, respectively. The comparison demonstrates that with a reduction in sample size of approximately an order of magnitude, the online-DTIA method can accurately determine the isotopic composition of GHW across a wide range of values to within about 0.4 and 1.3 ‰ for $\delta^{18}O$ and δD, respectively. Measurement precision of the DTIA method is high across the sample set when measuring total gypsum water through the two peak dehydration, averaging 0.20 ‰ for $\delta^{18}O$ and 0.4 ‰ for δD.

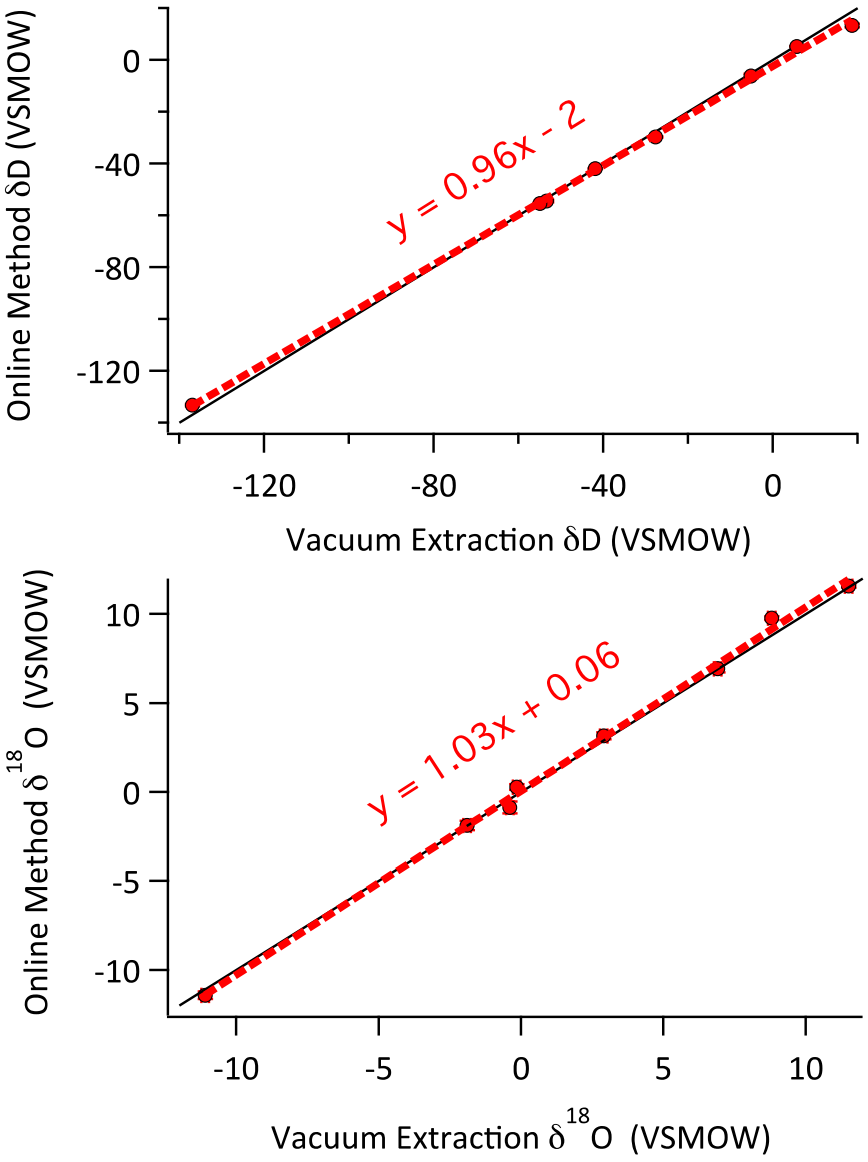

Figure 2.3. The precision and accuracy of gypsum measurements, as shown by plots of total gypsum hydration water $\delta^{18}O$ and δD in natural and synthetic gypsum samples (eight total) from a high-precision, offline vacuum extraction technique (Gázquez *et al.*, 2015) and the online-DTIA technique. The black solid lines represent the 1:1 line of coincidence between the two methods.

2.4.2 Kaolinite and Montmorillonite: High-temperature Dehydroxylation Examples

In addition to providing precise and routine isotopic measurements on relatively small samples, a significant innovation of the system is the capability of separating different types of bonded water. This chapter presents preliminary measurements of the isotopic composition of samples of kaolinite (source: Blackpool Pit, St. Austell pluton, Cornwall, UK (Sheppard, 1977)) and montmorillonite (source: Clay Minerals Society Stx-1b). Kaolinite, $Al_2Si_2O_5(OH)_4$, is a simple clay with only bonded hydroxyl; kaolinite can therefore be used to compare the online-DTIA method to an offline clay hydroxyl isotopic composition measurement technique. Montmorillonite is a clay with both interlayer water and bonded hydroxyl, whose members follow the formula $(Na,Ca)_{0.33}(Al,Mg)_2(Si_4O_{10})(OH)_2 \cdot nH_2O$, and which is a more representative example of water found in phyllosilicates. Examples of the weight %, H_2O, $\delta^{18}O$ and δD traces are shown in Figure 2.4.

Kaolinite undergoes dehydroxylation from ~450 to 650 °C, producing a relatively symmetric peak in H_2O (note the mass increase at 300 °C is an uncorrected artefact from an increase in the temperature ramp rate). Based on four replicate measurements with the online-DTIA system using ~7.2 mg of kaolinite, the $\delta^{18}O$ and δD of the hydroxyl water is 6.63 ± 0.7 ‰ and –62.2 ± 0.7 ‰ respectively. These results agree within error of offline in vacuum extractions (n = 5) of significantly larger samples in our laboratory ($\delta^{18}O$ = 5.8 ± 0.5 ‰ and δD = –62.6 ± 3.7 ‰), and δD as determined by early offline extraction and gas-source mass spectrometry techniques (δD = –62 ‰ (Sheppard, 1977)). This demonstrates that water extraction at high-temperature with the online-DTIA method is free of any significant errors with respect to previously established methodologies.

The montmorillonite shows a highly convolved double peak from ~100-200 °C from interlayer and absorbed water with both $\delta^{18}O$ and δD trending towards enriched values. From 200-500 °C, the sample continues to slowly lose mass (~0.003 wt% / °C). This leads to elevated water vapour levels between 2000 and 3000 ppm. Dehydroxylation appears to begin at about 500 °C with a significant acceleration of water loss between 600 and 700 °C. In cases like this, an isothermal interval can be employed to increase separation between peaks. Using this technique (see Chapter 4 for a full description of the montmorillonite measurement

program), replicate measurements (n = 4) constrain the $\delta^{18}O$ and δD of the hydroxyl peak to 13.42 ± 0.13 ‰ and –41.6 ± 0.6 ‰, respectively. This demonstrates the possibility for high-precision measurements of clay mineral hydroxyl oxygen and hydrogen isotopic composition. Attempts to separate and measure the hydroxyl water with offline extraction proved unsuccessful, highlighting the utility of the online-DTIA method but limiting our ability to assess the accuracy of the online-DTIA method.

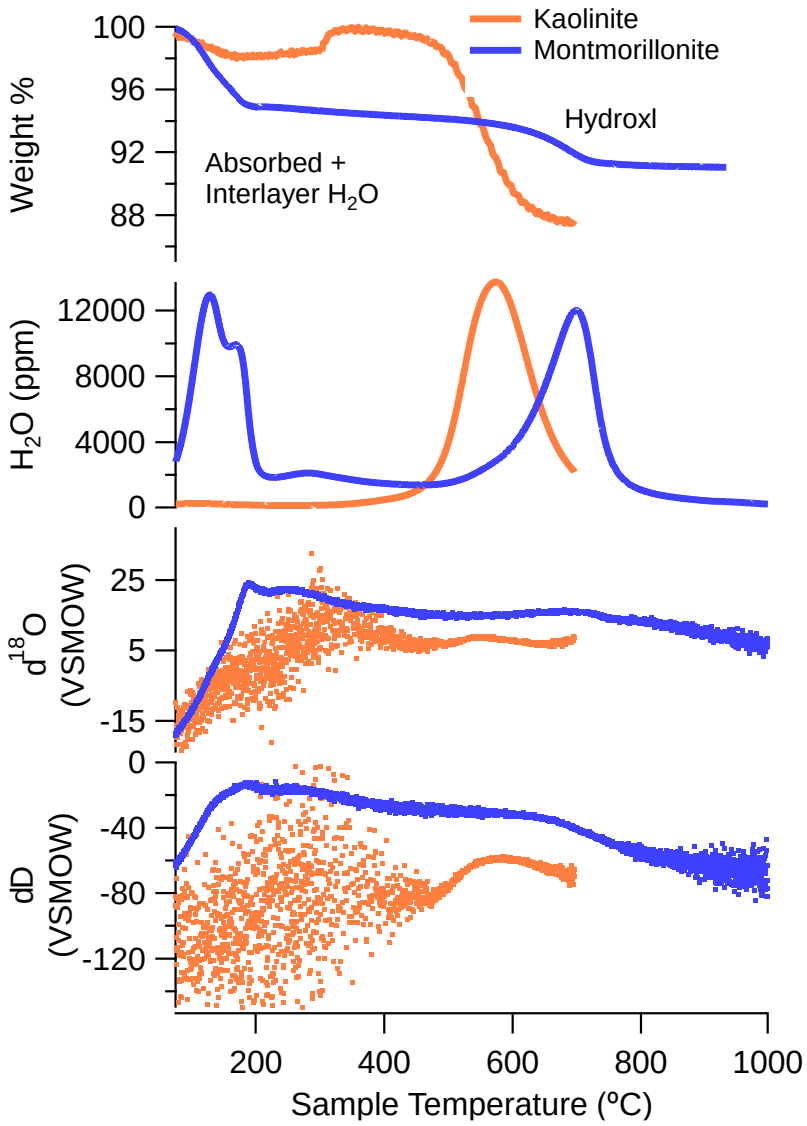

Figure 2.4. A comparison of the kaolinite (orange) dehydroxylation centred around 550 °C and the montmorillonite interlayer and absorbed water dehydration around 150 °C and dehydroxylation which peaks at around 650 °C.

2.5 Conclusions

A new method capable of measuring the isotopic composition of multiple forms of bonded water in hydrous minerals has been developed. The online DTIA method simultaneously provides $\delta^{18}O$ and δD data at precisions of 0.12 and 0.8 ‰ respectively. These precisions are comparable to previous methodologies for natural samples, if not a slight improvement (see Table 2.1 for comparison). However, the new method requires about ~1.4 µl of water and is thus a slight compromise on sample size, particularly when compared to online-IRMS methods capable of measurements of only 0.1 µl of water. Compared to offline differential thermal separation the online-DTIA is significantly less labour intensive, and has significantly lower risk of water re-adsorption compared to methods where samples are partially dehydrated before being transported to measurement instruments (Bauer and Vennemann, 2014). The instrumental setup also requires much lower capital and consumables costs compared to methods utilizing gas-source mass spectrometers.

Method	**Sample Size**	**Precision (1-sigma s.d.)**		**Reference**
	H_2O (µl)	**$\delta^{18}O$ (‰)**	**δD (‰)**	
Online DTIA	~1.4	0.20	0.4	This study
Vacuum Extraction - CRDS	40	0.13	0.5	Gázquez *et al.*, 2015
TCEA-IRMS	0.1	0.2	2	Sharp *et al.*, 2001
Online combustion OA-ICOS	0.4	-	3 to 4	Koehler and Wassenaar, 2012
Online reduction-IRMS	1.00×10^{-5}	-	1 to 2	Eiler and Kitchen, 2001
Fluid Inclusion CRDS	0.3 to 1.0	0.5	2	Arienzo *et al.*, 2013
	> 0.5	0.4	1.5	Affolter *et al.*, 2014
	0.05 to 0.25	0.05 to 0.6	0.0 to 3.0	Uemura *et al.*, 2016

Table 2.1. Summary of the precisions of and sample sizes required for a number of methods for isotopic composition analysis. DTIA has a comparable precision to existing methods, and in most cases is more precise.

The primary advantage of the DTIA method is the ability to rapidly characterise the wt % and isotopic composition of multiple forms of bonded H_2O or bonded OH^- in a sample. By separating these different forms of water, factors that control the isotopic composition of the water species, such as isotopic fractionation during formation and post-depositional exchangeability, can now be studied. The same principle could also provide a way to separate water from different minerals in natural samples of mixed mineralogy.

3 An Examination of the Palaeoclimatic and Structural Implications of the Two-Step Gypsum Dehydration Mechanism using DTIA

3.1 Abstract

This chapter reports the results of experiments to determine the origin of gypsum's two-step dehydration. In particular, I show that the dehydration mechanism is strongly affected by changes in sample grain size and in the partial pressure of water present in the environment under which gypsum dehydration occurs. Attempts to use the two-step dehydration to recover further palaeoclimatic information were unsuccessful, as it appears that isotopic fractionation between the gypsum → bassanite and bassanite → anhydrite dehydration steps are not driven by differences in water bonding environment, but rather by kinetic factors upon dehydration, which are difficult to isolate due to the rapid rehydration of γ-anhydrite under atmospheric conditions. Attempts to synthesise bassanite, in order to determine bassanite-water fractionation factors, were also broadly unsuccessful, giving low yields of bassanite and inaccurate fractionation factors. Further attempts to calculate bassanite-water fractionation by rehydrating anhydrite also proved inaccurate; improvements for more accurate measurements using anhydrite rehydration are suggested. Accurate determination of the bassanite-water fractionation factors would allow for bassanite to be used like gypsum as a palaeoclimatic proxy – this holds particular relevance for determination of the Martian palaeoclimate, where gypsum and bassanite are found.

3.2 Introduction

Gypsum ($CaSO_4 \cdot 2H_2O$) is the hydrated endmember of the calcium sulphate minerals (gypsum-bassanite-anhydrite) and is a mineral common to terrestrial environments, often forming as a result of evaporation of $CaSO_4$ bearing waters. Gypsum hydration water, in particular, has found use as a proxy for the hydrological conditions of its formation, through analysis of the isotopic composition (both oxygen isotopes and hydrogen isotopes) of the hydration water (e.g. Pierre and Fontes, 1978; Sofer, 1978; Hodell *et al.*, 2012; Gázquez *et al.*, 2013, 2017; Evans *et al.*, 2015), and also in conjunction with other proxies such as fluid inclusion salinity (Evans *et al.*, 2015). Furthermore, the recent discovery of bassanite ($CaSO_4 \cdot 0.5H_2O$) veins on Mars (Wray *et al.*, 2010; Rapin *et al.*, 2015), as well as widespread gypsum deposits (Langevin *et al.*, 2005; Gendrin *et al.*, 2005), has prompted a renewed interest in the hydration water of the gypsum-bassanite-anhydrite system and its potential applications as a palaeo-proxy.

The dehydration of gypsum to anhydrite ($CaSO_4$) is thought to proceed via the intermediate bassanite (Bezou *et al.*, 1995; Christensen *et al.*, 2008; Jacques *et al.*, 2009). The structure of bassanite is close to that of γ-anhydrite (anhydrite III, soluble anhydrite) – one of three phases that anhydrite can form, the others being β-anhydrite (anhydrite II, insoluble anhydrite), which forms at temperatures >300 °C, and α-anhydrite (anhydrite I), which forms at temperatures >1180 °C (Prieto-Taboada *et al.*, 2014). Both have a channel structure (Bezou *et al.*, 1995), which in bassanite contains the structural water. However, the dehydration of gypsum is strongly affected by reaction conditions (Paulik *et al.*, 1992), and under some conditions (low partial pressure of water being the most prominent) the two-phase dehydration is not seen. Because of this, and the fact that a number of the phases in the gypsum dehydration are metastable, the exact mechanisms for gypsum dehydration are still not known, despite a great deal of research on the subject. As such, here I use DTIA to measure the dehydration profile of gypsum, and interpret these in light of other published findings on the mechanism of gypsum dehydration.

The two-step dehydration is also of interest for palaeoclimatology. Mandal and Mandal (2012) proposed from IR data that the two-step dehydration is driven by gypsum containing water in two different bonding environments; one water fraction consisting of more loosely

bonded water bound to calcium, which is removed during the gypsum → bassanite dehydration, and the other smaller water fraction consisting of water bonded to sulphate with stronger hydrogen bonds. This more strongly bonded water was hypothesized as being the water removed in the bassanite → anhydrite dehydration. If this is indeed the case, the stronger anion-bonded water ("anion water") is less likely to undergo isotope exchange and more likely to preserve the isotopic composition of the formation water. This has potential significance to palaeoclimatology, where it could allow for partially exchanged gypsum hydration waters to still be used as a palaeoclimatic proxy, by isolation of the bassanite water. It could also help explain the mechanism of gypsum dehydration and why the second dehydration peak is always isotopically enriched relative to the first (Table 3.1). To test this "anion water" hypothesis, I present the results of a series of experiments designed to test for the presence of "anion water", and if present, whether it was suitable for use as a palaeoclimatic proxy. Critically, if the "anion water" hypothesis is correct, then the second step of the two-step gypsum dehydration will not be isotopically affected by changes to the water of the first dehydration step.

Furthermore, in order to use bassanite water as a palaeoclimatic proxy, the isotopic fractionation between bassanite and its mother water must be known. There are no reported experimental values for the hydrogen and oxygen bassanite-water fraction factors in the literature. As such, I present the results of a series of experiments which attempt to synthesize bassanite and measure the fractionation. These results are compared to a theoretical prediction of the bassanite fractionation factors, calculated using density functional theory (DFT) (Liu *et al.*, 2018).

The hydration water of bassanite is also of interest independent of the "anion water" hypothesis. While bassanite is a rare mineral on Earth due to its instability at 100% relative humidity (Robertson and Bish, 2012), the fact that bassanite has been discovered on Mars has made finding the bassanite-water fractionation factors a worthy goal.

Samples	Total $\delta^{18}O$ / ‰	1st Peak $\delta^{18}O$ / ‰	2nd Peak $\delta^{18}O$ / ‰	2nd - 1st Peak $\delta^{18}O$ / ‰	Total δD / ‰	1st Peak δD / ‰	2nd Peak δD / ‰	2nd - 1st Peak δD / ‰
V22L Entrada	–11.41 ± 0.21	–12.99 ± 0.41	–7.04 ± 0.37	5.95	–133.21 ± 0.51	–136.54 ± 0.01	–124.06 ± 1.90	12.48
BG-10	–1.87 ± 0.27	–3.41 ± 0.21	3.20 ± 1.39	6.60	–54.45 ± 0.53	–56.68 ± 0.32	–47.20 ± 1.27	9.49
CRI-01	–0.29 ± 0.16	–1.45 ± 0.15	6.16 ± 0.40	7.61	–41.97 ± 0.16	–44.78 ± 0.18	–32.50 ± 0.52	12.28
CM	–0.86 ± 0.34	–2.41 ± 0.24	4.19 ± 0.89	6.60	–55.35 ± 0.27	–57.75 ± 0.16	–47.55 ± 0.70	10.19
SBL-2.3	3.16 ± 0.20	1.68 ± 0.23	7.78 ± 0.74	6.10	–29.73 ± 0.30	–32.30 ± 0.32	–21.65 ± 1.20	10.65
Bosque-18	6.93 ± 0.22	5.28 ± 0.24	12.12 ± 0.66	6.84	–6.20 ± 0.86	–9.63 ± 0.75	4.56 ± 1.75	14.19
PI MIX	9.78 ± 0.10	8.07 ± 0.10	15.43 ± 1.12	7.37	5.27 ± 0.01	1.84 ± 0.55	16.60 ± 2.50	14.77
Salina 5	11.58 ± 0.08	9.12 ± 0.13	17.75 ± 0.65	8.63	13.30 ± 0.67	8.79 ± 0.53	26.71 ± 1.97	17.92

Table 3.1. A summary of DTIA measurements of the eight gypsum samples presented in Chapter 2 (Figure 2.3), showing total isotopic compositions, first peak and second peak isotopic compositions, the associated errors, and the difference in isotopic composition between the first and second peaks. The second dehydration water is always more enriched than the first in both oxygen and deuterium. The differences between the first and second peaks are similar for $\delta^{18}O$ across the samples.

3.3 Materials and Methods

All DTIA measurements of gypsum were carried out using the gypsum dehydration method described in Chapter 2, to ensure a consistent dehydration profile for measurement. A dry N_2 gas stream was used with no catalyst for the removal of organics. Furthermore, only $^{18}O/^{16}O$ and D/H are measured with DTIA, so all references to oxygen fractionation in the text refer to $\alpha^{18}O$, and all references to hydrogen fractionation refer to αD.

3.3.1 Materials

The internal lab standard New Gyp (a synthesised gypsum) was used for all experiments in this chapter. The aluminium crucibles refer to a 99.5 % purity 25 µl aluminium crucible and lid sourced from Netzsch for use with Netzsch DSC and TG systems.

3.3.2 Investigating the Two-Step Dehydration

3.3.2.1 Partial Dehydration Experiments

In order to more closely examine the exact nature of the gypsum → bassanite → anhydrite transition, and whether the water in bassanite represented a separate pool of water to the water lost in the gypsum → bassanite dehydration, I partially dehydrated a set of gypsum samples, in order to determine whether only the gypsum → bassanite water isotopic composition was affected, or if the isotopic compositions of both the gypsum → bassanite and the bassanite → anhydrite dehydration waters were changed. Owing to difficulties in reproducibly measuring a two peak dehydration for partially dehydrated gypsum, I then carried out a number of partial dehydration → rehydration experiments, in order to determine whether water re-entering the gypsum structure could influence the bassanite dehydration isotopic composition or not.

3.3.2.1.1 Partial Dehydration – in Furnace

The first attempts to partially dehydrate a gypsum sample were carried out using a furnace set to 60 °C under an initial vacuum pressure of 6×10^{-3} mbar (which increased as water was

liberated from the gypsum, as the gypsum was left isolated from the vacuum during heating). To optimise the amount of time it would take to achieve significant but not total dehydration of gypsum, a first experiment was carried out where 5 gypsum samples were loaded into the furnace, and one removed every 30 minutes to measure the weight loss of the sample. I found that after 120 minutes in the furnace, approximately 53 % of the water was lost. As the bassanite → anhydrite transition should account for the final 25 % of water in the sample, I decided that 120 minutes resulted in enough water removal to make a significant change to the first dehydration peak, without being so long as to be likely to dehydrate significant amounts of bassanite to anhydrite. An analysis of the IR water peaks of the 120 minute-dehydrated sample found that both gypsum and bassanite water peaks were present; however, as the anhydrite structure would simply result in a lack of water peaks, it was unknown whether the sample also contained anhydrite.

A second 120 minute furnace run was carried out, yielding a mass loss of 9.1 % and hence a water loss of 42 %, and a number of dehydration measurements made as per the standard procedure, using between 7.3 and 8.9 mg of sample. When the masses of the samples were measured, it was found that they were slowly increasing on the balance, suggesting atmospheric water absorption.

3.3.2.1.2 Partial Dehydration – Rehydration in Air

To try to work around the problems with the very dehydrated gypsum samples from the furnace experiments, which appeared to absorb atmospheric water, and were difficult to use to measure a reliable two peak dehydration, I carried out a new set of experiments, which used the Netzsch for finer control over the partial dehydration, and then let some of the sample rehydrate under a hydrated nitrogen gas flow. For these experiments, a partially dehydrated gypsum was prepared by heating a large sample (325 mg) of the synthetic standard New Gyp in a large aluminium oxide crucible to 125 °C, at a rate of 5 K / minute. The sample was heated under air, to improve the peak separation. Using thermal gravimetric analysis (TGA), the weight loss was found to be 2.96 %, and hence the water loss was found to be 14.1 %; when a portion of the partially dehydrated gypsum was set aside and dehydrated fully (the air initial gypsum), a further 87 ± 3 % of water was driven off,

suggesting that the partially dehydrated gypsum had taken on very little, if any, additional water before being placed in a controlled atmosphere.

Following the partial dehydration, the sample was split into two portions: one was subsequently dehydrated fully, using the standard method described previously (each sealed aluminium crucible containing between 7 – 8 mg of partially dehydrated gypsum), while the second portion was placed into a controlled water atmosphere, achieved using the setup shown in Figure 3.1 with an enriched spiked water. The isotopic composition of the water vapour was found by directing the wet N_2 flow to the CRDS spectrometer, through the heated box. This second portion of gypsum was sampled at 99 and 172 hours, and two DTIA measurements using the standard sealed aluminium crucible method were made for each time.

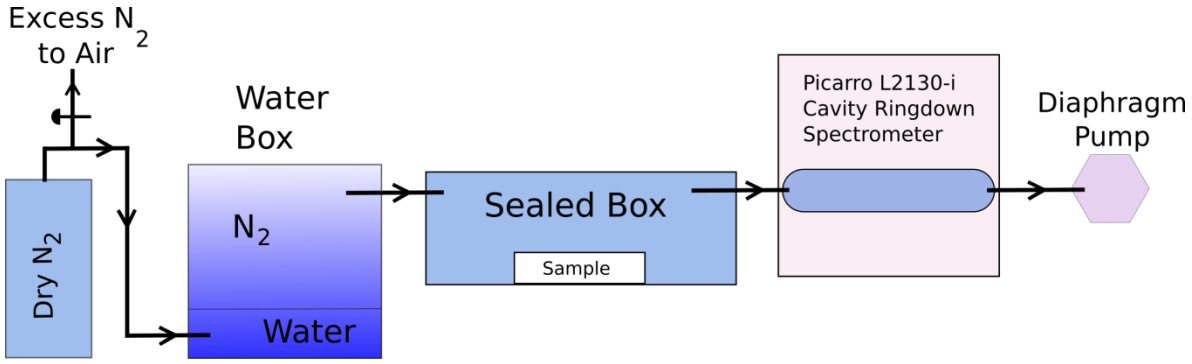

Figure 3.1. Diagrammatic representation of the experimental setup required to rehydrate a partially dehydrated gypsum sample under a known controlled water vapour. Nitrogen gas is bubbled through a submerged opening into a sealed water box containing water of a known isotopic composition. Excess nitrogen pressure is vented to atmosphere through a Teflon tube, where flow is restricted by a screw valve. A diaphragm pump attached to the CRDS draws nitrogen at the required pressure from the water box, over the sample held in a second sealed box, to the CRDS.

3.3.2.1.3 Partial Dehydration – Rehydration in Water

To further increase reliability by giving a fully rehydrated gypsum sample, I ran a final set of experiments, where partially dehydrated gypsum was similarly prepared by heating in the Netzsch, before rehydration in solution. A larger sample of 625.7 mg of the synthetic standard New Gyp was heated under air in a large aluminium oxide crucible to 128 °C, at a rate of 5 K / minute, in order to slightly increase the amount of water initially driven off. The weight loss (from TGA) was found to be 4.55 %, implying a water loss of 21.7 %; when a portion of the partially dehydrated gypsum was set aside and dehydrated fully (the water initial gypsum), a further 78 ± 5 % of water was driven off, suggesting that the partially dehydrated gypsum had not taken on any additional water before being placed into solution.

After the partially dehydrated sample had cooled, the sample was split into four portions – three portions were placed into three different solutions. The fourth portion of partially dehydrated gypsum was measured four times using the standard DTIA procedure, using 7 – 8 mg of sample sealed in aluminium crucibles. These were used to find the initial hydration and isotope ratios of the partially dehydrated gypsum. The aluminium crucibles were sealed just before the gypsum portions were placed into solution, so that all portions of partially dehydrated gypsum spent the same amount of time exposed to air.

The three solutions used were all saturated with respect to $CaSO_4$, to prevent loss of sample to dissolution. The first solution consisted of only water and $CaSO_4$. The second solution, after saturation with $CaSO_4$, had $NaSO_4$ dissolved into it, up to a concentration of 0.0838 $moldm^{-3}$. The third solution, after saturation with $CaSO_4$, had a small amount of polyacrylic acid dissolved into it (12.2 mg of polyacrylic acid into 125 ml of saturated water). Polyacrylic acid is thought to inhibit precipitation of gypsum from solution (Amjad, 1988), while $NaSO_4$ is commonly used as an activator when rehydrating anhydrite through reprecipitation (Conley and Bundy, 1958). The partially dehydrated gypsums were left in the saturated solutions for 24 hours, to ensure complete rehydration. After this, the gypsum samples were filtered and dried in an oven at 40 °C for at least 48 hours, before standard DTIA measurements using sealed aluminium crucibles and 7-8 mg sample were made.

3.3.2.2 Grain Size Experiments

In order to further test how the dehydration profile of gypsum is affected by kinetic factors, I carried out DTIA measurements on a set of three grain sizes: finely ground New Gyp (8.6 mg, grain size <64 μm), normal New Gyp (8.4 mg, grain size ≈ 100 μm), and a New Gyp single crystal (8.3 mg, grain size > 100 μm). I measured each using unsealed aluminium crucibles under dry nitrogen gas, following the standard DTIA procedure.

3.3.2.3 FTIR Experiments

Having assessed that the gypsum → anhydrite transition is primarily driven by kinetics, I looked to recreate the results reported in Mandal and Mandal, 2001, whereby the IR spectrum recorded from a dehydrated gypsum sample resembled the bassanite IR spectrum until the gypsum sample was heated as high as 350 °C. Using a Bruker TENSOR 27 FTIR spectrometer and the standard New Gyp, I took measurements of unheated gypsum, bassanite and two anhydrites. The bassanite was obtained by heating a sealed aluminium capsule to 150 °C, before ending the heating run between the first and second peaks of dehydration. The two anhydrites were obtained by heating to 250 °C and 350 °C respectively.

3.3.3 Measuring Bassanite-Water Isotopic Fractionation

3.3.3.1 Anhydrite-Bassanite Rehydration Experiments

Following the results of the IR measurements, a gypsum sample was heated to 250 °C, removing all water, then, after cooling, removed from the Netzsch and allowed to sit under air for a few minutes. The dehydrated gypsum was then reheated to 250 °C, and it was found that more water was removed – confirming that anhydrite had rehydrated to bassanite under air. It therefore seemed likely that the as yet unmeasured bassanite-water fractionation factor could be determined from rehydration under air, so I conducted a series of experiments to find the bassanite-water vapour fractionation factor.

Our initial experiments to determine the bassanite-water vapour fractionation factor consisted of a four-phase process. Firstly, a gypsum sample would be heated in the Netzsch under

nitrogen gas to 250 °C, to remove all water. Secondly, while still recording the mass of the sample using the TGA, atmospheric air would be drawn into the Netzsch by the Picarro vacuum pump (limiting the air flow to less than 30 ml per minute). Thirdly, after the sample had fully rehydrated to bassanite, the sample was removed from the Netzsch and the furnace was heated to 250 °C again, to clean the furnace of any excess water before measurement. Finally, the bassanite was loaded back into the furnace and a DTIA measurement made. The isotopic composition of atmospheric water vapour was measured directly by drawing lab air directly into the Picarro CRDS during the cleaning phase, and taking an average of the recorded isotopic composition.

The error in measurement at this stage was quite large, so the experiment was repeated a number times until an optimum weight of 16.6 mg was chosen, and time required for the rehydration to bassanite found (48 minutes). Finally, it was decided that the same gypsum sample could be used repeatedly – such that the bassanite dehydrated for the first measurement could be rehydrated back to bassanite for the second measurement. This was to eliminate any variation arising from changes in the sample mass or grain size. The bassanite-water vapour fractionation factor was converted to a bassanite-water fractionation factor by dividing the measured bassanite-water vapour fractionation factor by the water-water vapour fractionation factor.

3.3.3.2 Bassanite Precipitation Experiments

As the bassanite-water fractionation factor determined from the air rehydration experiments did not correspond to predicted theoretical fractionation factors for bassanite, I attempted to measure the bassanite-water fractionation factor directly by precipitating bassanite out of solution.

Our first approach for this was based on the work of Tritschler *et al.* (2015), who had precipitated bassanite in solution by using an alcohol to inhibit hydration and reduce the effective concentration of water. While alcohols are unsuitable for use when determining water fractionation factors (as there will be isotopic exchange between the alcohol hydroxyl and the water used), it is possible that other polar organic solvents can facilitate bassanite precipitation without isotopic exchange. I therefore tried the use of the solvent acetonitrile

(CH_3CN), a highly polar anoxic solvent. For these experiments, 9 ml of 50 mM solutions of both $CaCl_2$ and Na_2SO_4 were mixed, briefly shaken, then poured into 107 ml of acetonitrile. The resulting solid was collected, centrifuged, and dried in a 45 °C oven overnight. I also tried precipitation from ethanol, again using 9 ml of $CaCl_2$ and Na_2SO_4 solution (50 mM) and 120 ml ethanol, for comparison of bassanite purity between the two methods. The percentage bassanite in each case was determined by comparing the water per mg of sample to the measured water per mg gypsum (using New Gyp) and measured water per mg bassanite (from the air rehydration experiments). Removal of solvent before DTIA measurement was confirmed with IR spectroscopy.

One final attempt was made to precipitate bassanite using an older method described by Conley and Bundy (1958), where bassanite was precipitated at high temperatures. To do this, 0.5 M solutions of $CaCl_2$ and Na_2SO_4 were made up and heated in a heated block at 95 °C. The solutions were rapidly mixed after heating for 75 minutes in sealed tubes, and the precipitate was then filtered out (a fast process due to the high temperature of the water). The material was dried overnight in a 45 °C oven, then, after a DTIA measurement was carried out to determine the optimum amount of sample required, four measurements were made using 11.1 mg of precipitate.

3.4 Results

3.4.1 Investigating the Two-Step Dehydration

3.4.1.1 Partial Dehydration Experiments

I compare the results of DTIA measurements of all partial dehydration samples, both total isotopic composition and individual water peak isotopic composition, to the measured values for New Gyp, shown in Table 3.2. The dehydration profiles for these samples are shown together in Figure 3.2. The New Gyp standard and samples rehydrated in solution are found to have the highest amount of total water per mg mass of sample measured (between 7.4×10^5 and 7.6×10^5 ppm mg^{-1}), suggesting that these samples are fully hydrated gypsum samples, while the others are not. It is worth noting that, as expected, the total water isotopic composition has changed from New Gyp for all samples for both oxygen and hydrogen, and that, as a whole, the partial dehydration experiments show the majority of water being removed from the first peak of the dehydration – the gypsum → bassanite transition.

3.4.1.1.1 Partial Dehydration – in Furnace

The oxygen and hydrogen isotopic composition of the hydration water for these furnace dehydrated gypsum samples is lower than that of New Gyp for both peaks (Table 3.2). These partially dehydrated gypsum samples also show the lowest amount of water per mg sample, as expected from the larger initial weight loss of the sample. As a result of this lower amount of water, reliably reproducing the two peak dehydration was difficult, as the dehydration profile changes depending on the partial pressure of water in the system. Most samples show a sudden release of water at the start of dehydration, and dehydration of the second peak begins before the first peak has finished dehydrating. The typical profile for these samples is compared to the one measurement where peak separation was preserved in Figure 3.3.

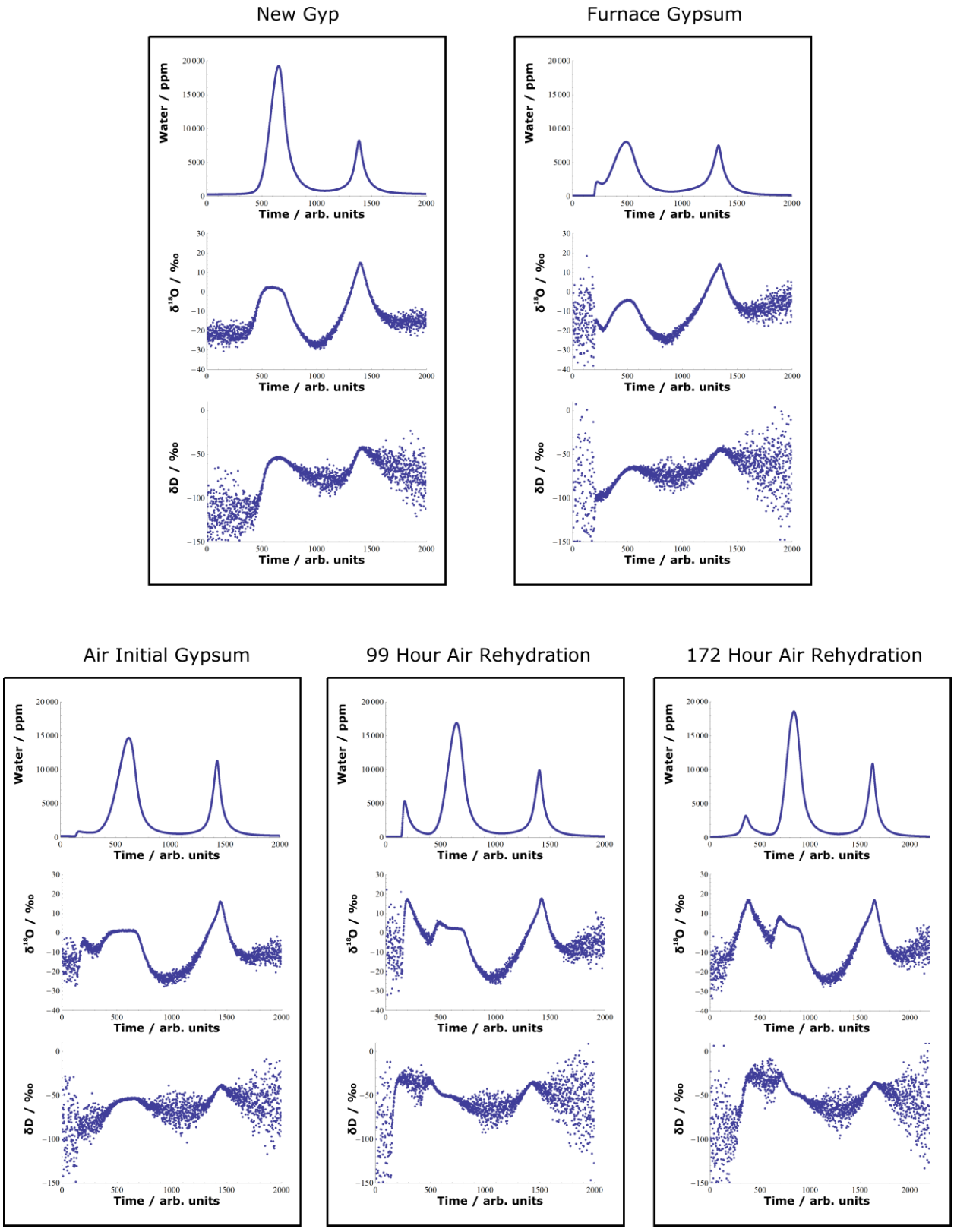

Figure 3.2 (a). The dehydration profiles for the partially dehydrated gypsum samples, showing that the water-rehydrated samples are consistent with the New Gyp sample. The partially dehydrated samples are also consistent, but the ratios of water amounts between the first and second peaks are smaller. The air-rehydrated samples show a slightly different dehydration profile, with an initial small third peak.

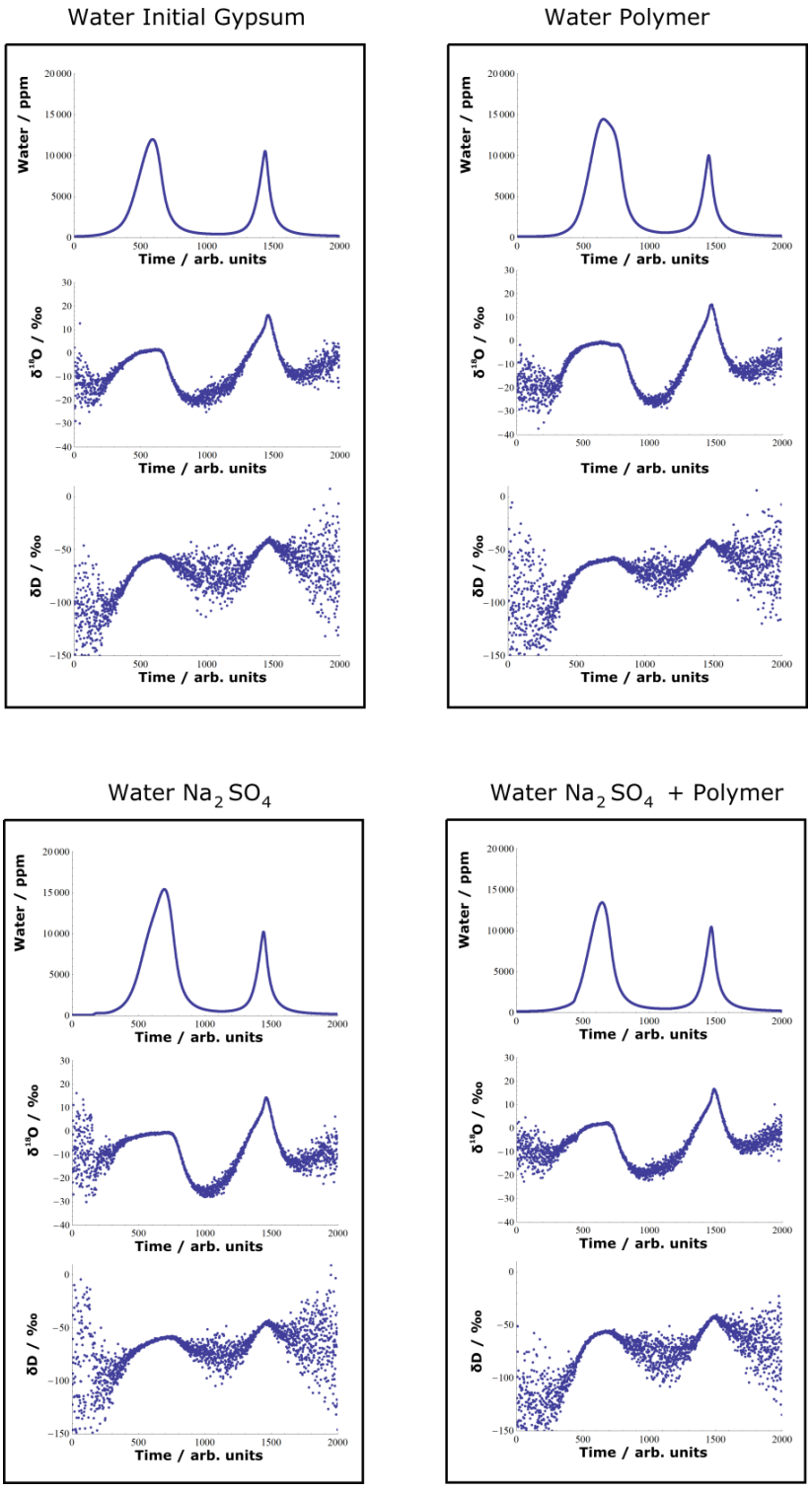

Figure 3.2 (b). Continuation of Figure 3.2 (a).

Sample Total Water	No. Repeats	Avg Mass / mg	H_2O per mg	H_2O	H_2O Error	δD / ‰	δD Error	$\delta^{18}O$ / ‰	$\delta^{18}O$ Error
New Gyp	2	6.82	7.43×10^5	5.07×10^6	2.90×10^5	–55.07	0.22	0.19	0.26
Furnace 120 Gypsum	1	7.25	5.17×10^5	3.75×10^6	-	–64.75	-	–4.72	-
Air Gypsum Initial	1	7.53	6.43×10^5	4.84×10^6	-	–53.53	-	0.56	-
Air Gypsum 99 Hour	2	7.51	7.05×10^5	5.29×10^6	2.10×10^5	–46.30	0.08	2.33	0.12
Air Gypsum 172 Hour	2	7.55	7.16×10^5	5.41×10^6	9.22×10^3	–44.17	0.19	2.55	0.16
Water Gypsum Initial	3	7.48	6.04×10^5	4.52×10^6	3.04×10^5	–56.58	0.21	0.99	0.30
Water Polymer	4	7.46	7.50×10^5	5.59×10^6	2.35×10^4	–58.66	0.97	–1.09	0.23
Water Na_2SO_4	4	7.47	7.47×10^5	5.58×10^6	1.85×10^4	–60.82	0.46	–1.33	0.11
Water Na_2SO_4 + Polymer	4	7.43	7.54×10^5	5.60×10^6	2.43×10^4	–60.37	1.04	–s1.42	0.14

Table 3.2 (a). Summary of total water results for gypsum partial dehydration experiments compared to measurements of the New Gyp sample without any partial dehydration. Considering the water per mg (ppm mg^{-1}) for each sample, only the initial New Gyp and the water-rehydrated samples can be fully hydrated gypsum.

Sample First Peak Water	No. Repeats	Avg Mass / mg	H_2O per mg	H_2O	H_2O Error	δD / ‰	δD Error	$\delta^{18}O$ / ‰	$\delta^{18}O$ Error
New Gyp	2	6.82	5.64×10^5	3.85×10^6	2.40×10^5	–57.35	0.28	–1.50	0.31
Furnace 120 Gypsum	1	7.25	3.17×10^5	2.30×10^6	-	–72.76	-	–9.37	-
Air Gypsum Initial	1	7.53	4.52×10^5	3.41×10^6	-	–56.67	-	–1.64	-
Air Gypsum 99 Hour	2	7.51	5.17×10^5	3.88×10^6	1.62×10^5	–47.46	0.06	1.02	0.05
Air Gypsum 172 Hour	2	7.55	5.21×10^5	3.94×10^6	4.03×10^3	–44.69	0.02	1.40	0.11
Water Gypsum Initial	3	7.48	4.10×10^5	3.06×10^6	3.22×10^5	–61.08	0.37	–1.60	0.39
Water Polymer	4	7.46	5.65×10^5	4.21×10^6	2.23×10^4	–61.64	1.19	–2.74	0.32
Water Na_2SO_4	4	7.47	5.60×10^5	4.19×10^6	1.27×10^4	–63.58	0.56	–2.96	0.13
Water Na_2SO_4 + Polymer	4	7.43	5.68×10^5	4.22×10^6	1.89×10^4	–63.13	1.19	–3.08	0.20

Table 3.2 (b). Summary of first peak water results for gypsum partial dehydration experiments compared to measurements of the New Gyp sample without any partial dehydration. This peak shows the largest difference in amount of water per mg (ppm mg^{-1}) of sample, and shows significant changes in the δD and $\delta^{18}O$ of the samples.

Sample Second Peak Water	No. Repeats	Avg Mass / mg	H_2O per mg	H_2O	H_2O Error	δD / ‰	δD Error	$\delta^{18}O$ / ‰	$\delta^{18}O$ Error
New Gyp	2	6.82	1.79×10^5	1.22×10^6	5.22×10^4	–47.82	0.14	5.54	0.03
Furnace 120 Gypsum	1	7.25	2.00×10^5	1.45×10^6	-	–52.04	-	2.66	-
Air Gypsum Initial	1	7.53	1.91×10^5	1.44×10^6	-	–46.10	-	5.76	-
Air Gypsum 99 Hour	2	7.51	1.88×10^5	1.41×10^6	4.76×10^4	–43.12	0.10	5.94	0.26
Air Gypsum 172 Hour	2	7.55	1.95×10^5	1.47×10^6	1.33×10^4	–42.80	0.63	5.60	0.28
Water Gypsum Initial	3	7.48	1.95×10^5	1.46×10^6	1.86×10^4	–47.65	0.62	6.12	0.32
Water Polymer	4	7.46	1.84×10^5	1.38×10^6	4.74×10^3	–49.55	0.37	3.95	0.08
Water Na_2SO_4	4	7.47	1.87×10^5	1.40×10^6	6.30×10^3	–52.55	0.22	3.55	0.09
Water Na_2SO_4 + Polymer	4	7.43	1.86×10^5	1.39×10^6	6.11×10^3	–51.95	0.61	3.62	0.07

Table 3.2 (c). Summary of second peak water results for gypsum partial dehydration experiments compared to measurements of the New Gyp sample without any partial dehydration. The amount of water per mg (ppm mg^{-1}) for each sample is very similar when comparing only the second peaks. Despite this, there are significant changes in the second peak isotopic composition upon rehydration.

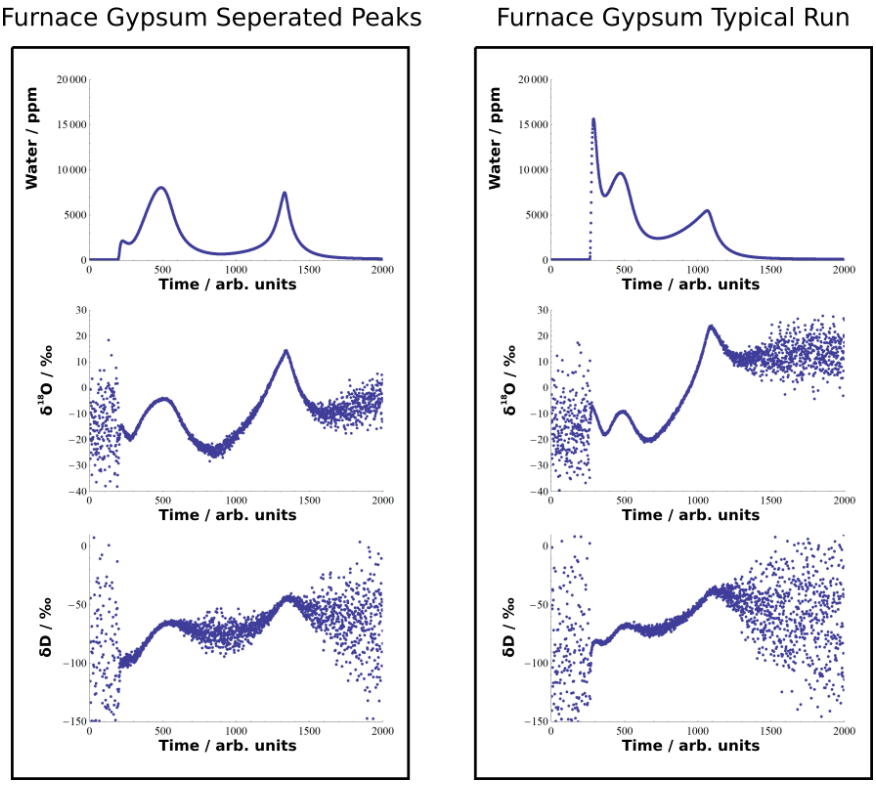

Figure 3.3. Comparison of the two dehydration profile types seen when measuring the furnace dehydrated gypsum. While both show a sudden jump in the water partial pressure, the size of the jump is very different, and in the typical runs seems to cause the dehydration peaks to coalesce.

3.4.1.1.2 Partial Dehydration – Rehydration in Air

The water amounts per mg sample (Table 3.2) show that these samples did not fully rehydrate to gypsum, but comparison between the initial gypsum (measured directly after the initial hydration) to the gypsum left under a hydrous nitrogen flow show that some water has been absorbed by the sample. This rehydration appears to have occurred mostly within the first 99 hours – after this point, sample water content does not significantly increase (at 99 hours, sample has 94.8 % of the water amount that New Gyp has, and at 172 hours, sample has 96.4 % of the water amount that New Gyp has), and there is only a small further change in the measured δD and $\delta^{18}O$ values. Moreover, the water regained by the sample is removed before the bassanite → anhydrite dehydration – the second peak contains the same amount of water per mg sample for both the initial and rehydrated gypsums. Rather, the water absorbed by the sample appears to dehydrate first, almost entirely contained within a third small

dehydration peak which is removed at a lower temperature (Table 3.3). Interestingly, the isotopic composition of the hydration water of the gypsum still appears to have been changed even when this secondary peak is excluded, and though the magnitude of the isotopic change is smaller for oxygen when the secondary peak is excluded, the isotopic change is almost the same size for deuterium regardless of whether the secondary peak is included (Table 3.3).

Compared to New Gyp, the gypsum samples rehydrated in air show isotopic enrichment, due to the use of enriched water in the hydrous nitrogen flow. Significant isotopic enrichment is seen in both peaks. The implied sample-vapour fractionation factors for this rehydration are shown in Table 3.4 (found by using the difference in water content and isotopic composition between the initial gypsum and the 99 and 172 hour gypsums, assuming that none of the water present in the initial gypsum has exchanged), as are the calculated sample-liquid water fractionation factors (calculated following Méheut *et al*., 2007, using experimental fractionation factors for oxygen (e.g. Majoube, 1971, Barkan and Luz, 2005) and hydrogen (Mook, 2001) for water evaporation; the isotopic composition of the water vapour was found to be –19.75 ‰ and 13.41 ‰ for δD and $\delta^{18}O$ respectively).

3.4.1.1.3 Partial Dehydration – Rehydration in Water

Here the samples contain as much water as New Gyp which has not been at all dehydrated (Table 3.2), suggesting that these samples have fully rehydrated to gypsum. Rehydration appears to primarily have affected the first peak, which shows a large increase in water between the partially dehydrated state and the rehydrated state. All three rehydrated samples show a change in the isotopic composition of both dehydration peaks, though the solutions containing Na_2SO_4 show a larger depletion. The initial partially dehydrated gypsum also shows a slight enrichment relative to the initial New Gyp isotopic composition; this is consistent with lighter isotopes being removed earlier during dehydration. The implied fractionation factors for these rehydrations are shown in Table 3.4 (found by using the difference in water content and isotopic composition between the initial gypsum and fully hydrated gypsum, assuming that none of the water present in the initial gypsum has exchanged; the isotopic composition of the water was found to be –48.86 ‰ and –7.76 ‰ for δD and $\delta^{18}O$ respectively).

Water Portion	Sample	H_2O Amount	H_2O per mg	δD / ‰	δD Error	$\delta^{18}O$ / ‰	$\delta^{18}O$ Error
Total Water	New Gypsum	5.07×10^6	7.43×10^5	–55.07	0.22	0.19	0.26
	Air Gypsum Initial	4.84×10^6	6.43×10^5	–53.53	-	0.56	-
	Air Gypsum 99 Hour	5.29×10^6	7.05×10^5	–46.30	0.08	2.33	0.12
	Air Gypsum 99 Hour Excl. 2° Peak	4.84×10^6	6.45×10^5	–47.12	0.12	1.61	0.13
	Air Gypsum 172 Hour	5.41×10^6	7.16×10^5	–44.17	0.19	2.55	0.16
	Air Gypsum 172 Hour Excl. 2° Peak	5.09×10^6	6.74×10^5	–44.42	0.64	2.12	0.20
First Peak	New Gypsum	3.85×10^6	5.64×10^5	–57.35	0.28	–1.50	0.31
	Air Gypsum Initial	3.41×10^6	4.52×10^5	–56.67	-	–1.64	-
	Air Gypsum 99 Hour	3.88×10^6	5.17×10^5	–47.46	0.06	1.02	0.05
	Air Gypsum 99 Hour Excl. 2° Peak	3.43×10^6	4.57×10^5	–48.76	0.12	–0.16	0.07
	Air Gypsum 172 Hour	3.94×10^6	5.21×10^5	–44.69	0.02	1.40	0.11
	Air Gypsum 172 Hour Excl. 2° Peak	3.62×10^6	4.79×10^5	–45.10	1.19	0.69	0.46
Second Peak	New Gypsum	1.22×10^6	1.79×10^5	–47.82	0.14	5.54	0.03
	Air Gypsum Initial	1.44×10^6	1.91×10^5	–46.10	-	5.76	-
	Air Gypsum 99 Hour	1.41×10^6	1.88×10^5	–43.12	0.10	5.94	0.26
	Air Gypsum 172 Hour	1.47×10^6	1.95×10^5	–42.80	0.63	5.60	0.28

Table 3.3. Summary of the air rehydration results, offering a closer examination of the implications of the small third peak seen in these samples. Results for the measured total water and first peak water are compared to the isotopic composition and water amount values found when excluding the secondary dehydration peak seen at lower temperatures in the dehydration. Although the secondary peak seems to contain most of the water regained by the sample, its effect on the isotopic composition is less pronounced. The second dehydration peak is unaffected by the presence of the secondary small dehydration peak, so no comparison is shown.

Sample Fractionation Factor	**αD**	**$\alpha^{18}O$**
Water Vapour – Liquid Water	1.0936	1.0117
Air 99 Hours (Measured)	1.0410	1.0150
Air 172 Hours (Measured)	1.0590	1.0130
Air 99 Hours (Calculated)	0.9515	1.0029
Air 172 Hours (Calculated)	0.9687	1.0008
Polymer	0.9812	0.9986
Na_2SO_4	0.9706	0.9975
Na_2SO_4 + Polymer	0.9763	0.9971
Gypsum - Water (Theoretical)	0.9809	1.0035
Bassanite - Water (Theoretical)	0.9667	1.0035

Table 3.4. Fractionation factors for the rehydration of partially dehydrated gypsum. The calculated air fractionation factors are found by combining the measured fractionation factors for the rehydration from water vapour with the water vapour – liquid water fractionation factors from the literature (Majoube, 1971; Barkan and Luz, 2005; Mook, 2001).

The change in hydration state is considered in more detail in Table 3.5. In particular, the amount of water each gypsum sample contains is found by comparing the water per mg of the total dehydration water to that of New Gyp. This is used to calculate the mass of $CaSO_4$ present in each sample according to the following equation:

$$mass_{CaSO_4} = mass_{sample} \times \frac{Mr_{CaSO_4}}{Mr_{CaSO_4.xH_2O}}$$

Where Mr represents the molecular mass and x is the water fraction determined from the comparison of water per mg between the sample and New Gyp. The expected second peak water per mg for the rehydrated samples can then be determined by scaling the initial gypsum's second peak water by the ratio of initial and rehydrated sample masses:

$$expected\ water_{rehyd\ sample} = expected\ water_{inital\ gysum} \times \frac{mass_{inital\ gysum}}{mass_{rehyd\ sample}}$$

The expected water amounts agree with the measured water amounts.

	New Gypsum	Water Gypsum Initial	Water Polymer	Water Na_2SO_4	Water Na_2SO_4 + Polymer
Avg Mass / mg	6.82	7.48	7.46	7.47	7.43
Total H_2O per mg x10^5	7.43	6.04	7.50	7.47	7.54
Percentage Hydration w.r.t. New Gyp	100	81	101	101	101
Molecular Mass of H_2O in Sample	36.03	29.29	36.33	36.22	36.54
Molecular Mass of Hydrated $CaSO_4$	172.17	165.43	172.47	172.36	172.68
Mass of $CaSO_4$ in sample / mg	5.39	6.15	5.89	5.90	5.86
Expected Second Peak H_2O per mg x10^5	-	-	1.86	1.87	1.85
Measured Second Peak H_2O per mg x10^5	1.79	1.95	1.84	1.87	1.86

Table 3.5. Data for calculating the expected water amounts in the second dehydration peak of the water rehydrated gypsums, assuming that the initial gypsum is comprised entirely of partially dehydrated gypsum which dehydrates via the bassanite phase in its second dehydration peak. The measured and expected water amounts agree.

3.4.1.2 Grain Size Experiments

I compare the DTIA profiles from the three grain sizes in Figure 3.4. For the lower grain sizes (<64 μm and ≈100 μm), there are two peaks in the isotope signals, despite the dehydration water seeming to emit in a single peaked dehydration. At larger grain sizes (>500 μm) gypsum shows little change in the hydrogen or oxygen isotopes across the dehydration and the $\delta^{18}O$ and δD values remain reasonably constant at. –3.34 ‰ and –64.9 ‰, respectively, with a slight shoulder after the water peak maximum. Smaller grain sizes were found to begin dehydration at lower temperatures, consistent with previous results (Khalil, 1982).

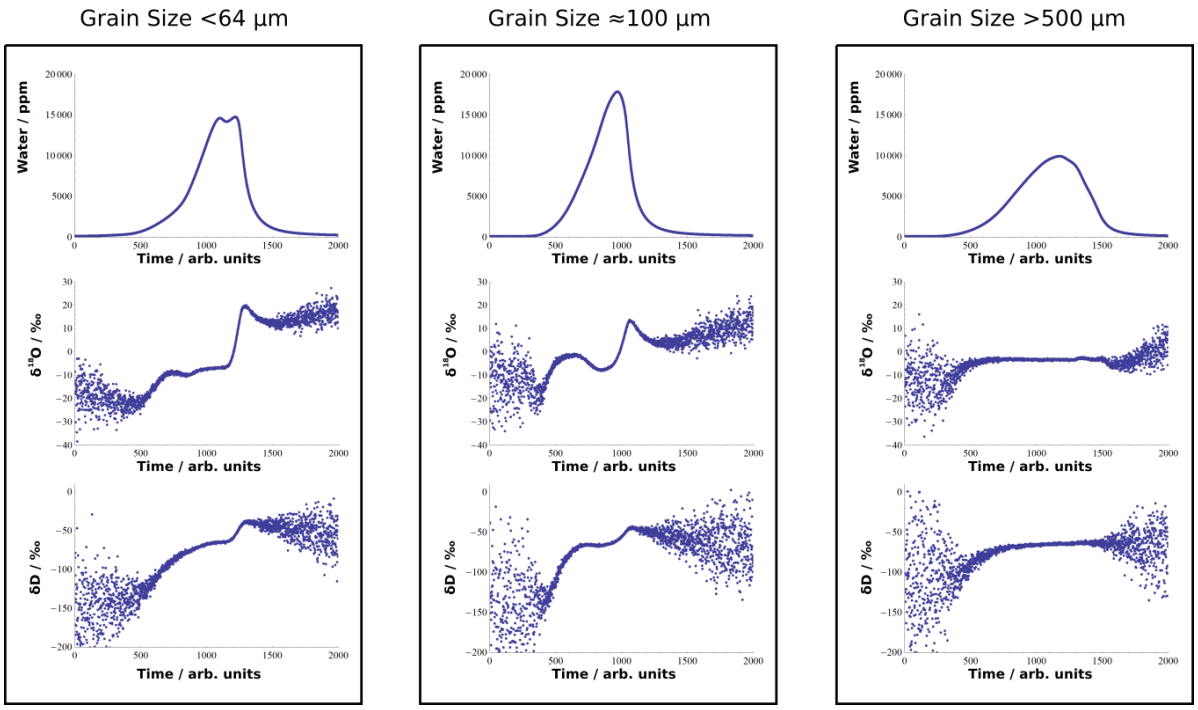

Figure 3.4. Comparison of the dehydration profiles of gypsum at different grain sizes. The gypsum-bassanite peak separation does not occur because these samples were measured in unsealed crucibles under a nitrogen atmosphere. As the grain size decreases, however, the dehydration becomes more like that of the two-step gypsum → bassanite → anhydrite dehydration.

3.4.1.3 FTIR Experiments

The IR spectra for gypsum, gypsum dehydrated to bassanite (by stopping heating after the first peak of the two peak dehydration) and gypsum heated to 250 °C and 350 °C are shown in Figure 3.5. The IR spectrum of gypsum heated to 250 °C, which is past the end temperature of the two peak dehydration, is the same as that of bassanite, with water peaks present at 3606, 2555 and 1616 cm^{-1}, as reported in Mandal and Mandal (2001). Once the gypsum is heated to 350 °C, these water peaks no longer occur in the IR, indicating anhydrite II (β-anhydrite) formation.

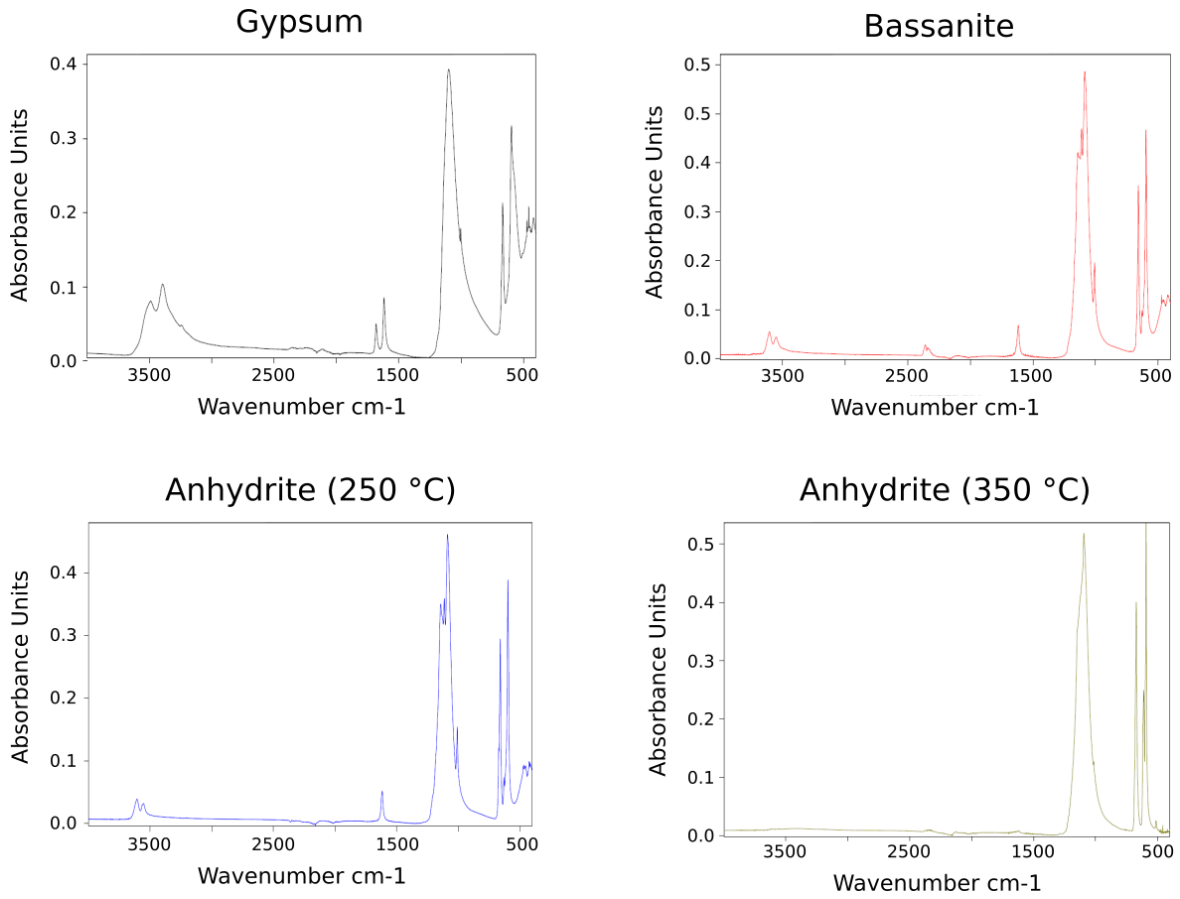

Figure 3.5. Comparison of the FTIR of gypsum, bassanite, and "anhydrite" formed by heating gypsum to two different temperatures. The peaks of interest are found in the 3300-3600 and 1550-1650 cm^{-1} regions of the spectra – corresponding to O-H stretches and H_2O bends respectively. These are, as expected, seen both in gypsum and bassanite, and are larger in gypsum, which has a higher water content. They are not seen in the anhydrite heated to 350 °C, as expected. However, they are seen in the "anhydrite" formed by heating gypsum to 250 °C.

3.4.2 Measuring Bassanite-Water Isotopic Fractionation

3.4.2.1 Anhydrite-Bassanite Rehydration Experiments

The TG data for a set of anhydrite-bassanite rehydration experiments is shown in Figure 3.6. After gypsum is dehydrated to anhydrite III (γ-anhydrite), the newly formed anhydrite readily rehydrates to bassanite under even modest partial pressures of water (water concentration of ≈ 12000 ppm). The TG data for the dehydration runs have some error due to increased buoyancy at higher temperatures – expressed as an initial increase in mass loss before dehydration. The measured bassanite-water vapour fractionation factors (^{18}O and D) and calculated bassanite-water fractionation factors are shown in Table 3.6 (calculated following Méheut *et al.*, 2007), alongside the experimental oxygen (e.g. Majoube, 1971, Barkan and Luz, 2005) and hydrogen fractionation factors (Mook, 2001) for water evaporation. Both oxygen and hydrogen fractionation factors for bassanite-water are much lower than expected compared to theoretical predictions, and much lower than those for gypsum.

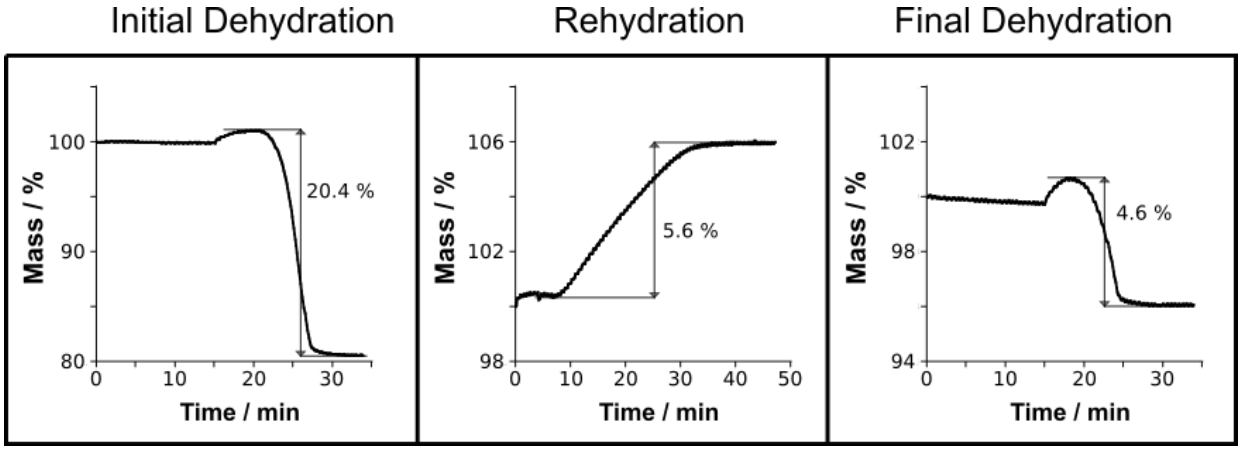

Figure 3.6. Series of TG measurements showing the reabsorption of water by anhydrite III after dehydration. The percentage changes labelled on the TG profiles have been scaled to the weight of the original gypsum sample, though some inaccuracy remains in the final mass changes due to increased gas pressure in the TG furnace upon heating.

Fractionation Factor	αD	αD Error	$\alpha^{18}O$	$\alpha^{18}O$ Error
Water Vapour - Water	1.0936	-	1.0117	-
Bassanite - Water Vapour (Measured)	1.0518	0.0011	1.0042	0.0003
Bassanite - Water (Calculated)	0.9618	0.0010	0.9926	0.0003
Bassanite - Water (Theoretical)	0.9667	-	1.0035	-

Table 3.6. Summary of the fractionation factors measured for the anhydrite → bassanite hydration, when rehydration occurred through water vapour, compared to the theoretical bassanite-water fractionation factors found by DFT (Liu *et al.*, 2018).

3.4.2.2 Bassanite Precipitation Experiments

The fractionation factors for oxygen and hydrogen of the bassanite-water system are reported in Table 3.7, alongside the predicted percentage bassanite (assuming the sample is made up of $CaSO_4 \cdot 2H_2O$ and $CaSO_4 \cdot 0.5H_2O$, though bassanite can take a range of hydration values). Considering the bassanite samples precipitated at room temperature, the measured oxygen fractionation appears similar for both precipitation in ethanol and precipitation in acetonitrile, despite the fact that the percentage bassanite is very different when comparing ethanol precipitation (>70 % bassanite) to acetonitrile precipitation (<20 % bassanite). Because of potential isotope exchange between ethanol and water, the measured bassanite-water fractionation factors may not be accurate for ethanol-precipitated bassanite. Agreement with the theoretical value is poor for both low temperature and high temperature precipitation experiments, and for the previous anhydrite rehydration experiments.

Fractionation Factor	**% Bassanite (By Water)**	**αD**	**αD Error**	**$\alpha^{18}O$**	**$\alpha^{18}O$ Error**
Water Vapour	-	1.0936	-	1.0117	-
Ethanol Precipitation	74.7	0.9710	0.0010	1.0160	0.0001
Acetonitrile Precipitation	16.1	1.0085	0.0003	1.0136	0.00003
High Temperature Precipitation	65.2	1.0029	0.0009	1.0076	0.0001
Gypsum - Water (Theoretical - 30 °C)	-	0.9809	-	1.0035	-
Bassanite - Water (Theoretical - 30 °C)	-	0.9667	-	1.0035	-

Table 3.7. Summary of the fractionation factors measured for the anhydrite → bassanite hydration, when attempting to directly precipitate bassanite, compared to the theoretical bassanite-water fractionation factors found by DFT (Liu *et al.*, 2018).

3.5 Discussion

3.5.1 Investigating the Two-Step Dehydration

While the mechanisms and structural changes of gypsum during dehydration have been studied by many authors (e.g. Ball and Norwood, 1969; Paulik *et al.*, 1992; Lou *et al.*, 2011), the relationship between the two-step dehydration and the isotopic composition of the hydration water has not been examined previously. The implications of the two-step dehydration are discussed with respect to individual experiments below.

3.5.1.1 Partial Dehydration Experiments

Considering the results from the partial dehydration experiments as a whole, the isotopic composition of the water removed in the bassanite dehydration peak is altered by even small amounts (as little as 7.3 %) of rehydration of the sample. This holds true even when the amount of water in the bassanite dehydration peak is unchanged by rehydration. As such, we can infer that it is not possible to draw further information about gypsum formation environments from the second dehydration peak. This finding also weakly contradicts the "anion water" theory proposed in Mandal and Mandal (2012); if a set of more strongly bonded water was responsible for the two-step dehydration, we would expect to be able to distinguish this water isotopically from the more weakly bonded water. Rather, my results are more consistent with previous x-ray diffraction (XRD) and neutron diffraction measurements of the gypsum structure (e.g. Atoji and Rundle, 1958; Cole and Lancucki, 1974; Pedersen and Semmingsen, 1982), which generally report that the gypsum water sits in identical positions within the structure.

It is still interesting that, isotopically, the two dehydration steps are distinct, with the second step always being isotopically enriched relative to the first. This could be due to simple kinetics, whereby the isotopically heavier water takes more energy to be removed from the gypsum structure, or due to minor differences in bond strength between heavier water and the $CaSO_4$ structure.

The individual partial dehydration experiments are discussed in more detail below.

3.5.1.1.1 Partial Dehydration – in Furnace

For the heavily dehydrated gypsum (53 % water removed), the isotopic composition of the remaining water appears lighter than for undehydrated New Gyp. This is unexpected, as during DTIA measurements of gypsum, not only is the first water peak always isotopically lighter than the second, but also lighter isotopes are removed first from each peak. The answer likely lies in the amount of water recorded for the sample; while a 53 % water loss was measured from the decrease in mass, the sample still had 70 % of the water per mg as New Gyp. This indicates significant amounts of rehydration under atmosphere between the measurement of mass loss and the DTIA measurement. It is unclear which phase of calcium sulphate (gypsum, bassanite, or γ-anhydrite) is responsible for the atmospheric water absorption. Detecting this using IR would be difficult, not only because γ-anhydrite absorptions would be coincident with those of bassanite and gypsum in a mixture, but also because γ-anhydrite is likely to rehydrate before such a measurement can be made. This means that it is very difficult to tell from these experiments whether partial dehydration of gypsum affects the isotopic composition of the bassanite → anhydrite peak.

It is likely that the difficulty in recording a separated two peak dehydration is due to this water absorption. The DTIA profiles all show a sudden release of water from the sample – combined with DSC and TG data, water appears to have been driven out of the structure in a secondary peak before the first dehydration peak, but in too small an amount to break the seal of the aluminium crucible. Because the pressure inside the crucible was now higher, when the larger first peak dehydration started, the crucible seal broke suddenly, releasing enough water to change the dehydration pathway. Comparing the temperature at which the small secondary dehydration peak is seen to later results dehydrating bassanite, where bassanite began dehydration at a lower temperature than gypsum, it seems likely that the secondary peak is due to the γ-anhydrite → bassanite reaction under air.

3.5.1.1.2 Partial Dehydration – Rehydration in Air

As in the previous partial dehydration experiment, determining what phases of calcium sulphate formed during the initial dehydration, and which phases were subsequently rehydrated, is critical to understanding the results of the rehydration in air experiments. If

bassanite and gypsum are the major reaction products of partial dehydration, then the change in isotopic composition of the second peak hydration water on rehydration must mean that there is no separate bassanite pool of water. If, on the other hand, γ-anhydrite and gypsum are the major products of partial sample dehydration, then the changing isotopic composition of the bassanite dehydration peak would be explained by loss of water from this peak during the initial dehydration, which is replaced with water of different isotopic composition on rehydration.

We should be able to identify these two cases from the amount of water measured in the second peak. If significant amounts of γ-anhydrite are being formed during the initial dehydration, and later rehydrated to bassanite, the amount of water in the second peak should increase during rehydration. We do not see an increase in second peak water amount in our results – therefore, rehydration of γ-anhydrite to bassanite cannot be responsible for the isotopic change of the second peak. We can also discount rehydration of bassanite to gypsum – other studies (e.g. Vaniman *et al.*, 2009; Harrison, 2012) have found that bassanite is relatively inert to rehydration, occurring on a timescale of thousands of hours. Therefore, the most likely scenario is that we are dehydrating gypsum partially, resulting in variably hydrated gypsum (e.g. $CaSO_4 \cdot 1.5H_2O$, or other fractions of water) which slowly rehydrates towards $CaSO_4 \cdot 2H_2O$.

It is also possible that we are seeing some rehydration of γ-anhydrite to bassanite, but that this bassanite is then dehydrated at a lower temperature, explaining the small secondary peak seen at the start of dehydration. This would be consistent with the later bassanite dehydration measurements, where pure bassanite samples are found to begin dehydrate at lower temperatures than gypsum samples. This would still lead to the conclusion that there is no separate bassanite water pool which is more strongly bonded; and the measured fractionation factors for deuterium are more consistent with the predicted bassanite fractionation factors. However, this rehydration occurs very rapidly, completing within an hour even at partial pressures of water lower than atmospheric water partial pressure, so in this case, it is not clear why the secondary peak would continue to increase in size between the 99 hour and 172 hour measurements. We also cannot assume that the isotopic fractionation for hydration of partially dehydrated gypsum is the same as for hydration of anhydrite. The secondary peak could also therefore be the result of water absorbed on the surface of the gypsum, or the result

of a slight structural change of the gypsum on heating (e.g. sintering of grains (Paulik *et al.*, 1992)).

3.5.1.1.3 Partial Dehydration – Rehydration in Water

In the previous set of partial dehydration experiments, it was not possible to fully establish which phases of calcium sulphate formed during partial dehydration. Some confusion remained as to whether the experiments observed rehydration of γ-anhydrite, partially dehydrated gypsum, or of bassanite – though bassanite rehydration was established as unlikely. Carrying out similar experiments, but rehydrating the partially dehydrated sample under water, allows us to examine the effects of partial dehydration more closely.

Unlike in the rehydration under air experiments, we can be certain that by rehydrating the sample under water, the final samples will be fully hydrated gypsum. As such, if any gypsum was converted to bassanite or γ-anhydrite during the initial partial dehydration, we would observe an increase in the amount of water per mg in the second peak after rehydration. We do not see an increase in the amount of second peak water, even when correcting the water per mg of sample by the fact that the rehydrated samples will have a smaller amount of $CaSO_4$ per unit mass, because they contain more water overall. Our values for the predicted amount of water in the second peak, assuming that the initial sample is fully hydrated with respect to the bassanite dehydration peak, fall within 1 % of the measured amounts of water. This suggests that very little gypsum has changed phase to bassanite or γ-anhydrite during partial rehydration; and therefore that there is no pool of more strongly bound water in bassanite.

There are two further points of interest from the data. The first is that the presence of polyacrylic acid, a polymer used to inhibit gypsum reprecipitation (Amjad, 1988), does not affect the isotopic composition of the rehydration water, suggesting that reprecipitation is not a factor here. The second is that Na_2SO_4 does affect the isotopic composition of the rehydration water. Na_2SO_4 is thought to act as an activator for γ-anhydrite rehydration (Conley and Bundy, 1958). It is therefore possible that Na_2SO_4 also acts as an activator for rehydration of partially dehydrated gypsum, or that Na_2SO_4 acts as an activator for gypsum

reprecipitation, but this would require further experimentation to verify and falls outside of the scope of this study.

3.5.1.2 Grain Size Experiments

The three DTIA profiles for different grain sizes of gypsum clearly demonstrate that the dehydration is grain size-dependent. The isotopic profiles suggest that for both the <64 μm and ≈100 μm samples, the gypsum dehydrates via bassanite, even though no second dehydration peak is seen for the ≈100 μm sample, and even the <64 μm shows very little peak separation for the dehydration. By contrast, the isotope dehydration profile of the larger single crystal (>500 μm) does not go through distinct gypsum → bassanite → γ-anhydrite phases. The fact that the isotope profile is flat suggests that the various component calcium sulphate structures are all dehydrating at a constant rate (i.e. the amount of $CaSO_4 \cdot 2H_2O$, $CaSO_4 \cdot 0.5H_2O$, and calcium sulphate with every amount of water in between dehydrating at any one time is constant once dehydration starts until the end of dehydration). This implies that there is an interface between calcium sulphate phases, that moves through the crystal as more of the crystal is dehydrated.

To verify this, measurements were taken by Nick Evans and Gernot Nehrke (unpublished) using *in situ* Raman spectroscopy on similar grain sizes of gypsum heated under the same conditions (unsealed crucible, 5 K / min heating ramp). The presence of gypsum, bassanite and γ-anhydrite can be found from shifts in the position of the sulphate ν_2 stretch, which appears at around 1008 cm^{-1} for gypsum, 1015 cm^{-1} for bassanite and 1025 cm^{-1} for γ-anhydrite. These experiments found that the presence of bassanite could be measured for the <64 μm and ≈100 μm samples (similar to the results from Fusseis *et al.*, 2012, where X-ray micro-tomography was used to identify a moving dehydration front for a gypsum of grain size 120 μm), but not for the >500 μm sample, which seemed to transition from gypsum directly to anhydrite. The bassanite phase may be too transient to measure by Raman spectroscopy, as Raman spectroscopy has limited sample penetrativity.

3.5.1.3 FTIR Experiments

The results here clearly indicate that the γ-anhydrite structure changes back to bassanite very quickly under air (within 5 minutes), though does not necessarily achieve full bassanite hydration during this time. Equally, combined with the TG / water data from these runs, it is clear that anion water (Mandal and Mandal, 2001) is not the cause of water peaks being present in the IR measurements of gypsum heated to 250 °C, as no water is released by the gypsum between 220 °C and 350 °C.

Other studies have found that γ-anhydrite displays this rehydration behaviour (e.g. Vaniman *et al.*, 2009; Harrison, 2012), so these results are not ground breaking, but rather were very important to forming other ideas for experiments and explaining previous data in this thesis.

3.5.2 Measuring Bassanite-Water Isotopic Fractionation

While the previous partial dehydration experiments suggest that the second peak dehydration water is not an important palaeoproxy, as the bassanite water does not exist in a distinct less exchangeable form than the gypsum hydration water, bassanite is still important as a proxy. Bassanite's natural occurrence on Earth is rare, typically limited to arid environments, due to the fact that bassanite is metastable under non-arid conditions. However, bassanite has been detected on Mars (e.g. Wray *et al.*, 2010; Rapin *et al.*, 2016), so knowing how water fractionates when entering the bassanite structure is important.

Unfortunately, it proved very difficult to precipitate bassanite samples of high enough purity for accurate fractionation factor measurement. The most reliable method in the literature for precipitating bassanite involves the use of large amounts of ethanol (Tritschler *et al.*, 2015); however, I was unable to reproduce the high (> 90 %) purity of this study. Moreover, ethanol precipitation isn't suitable for fractionation factor measurements, as the hydrogen of the alcohol will exchange with the hydrogen of the water required for anhydrite rehydration. The research of Tritschler *et al.* (2015) also suggested that bassanite precipitation purity was correlated with the polarity of the non-water solvent used (where more polar alcohols, such as ethanol, gave higher bassanite yields than less polar alcohols, such as iso-propanol). As such, I repeated the bassanite precipitation experiments using acetonitrile, a highly polar organic

solvent which does not contain exchangeable hydrogen. The dielectric constant (a measure of solvent polarity) of acetonitrile is 37.5 – which, using the predicted trend of bassanite purity against solvent dielectric constant presented in Tritschler *et al.* (2015), would predict a bassanite purity of 100 %. The measured bassanite purity using acetonitrile was only 16 %.

The high temperature precipitation experiments similarly did not produce as high a purity of bassanite as required for accurate bassanite-water fractionation factor experiments. These experiments were, however, reasonably reproducible, despite the limitations of the experimental setup (where bassanite was made in multiple test tubes, due to the size limits of the heated block, and the final temperature of the water at time of mixing is unknown). One difficulty of using high temperature experiments for fractionation factor determination is that the high temperatures will lead to evaporation of water, changing the water isotopic composition. A more specialised experimental setup could heat much larger amounts of water, monitoring the temperature of the water directly, such that the effect of bassanite precipitation on the water isotopic composition could be considered negligible, and then the isotopic composition of the water could be measured after heating and precipitation (keeping the water sealed to atmosphere to avoid further evaporation). However, this method for obtaining bassanite reflects natural formation conditions of bassanite least well, and further modelling work would be required to link bassanite fractionation at high temperatures to the expected fractionation at lower temperatures representative of arid terrestrial climates (and potentially Martian climates).

A further confounding factor for experimental measurement is that the bassanite structure of calcium sulphate can contain variable amounts of water (e.g. Bezou *et al.*, 1995; Vaniman *et al.*, 2009; Harrison, 2012); this makes it unclear whether measuring the amount of water present in a bassanite sample is an appropriate method for calculating the purity of bassanite in a sample, as it may underestimate bassanite purity if bassanite is more hydrated than expected, or whether a method that measures the structure, such as XRD or IR spectroscopy, where water amounts may not match those of natural bassanites, would be more appropriate. Bassanites of different hydration states may even fractionate oxygen and hydrogen isotopes differently upon hydration, further decreasing the clarity of experimental measurement.

In contrast to the bassanite precipitation experiments, rehydration of γ-anhydrite to bassanite under hydrous atmospheres reliably produced high purity bassanite. This is consistent with the fact that these conditions more closely represent the conditions under which terrestrial bassanite might form. However, the measured bassanite-water vapour fractionation factors do not agree with the predicted bassanite-water fraction factors found in Liu *et al.* (2018), especially for oxygen – where the measured bassanite-water vapour fraction factor actually matches closely to the predicted bassanite-water fractionation factor. Given that the oxygen fractionation factor measurement is more likely to be accurate in this case, due to issues with bassanite sample size, it is possible that the equilibrium fractionation factors for water condensation are not appropriate for use in bassanite rehydration from atmospheric water. It is unclear if a more controlled experiment could remove the observed kinetic effects, or drive the condensation to be entirely kinetically driven, such that the condensation fractionation factors could be considered as equal to one. However, this bassanite formation method appears the most likely to yield accurate bassanite fractionation factors which can be compared to the theoretical fractionation factors found in Liu *et al.* (2018). As such, further experiments using more bassanite, and a more tightly controlled water atmosphere, are warranted to verify the accuracy of the theoretical calculations of bassanite-water isotopic fraction.

The individual bassanite fractionation factor experiments are discussed in more detail below.

3.5.2.1 Anhydrite-Bassanite Rehydration Experiments

Comparison of the theoretical bassanite-water fractionation factors (Liu *et al.*, 2018) to the calculated bassanite-water fractionation factors (i.e. calculated from the bassanite-water vapour) finds the calculated bassanite-water fractionation factors to be very low for both isotopes. Some of this deviation may be due to the use of a sample which released insufficient water upon heating; for these measurements, only ≈0.8 μl of water was measured. Comparing this to results for low water concentrations from Bauska *et al.* (Bauska *et al.*, 2017), we would therefore expect deuterium results to be somewhat depleted. However, oxygen $\delta^{18}O$ measurements are only weakly affected by low water amounts, deviating by up to 1 ‰ from accurate measurements, which does not change the measured fractionation factor significantly.

Why then are the measured fractionation factors so low – and in particular, why is the measured bassanite-water vapour fractionation factor so similar to the theoretical value for the bassanite-water fractionation factor? The most likely explanation is that we are seeing significant kinetic effects in the measured fractionation. Given that kinetic effects drive the fractionation factors towards 1 (i.e. less fractionation occurs), and that the theoretical gypsum and bassanite fractionation factors are much closer to 1 than those calculated from bassanite-water vapour fractionation, these kinetic effects must be occurring upon condensation. The thermodynamic water-water vapour fractionation factors ($\alpha^{18}O = 1.0117$, $\alpha D = 1.0936$, taken from Majoube (1971) and Mook (2001) respectively) are very high, making the calculated bassanite-water fractionation factors very low. If condensation were primarily a kinetic process, then the water condensing around the bassanite would be predicted to be isotopically lighter, and hence the bassanite fractionation factors would become higher. This equally applies to the results from the vapour rehydration of the partially dehydrated gypsum – the fractionation factors are much lower than would be expected for gypsum or bassanite, particularly for the hydrogen fractionation.

The question becomes whether these kinetic effects can be controlled, or taken into account. If we can reduce the significance of the kinetic effects, or drive the condensation to be entirely kinetically driven by using a more/less hydrous atmosphere for the rehydration, then further γ-anhydrite rehydration experiments could be used to determine the bassanite-water oxygen and hydrogen fractionation factors experimentally.

3.5.2.2 Bassanite Precipitation Experiments

Comparing the bassanite-water oxygen fractionation factors from the ethanol and acetonitrile precipitation experiments, we can see that the results are broadly similar for both samples. However, both results are significantly larger than the predicted bassanite fractionation factor. It's unclear what the cause of this is; it seems unlikely that hydration to gypsum could cause this discrepancy in oxygen fractionation, because the predicted gypsum and bassanite oxygen fractionation factors are the same. The acetonitrile hydrogen fractionation factor is also significantly larger than the predicted hydrogen fractionation factors for bassanite or gypsum.

As previously mentioned, some of the error here may be caused by the production of a bassanite-structured calcium sulphate which contains more than 0.5 molecules of water per unit of calcium sulphate. Certainly, the theoretical predictions of bassanite-water isotopic fractionation assume a bassanite structure of $CaSO_4 \cdot 0.5H_2O$ (Liu *et al.*, 2018), which may or may not fractionate hydration water in the same way as bassanite with larger quantities of water. However, comparison of the theoretical bassanite fractionation factors ($\alpha^{18}O = 1.0035$ and $\alpha D = 9667$ at 30 °C (Liu *et al.*, 2018)) to measured ($\alpha^{18}O = 1.0035$ and $\alpha = 0.9812$ at 20 °C (Gázquez *et al.*, 2017) and theoretical ($\alpha^{18}O = 1.0035$ and $\alpha D = 0.9809$ at 30 °C (Liu *et al.*, 2018)) gypsum fractionation factors implies that there is little change in oxygen fractionation based on the structural variations of gypsum and bassanite. Therefore at this stage, the only explanation I can offer for the disagreement between measured and theoretical results is that the presence of organic solvents affects how water enters the gypsum structure, which in turn affects the fractionation factor. Kinetic effects cannot explain the results, as these make fractionation occur less strongly, tending towards one.

The high temperature results also recorded high fractionation factors for both oxygen and deuterium. It seems likely that this is due to water evaporation – although the solutions were sealed during heating, some water vapour would have evaporated into the air in the tubes and condensed around the neck of the tube, which was not uniformly heated. This could be avoided more if larger quantities of water were heated, and were heated in sealed tubes with very little air - which would require more specialised equipment than was available.

3.6 Conclusion

Unfortunately, my results show that it is not possible to retrieve more palaeoclimatic information from a gypsum sample by dehydrating it using DTIA and measuring the isotopic composition of the two dehydration peaks separately. Although the two dehydration peaks have different isotopic composition, this appears to be driven by kinetic factors, rather than the presence of a more strongly bound water pool in the gypsum structure. As such, the impact that DTIA can have on the study of gypsum is limited; however, DTIA can still be of some use in determining dehydration mechanisms, as demonstrated by the grain size experiments.

I was also unable to measure bassanite oxygen and hydrogen fractionation factors which were consistent with each other, or with published theoretical results (Liu *et al.*, 2018). Precipitation experiments involving the use of polar organic solvents turned out to be inappropriate for fractionation factor measurement, with issues of low bassanite yield and, in some cases, isotopic exchange between the required water and the organic solvent. High temperature precipitation techniques hold more promise for fractionation factor measurement, but existing predictions of gypsum and bassanite fractionation factors would have to be extended to higher temperatures to be able to compare theoretical and experimental results. Further experiments investigating the rehydration of anhydrite (primarily γ-anhydrite, but potentially long-term studies to investigate whether β-anhydrite will rehydrate over long time periods in a similar way) also hold promise for the determination of bassanite-water fractionation.

4 The Application of DTIA to and Practical Considerations for Clay Mineral Water Stable Isotopes

4.1 Abstract

For hydrated minerals, Differential Thermal Isotope Analysis (DTIA) is capable of providing accurate measurements of the $^{18}O/^{16}O$ and D/H isotopic composition of the hydration water. One of the greatest advantages of the DTIA method for water isotope measurement is that waters are released at different temperatures and can be separated and measured individually, rather than measuring the isotopic composition of the total water released. I therefore apply the DTIA method to clay minerals, which frequently contain multiple types of water (e.g. absorbed, interlayer, structural, hydroxyl), some of which are believed to undergo rapid kinetic isotopic exchange while the hydroxyl groups do not. I present the results of a series of experiments which show that clay hydroxyl isotopic composition can be accurately measured through DTIA, and present experiments highlighting some of the experimental concerns for the measurement and accurate interpretation of clay hydroxyl isotopes. Experimental errors are low for the final method, averaging at ± 0.48 ‰ and ± 0.19 ‰ for δD and $\delta^{18}O$ respectively, for natural mixed clay samples.

4.2 Introduction

Clay minerals are a geologically significant mineral group consisting of hydrous aluminium phyllosilicates of various structures. They are common in terrestrial environments, and evidence for the presence of clay minerals has also been found on Mars both in the Endeavour Crater (Wray *et al.*, 2009) and in the surrounding plains (Dobrea *et al.*, 2012), as well as on the dwarf planet Ceres (Rivkin *et al.*, 2006). These discoveries are of particular interest as the formation of clay minerals requires the presence of water.

Clay minerals have also found extensive use in studies of the Earth's climate history. For example, the Cretaceous-Palaeogene (K-Pg) boundary (formerly the Cretaceous-Tertiary K-T boundary) is marked by a clay layer enriched in iridium at many sites, such as Wyoming, US (Bohor *et al.*, 1987), Umbria, Italy and Stevns Klint, Denmark (Alvarez *et al.*, 1980). The Paleocene-Eocene Thermal Maximum (PETM) is also marked by changes in clay minerology in a number of sites: the North Sea Basin (Knox, 1996), New Jersey, US (Gibson *et al.*, 1993), Antarctica (Robert and Kennett, 1994) and across the Tethys region (Bolle *et al.*, 2000), among others. In all of these locations, the PETM is marked by the appearance of kaolinite, though it is unclear if the kaolinite proceeds or precedes the warming event at each site (and indeed, the relative timing of the kaolinite may well be different depending on location).

In addition, a number of studies have made use of clay stable isotopes to identify changes in local climate or environmental conditions. Measurements of the bulk oxygen isotopic composition have been used to identify clay source (John *et al.*, 2012), and hydrogen and oxygen isotope measurements have been combined to identify historic changes in meteoric water isotopic composition and palaeotemperatures (Mix and Chamberlain, 2014), as a proxy for chemical weathering intensity (Yang *et al.*, 2016) and as an indicator of mountain uplift (Chamberlain *et al.*, 1999).

The clay minerals can be divided into four main groups, which share common structural units. All clay minerals are comprised of layers of two-dimensional tetrahedral silicate sheets and octahedral hydroxyl sheets. The tetrahedral sheets are made up of SiO_4 units, where the Si^{4+} cation is surrounded by four O^{2-} anions spread regularly around the central Si^{4+} cation,

forming a tetrahedron. Tetrahedra are held together in a hexagonal network, as each tetrahedron shares three of the four apex oxygen anions with three neighbouring tetrahedra. The final oxygen anion projects out of the hexagonal sheet. The octahedral sheets, on the other hand, vary in chemical composition, but share the same structural framework regardless of composition – a central cation, typically Al^{3+}, Mg^{2+} or Fe^{2+}/Fe^{3+}, surrounded by six oxygen atoms (either as O^{2-} or as OH^{-}), forming an octahedron. The exact structure changes depending on the charge of the cation – octahedral layers with +2 charge cations have a brucite-like structure, where every octahedron contains a cation, whereas layers with +3 charge cations have a gibbsite-like structure, where every third octahedron is vacant. Different clay mineral groups are defined by the arrangements of the tetrahedral and octahedral structural units: the kaolin group consists of 1:1 layers of tetrahedral silica and octahedral alumina sheets, the smectite group (swelling clays) and illite (clay-mica) group consist of 2:1 tetrahedral and octahedral layers (where each octahedral layer is sandwiched between two tetrahedral layers) and the chlorite group takes a 2:1:1 structure, where 2:1 tetrahedral-octahedral layers are split by a layer by a layer of $M(OH)_6$ (M is either Fe^{3+} or Mg^{2+}), rather than a layer of water. The distinction between the smectite and illite groups arises from the ions in the interlayer region between adjacent tetrahedral layers – illite group clays tend to have Mg^{2+}, Ca^{2+} or K^{1+} interlayer cations, which prevent much water entering the interlayer space, whereas the smectite groups have smaller Na^{1+} interlayer cations and as a result can accommodate multiple water layers in the interlayer space.

The presence of interlayer water, alongside hydroxyl groups and in some cases bound (structural) water (H_2O molecules bonded to a metal centre) makes clays of great interest for investigation using the DTIA method. This is because the DTIA method allows for separation and measurement of each type of water in isolation, and measurement of oxygen and hydrogen isotopes simultaneously. Many studies of stable isotopes in clays (for example, Savin and Epstein, 1970a; Sheppard, 1977; Compton *et al.*, 1999; Vitali *et al.*, 2002; Mix and Chamberlain, 2014) rely on removal of interlayer and structural water through prolonged heating under vacuum (and often measured the bulk oxygen, rather than hydroxyl oxygen). However, clays are often hygroscopic (in particular smectite clays) and rehydrate in a matter of minutes under exposure to air, meaning that transfer of the samples from vacuum to measurement system is problematic. More recent measurements of clay isotopes (e.g. Bauer and Vennemann, 2014) have developed protocols for avoiding this problem, but they are labour intensive relative to the DTIA method, and rely on long dehydration steps for the

removal of interlayer water. Moreover, if useful palaeoclimatic information is contained in the interlayer and structural water isotopic composition, these can be measured using DTIA, unlike with other stable isotope methods.

In this chapter, I present a series of DTIA experiments, carried out with the aim to determine the optimum conditions for clay water isotope measurement, including sample treatment, measurement techniques and analytical procedures.

4.3 Materials and Methods

All clay DTIA measurements were carried out using a dry N_2 stream, without a catalyst for removal of organics. Only $^{18}O/^{16}O$ and D/H were measured. Larger samples were measured using a large 3.4 ml alumina (Al_2O_3) TG holder (order number GB445213), while smaller samples were measured using smaller TG/DSC crucibles, either a 85 µl 80/20 platinum-rhodium TG/DSC crucible (order number GB399205) or a 85 µl alumina crucible (order number GB399972).

4.3.1 Materials

The high-purity kaolinite used in this research was provided by IMERYS and is sourced from Blackpool Pit, St. Austell pluton, Cornwall, UK. The extraction process is described in Bidwell *et al.*, 1970. The montmorillonite Ethiudna refers to a montmorillonite sample sourced from the Ethiudna Mines, Mt Victor Plumbago Station, Olary Province, South Australia, Australia. The Syn Talc refers to a synthetic talc sample purchased from Fisher Scientific (MDL Number MFCD00084820). The chlorite sample is metamorphic but of unknown origin. The other eight clay samples were all purchased from the Clay Minerals Society. The sources of the clays are shown in Table 4.1.

Finally, the synthetic carbonate refers to a synthetic carbonate standard of 99.8 % purity, while the dolomite refers to a high purity dolomite sample.

4.3.2 Clay Dehydration Experiments

As a proof of concept for DTIA measurements of clay hydroxyl water isotopic composition, I carried out measurements of a number of clay minerals, optimising the DTIA process for each clay to achieve separation of water types within the clay. A summary of the methods used for the clay measurements are shown in Table 4.2. For these experiments, all “Isotherm 1” steps are 15 minutes long (Isotherm 1 steps are to remove air and allow the water background to return to low levels after opening the furnace – needed for the measurement of waters released at lower temperatures), while all other isotherm steps are 20 minutes long,

unless otherwise noted. All "Ramp 1" steps heat at a rate of 20 °C per minute, while all other ramp steps heat at a rate of 40 °C per minute.

For each clay, the optimal heating programs for water separation was determined by carrying out a DTIA measurement using a heating ramp of 5 °C per minute to precisely determine the temperature at which dehydroxylation started and finished, and to determine the start and end temperatures of the dehydrations of any other water released during heating. Isotherms were inserted between water dehydration and dehydroxylation peaks to increase peak separation between the various dehydrated waters. The measurement dehydration profiles for the clays are shown in Figure 4.1.

4.3.2.1 Kaolinite ($Al_2Si_2O_5(OH)_4$)

Kaolinite contains no structural water other than the hydroxyl groups, and only adsorbs a little water onto its surface. As such, it is an ideal clay for measuring the isotopic composition of using offline measurement processes (such as trapping). To measure it using DTIA as a comparison between online and offline measurements, I first used a 5 °C per minute heating ramp experiment to determine dehydroxylation temperature. I then used a DTIA measurement program consisting of a 10 minute isotherm at 25 °C, a 20 °C per minute heating ramp to 420 °C, a 20 minute isotherm at 420 °C and a heating ramp of 20 °C per minute up to 760 °C to determine the kaolinite hydroxyl isotopic composition. An average sample size of 7.2 mg kaolinite was used.

Clay	Further Details	Source
Beidellite SBCa-1		California, USA
Hectorite SHCa-1		Red Mountain Andesite formation (pliocene), County of San Bernardino, State of California, USA
Kaolinite	Provided by IMERYS	Blackpool Pit, St. Austell pluton, Cornwall, UK25
Montmorillonite Ethiudna		Ethiudna Mines, Mt Victor Plumbago Station, Olary Province, South Australia, Australia
Montmorillonite STx-1b	Ca-rich Montmorillonite	Manning formation, Jackson group (eocene), Gonzales County, Texas, USA
Montmorillonite SWy-3	Na-rich Montmorillonite	Newcastle formation, (cretaceous), Crook County, Wyoming, USA
Nontronite NAu-1	Al-enriched Nontronite	Uley Mine, South Australia
Palygorskite PFl-1		Hawthorne formation (miocene), Luten Mine, County of Gadsden, State of Florida, USA
Rectorite RAr-1		Garland County, Arkansas, USA
Sepiolite SepSp-1		Valdemore, Spain
Syn Talc		Fisher Scientific, MDL Number MFCD00084820

Table 4.1. A summary of the clays measured by DTIA including sources of clay and any further relevant information.

Clay	Mass Used / mg	Temperatures of Steps / °C					
		Isotherm 1	Ramp 1	Isotherm 2	Ramp 2	Isotherm 3	Ramp 3
Beidellite SBCa-1	20.6	25	25 → 320	320	320 → 640	-	-
Hectorite SHCa-1	59.8	25	25 → 540	540	540 → 900	-	-
Kaolinite	7.2	25 (10 minutes)	25 → 420	420	420 → 760 (20 °C per min)		
Montmorillonite Ethiudna	X	-	25 → 220	220 (60 minutes)	220 → 660 (20 °C per min)	-	-
Montmorillonite STx-1b	32.5	-	25 → 460	460	460 → 760	-	-
Montmorillonite SWy-3	23.1	25	25 → 460	460	460 → 760	-	-
Nontronite NAu-1	23.4	25	25 → 160	160	160 → 290	290	290 → 660
Palygorskite PFl-1	20.2	-	25 → 130	130	130 → 260	260	260 → 540
Rectorite RAr-1	43.2	25	25 → 220	220	220 → 340	340	340 → 760
Sepiolite SepSp-1	22.9	-	25 → 360	360	360 → 640	640	640 → 880
Syn Talc	25.6	25	-	-	25 → 740	740	740 → 1080

Table 4.2. A summary of the heating programs used for the DTIA measurements. Unless otherwise noted in the table, all isotherm 1 steps are of 15 minutes duration, while all other isotherm steps are of 20 minutes duration, and all ramp 1 steps are at a heating rate of 20 °C, while all other ramp steps are at a rate of 40 °C. Note that for Palygorskite, there are further steps not shown above: a fourth isotherm at 540 °C, and a fourth heating step from 540 °C to 940 °C, at a rate of 40 °C.

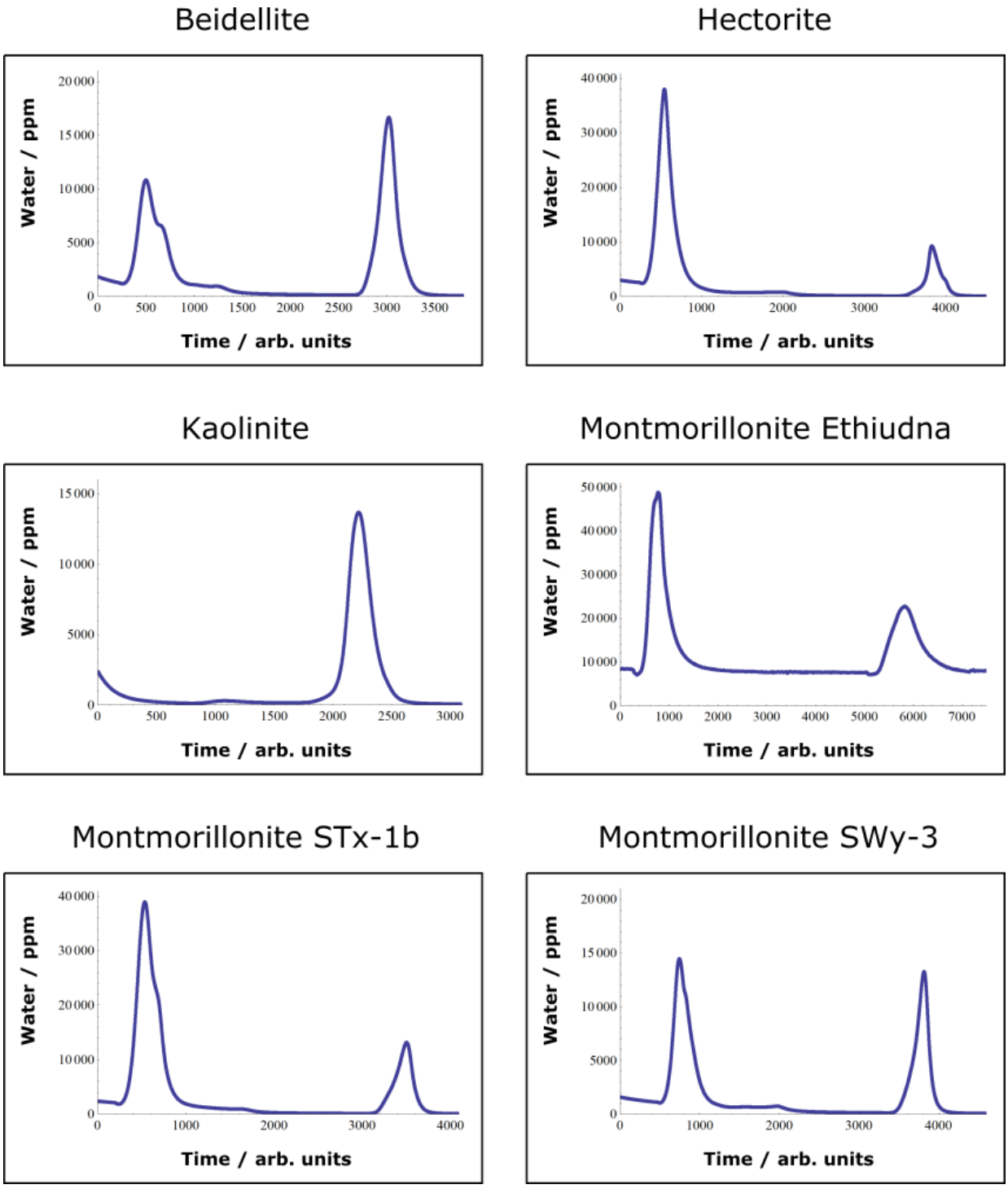

Figure 4.1 (a). The dehydration profiles for all measured clays as found using the measurement programs described in Table 4.2, demonstrating the water peak separation. The dehydration profile for Montmorillonite Ethiudna shows a raised background water level, because at this time a controlled water vapour background was in use, but this was removed for later measurements as it was found to be too unstable for accurate measurements.

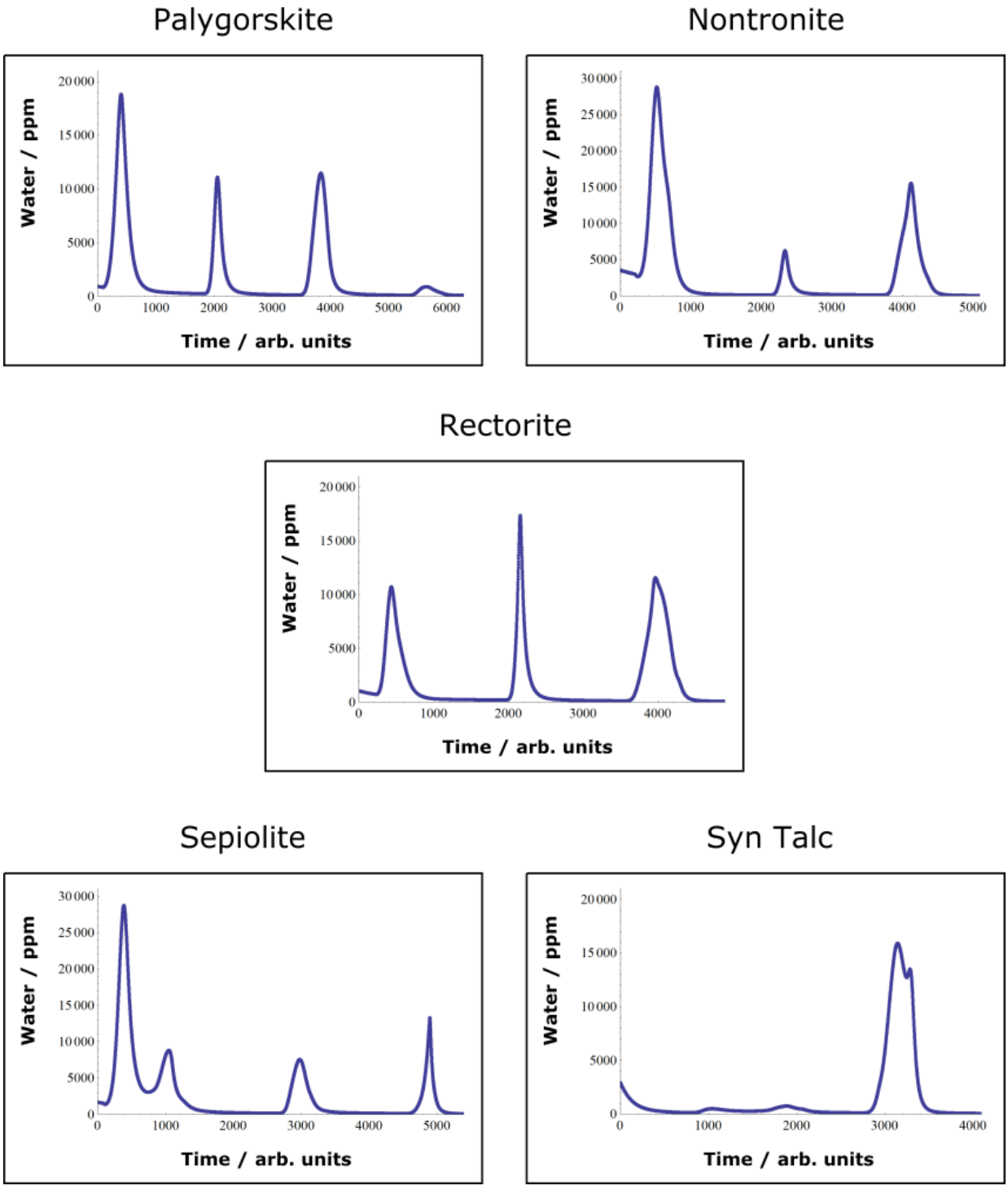

Figure 4.1 (b). Continuation of Figure 4.1 (a).

4.3.2.2 Montmorillonite ($(Na,Ca)_{0.33}(Al,Mg)_2(Si_4O_{10})(OH)_2 \cdot nH_2O$)

Montmorillonite is a typical smectite clay, containing variable amounts of interlayer water between layers in its structure as well as more strongly bonded hydroxyl groups. Following the standard procedure for determining a suitable DTIA heating program (using 5 °C per minute ramps to heat from room temperature until the end of dehydroxylation), measurements of the two clay mineral society high purity montmorillonites (STx-1b and SWy-3) were carried out using 20 °C per minute heating ramps to from 25 °C to 460 °C, 20 minute isotherms at 460 °C and then 40 °C per minute heating ramps up to 760 °C. For the montmorillonite SWy-3, a 15 minute isotherm at 25 °C was also used at the start of the run. However, in both cases, dehydration of the interlayer water began as soon as the sample was placed into the dry N_2 atmosphere, making the initial isotherm less important for montmorillonite. Sample sizes were on average 32.5 mg for montmorillonite STx-1b and 23.1 mg for montmorillonite SWy-3.

Unlike the two clay mineral society montmorillonite samples, the montmorillonite sample from the Ethiudna mine has a broad dehydroxylation (i.e. the dehydroxylation occurs over a larger temperature range, and at a lower temperature, than expected), in keeping with a degraded smectite (Cuadros and Altaner, 1998; Emmerich and Kahr, 2001). Being an earlier measurement before the DTIA process for clays was optimised, the DTIA program consists of a 20 °C per minute heating ramp to 220 °C, a 60 minute isotherm at 220 °C, then a heating ramp of 20 °C to 660 °C, and a water background was in use. The sample size was not recorded for these experiments.

4.3.2.3 Beidellite ($(Ca_{0.5},Na)_{0.3}Al_2(Si, Al)_4O_{10}(OH)_2 \cdot nH_2O$)

The optimum heating program for beidellite was determined to be a 15 minute isotherm at 25 °C followed by a 20 °C per minute heating ramp to 320 °C. Following a 20 minute isotherm at this temperature, a further 40 °C per minute heating ramp to 640 °C was used to measure the dehydroxylation. The sample size used was on average 20.6 mg.

4.3.2.4 Hectorite ($Na_{0.3}(Mg,Li)_3Si_4O_{10}(OH)_2$)

To measure the isotopic composition of hectorite, I used a heating program consisting of a 15 minute isotherm at 25 °C, a heating step using a 20 °C per minute ramp rate, a 20 minute isotherm at 540 °C and then a 40 °C per minute heating step to 900 °C. Interestingly, this hectorite sample seems to have a water pool not recorded in the general chemical formula for hectorite, as a large amount of water was released at temperatures <200 °C – at such low temperatures, it is likely a mixture of adsorbed and interlayer water. I was limited by crucible size during the measurement of hectorite, so I used 59.8 mg of sample to measure the isotopic composition, though using more sample would yield a more accurate result (approximately 50 % more sample would be required).

4.3.2.5 Nontronite ($CaO_{0.5},Na)_{0.3}Fe^{3+}_2(Si,Al)_4O_{10}(OH)_2 \cdot nH_2O$

The DTIA measurement of nontronite was carried out using three isotherms (a 15 minute isotherm at 25 °C, a 20 minute isotherm at 160 °C and a 20 minute isotherm at 290 °C) in order to separate the two low temperature dehydration peaks – the first peak corresponds to interlayer water, while the second peak may correspond to either the removal of the last layer of interlayer water, or to some kind of bound water not represented in general nontronites. The heating ramps used were a 20 °C per minute ramp between 25 °C and 160 °C, and two 40 °C per minute heating rate ramps for the 160-290 °C heating step and the final 540-940 °C heating step. The typical sample size used was 23.2 mg.

4.3.2.6 Palygorskite ($(CaO_{0.5},Na)_{0.3}Fe^{3+}_2(Si,Al)_4O_{10}(OH)_2 \cdot nH_2O$)

Palygorskite, as a pseudo-layer silicate, contains up to four different water types within its structure: in general, adsorbed water and zeolitic (or free) water are dehydrated at lower temperatures (<200 °C), water bound to the terminal ions of the octahedral-sheet like structure is removed next with increasing temperature, often dehydrating as two separate peaks at <300 °C and <600 °C, and finally the hydroxyl groups are removed at temperatures of approximately 800 °C. In my measurements, I observed peaks between 25-130 °C, 130-260 °C, 260-540 °C and 540-940 °C – for the first peak, a 20 °C per minute ramp was used, while a 40 °C per minute ramp was used for the measurement of other peaks. Isotherms were used at 25 °C (15 minutes), 130 °C (20 minutes, 260 °C (20 minutes) and 540 °C (20

minutes). Insufficient sample was used for accurate determination of the hydroxyl isotopic composition, but accurate measurements were made of the two bound water peaks by using 20.2 mg of sample. Approximately 15 times this amount of sample would be required for the accurate measurement of hydroxyl isotopic composition.

4.3.2.7 Rectorite ($(Na,Ca)Al_4((Si,Al)_8O_{20})(OH)_4 \cdot 2H_2O$)

Rectorite is a particular arrangement of the common interstratified illite-smectite clay mixture, containing a 1:1 ratio of dioctahedral smectite layers to dioctahedral mica layers. As such, when rectorite is heated, interlayer and adsorbed water are dehydrated from the structure first, followed by bound water (or this second peak could correspond to the final layer of interlayer water) and then by the hydroxyl water, giving a three step dehydration. For the measurement of the rectorite water isotopic composition, I used a heating program consisting of three isotherms (15 minutes at 25 °C, 20 minutes at 220 °C and 20 minutes at 340 °C), and three heating steps (a 20 °C per minute ramp between 25 °C and 220 °C, a 40 °C per minute ramp between 220 and 340 °C, and a 40 °C per minute ramp between 340 and 760 °C). An average sample size of 43.2 mg was sufficient for accurate hydroxyl group measurement.

4.3.2.8 Sepiolite ($Mg_4Si_6O_{15}(OH)_2 \cdot 6H_2O$)

Sepiolite, like palygorskite, is a pseudo-layer silicate and, as such, has multiple forms of water. Free water (found within channels in the sepiolite structure, as in palygorskite, and adsorbed on the surface) is removed first upon heating. The bound water, again as in palygorskite, is removed in two steps. In the case of sepiolite, this is thought to be due to changes in the structure upon heating, whereby the crystals fold, reducing the flow rate of water out of the channels (Kiyohiro and Otsuka, 1989). At higher temperatures (>660 °C, the hydroxyl water is released.

While it is possible to isolate the free water and first bound water for measurement, I only isolated the second bound water and hydroxyl water peaks for the DTIA measurements here. The heating program consisted of two 20 minute isothermal steps at 360 °C and 640 °C, a 20 °C per minute heating ramp between 25-360 °C and two 40 °C per minute heating ramps between 360-640 °C and 640-880 °C. For our initial DTIA measurements I used 22.9 mg of

sample - however, approximately twice as much sample would be required to yield sufficient water amounts for accurate hydroxyl group measurement.

4.3.2.9 Talc ($Mg_3Si_4O_{10}(OH)_2$)

The structure of talc contains only hydroxyl group water, and thus the main consideration for DTIA measurements is the removal of adsorbed water. As such, the synthetic talc samples were measured by running an isothermal step at 25 °C for 15 minutes to normalise the background, heating the talc sample at a high ramp rate (40 °C per minute) to 740 °C, where another 20 minute isothermal step was used to normalise the background and remove any water released within the furnace or by the sample during heating, and finally using a heating step to heat to 1080 °C with a 40 °C per minute ramp rate to liberate the hydroxyl water. Sample sizes for initial experiments were typically 25.6 mg.

However, the first of these experiments gave a very different result to the proceeding two measurements (giving the measurement set a large error), so further measurements were carried out using two different crucible types – the platinum-rhodium crucibles and the alumina crucibles, to compare the effects of crucible type on the measurement and potential memory effect. A final accurate measurement of talc was taken using a platinum crucible and a similar heating program, but with the second isotherm reduced to 10 minutes in duration (and is the result quoted in the results summary in Table 4.4.

4.3.2.10 Chlorite ($(Mg,Fe)_3(Si,Al)_4O_{10}(OH)_2 \cdot (Mg,Fe)_3(OH)_6$)

Chlorite is a member of the 2:1:1 clay group, so called because its structure consists of 2:1 talc-like layers of tetrahedral-octahedral-tetrahedral shape, and single brucite-like (e.g. $M(OH)_6$ where M can be Fe^{3+} or Mg^{2+}) layers between the talc-like layers. It is generally considered to undergo a two-step dehydration when heated. Although there is no bound water present, the hydroxyl groups are found in two different environments: the first to dehydroxylate are typically the interlayer hydroxyl groups (the hydroxyl groups attached to the brucite-like $(Mg,Fe)_3(OH)_6$ layer), while the hydroxyl groups associated with the mica sheet are typically released at higher temperatures. For chlorite, no measurements of the hydroxyl groups were carried out, as my primary interest was in determining at what temperatures we might expect chlorite to dehydroxylate at, in order to identify chlorite water

peaks in DTIA profiles of clay assemblages containing chlorite (see the PETM assemblage in Chapter 5).

4.3.3 Isotherm Length Experiments

DTIA requires optimisation of the heating programs to separate different types of structural water in the clay mineral. In order to examine whether the choice of heating program had significant effect on the measured hydroxyl isotopic composition, I carried out experiments measuring the effect of increasing isotherm length on the STx-1b montmorillonite sample. The heating program involved a 10 minute isotherm at 25 °C, a 40 °C pet minute ramp to 420 °C, an isotherm at 420 °C, and then a 40 °C per minute ramp to 760 °C. The isotherm at 420 °C before hydroxyl measurement was varied from 10 minutes to 60 hours.

4.3.4 Mixed Clay Experiments

Having demonstrated the separation of the different types of water found within a number of clay samples (and critically, the clay samples found within the PETM clays discussed in Chapter 5), I carried out experiments to see if the hydroxyl groups from different clays could be separated and measured individually, either by complete peak separation or by only analysing the parts of the dehydroxylation peaks that were not superimposed, and to determine if the presence of multiple clays had an effect on the measured total hydroxyl isotopic composition. Starting with a simpler test, mixtures of the Blackpool kaolinite and montmorillonite STx-1b were made yielding three different compositions: 21 % kaolinite, 31 % kaolinite and 40 % kaolinite. These mixtures were then measured using DTIA. The heating program used was similar to that used to measure pure montmorillonite but the pre-dehydroxylation isotherm temperature was lowered to ensure no partial dehydroxylation of kaolinite. It consisted of a 10 minute isotherm at 30 °C, a 40 °C / min heating ramp to 420 °C, a 10 minute isotherm at 420 °C, and finally a 40 °C heating ramp to 760 °C.

To find the expected values for the mixture's total hydroxyl isotopic composition, the hydroxyl water per mg of clay was found for the kaolinite and montmorillonite samples, and this was multiplied by the amount of each clay present to find the ratio of hydroxyl water from each clay. The expected mixture hydroxyl isotopic composition was then calculated by

summing the weighted hydroxyl isotopic compositions for each component, weighting by the percentage contribution to the total mixture hydroxyl water.

4.3.5 Carbonate Removal

The presence of carbonate can lead to oxygen exchange during DTIA measurement, and further DTIA experiments have found that the presence of dolomite, when added to pure synthetic talc samples, has a large effect on the measured $\delta^{18}O$ of the talc's hydroxyl water, as shown in Table 4.3 (both measured using platinum crucibles, and the heating program described in Table 4.2). The decarbonation of calcite/dolomite to CO_2 can isotopically exchange with water, thereby altering its oxygen isotopic composition (Gemery *et al.*, 1996). However, given that δD was also somewhat affected by CO_2 presence, it could also be that the presence of CO_2 in the carrier gas has a direct effect on the Picarro Water Isotope Analyzer's ability to accurately measure water vapour in the cavity (as carrier gas is known to have an effect on isotope measurement; Bauska *et al.*, 2017).

Because of this, I resolved to test methods for carbonate removal before measurement of natural mixed clay samples, which often contain some amount of carbonate. Previous studies have suggested that the best method for carbonate removal without sample degradation is to use a buffer solution of sodium acetate with acetic acid (Tessier *et al.*, 1979; Mseddi *et al.*, 2010.

In order to test whether the acid treatment affected measurements of $\delta^{18}O$ or δD, I acid treated a mixture of high-purity Blackpool kaolinite and a synthetic carbonate standard (99.8 % purity). I mixed 0.2323 g kaolinite with 0.2775 g carbonate, and placed the mixture into a 2 M buffer solution of sodium acetate and acetic acid. The buffer solution was made by mixing 20 ml of 2 M acetic acid with 80 ml of 2 M sodium acetate solution, chosen to give a theoretical pH of 5.2.

After leaving the mixture, with occasional stirring, for 90 minutes, the solids (0.1809 g) were recovered by filtration, washed several times with water, and then left in a 40 °C oven overnight to remove any excess water. Finally, the recovered mixture was measured using the DTIA system, using 8.95 ± 0.01 mg of sample, and a heating program of a 10 minute isotherm at 30 °C, followed by heating step using a 40 °C / min ramp rate to 760 °C.

	Syn Talc	Syn Talc + Dolomite
No. Repeats	3	3
Mass Talc / mg	25.62	31.58
Mass Dolomite / mg	-	8.69
H_2O	3.92×10^6	4.78×10^6
H_2O Error	9.12×10^3	1.78×10^4
δD / ‰	–67.11	–64.47
δD Error	0.39	0.32
$\delta^{18}O$ / ‰	–6.15	–3.08
$\delta^{18}O$ Error	0.04	0.08

Table 4.3. Comparison of the results of DTIA measurement of the talc hydroxyl water for two talc samples, where one sample has had dolomite (roughly 21.6 % of total) added before measurement. Note the shifted values for both $\delta^{18}O$ and δD.

4.3.6 Clay Exchange Experiment

One of the largest advantages of the DTIA method in measuring clay hydration water isotopic composition is that different water types in the clay can be measured separately. However, this is only useful if clay hydroxyl groups are indeed resilient to isotopic exchange than other water in the clay. To test this, a preliminary experiment was carried out, where a large sample of montmorillonite STx-1b was placed in water in a sealed conical flask, and left at 17 °C for approximately 23 months. After this time, the sample was filtered from solution, heated at 40 °C overnight to remove excess water, and then measured using the montmorillonite measuring program, but modified so that all ramps were at 40 °C per minute and the isotherm at 460 °C was altered to a 10 minute isotherm at 440 °C (a lower temperature here makes no difference to water separation, but may somewhat reduce the very small amount of exchange that can occur between the hydroxyl water and background water). Montmorillonite was chosen as it is a very common smectite, and is often the smectite that makes up illite-smectite clays (beidellite is also a smectite common in illite-smectite).

4.3.7 PETM Clay Measurement

In the following chapter (Chapter 5) the measurement of a set of PETM clays from a drill core in the North Sea Basin is discussed, along with the implications for the PETM of the isotopic trends recorded in the sample set. The development of the method for the measurement of the samples is discussed here. Initially, I measured a small portion of one of the samples (MPL 261) using a heating ramp of 5 °C per minute to 1030 °C (shown in Figure 4.2). Comparison with the 5 °C per minute dehydration profiles for rectorite, chlorite and kaolinite shows that in the PETM clay assemblage, the potential bound water / final interlayer water is removed at a higher temperature than in the pure rectorite, while the dehydroxylation begins at a slightly lower temperature. This could be because the rectorite is not an exact match to the illite-smectite of the PETM clay assemblage, which has a variable ratio of illite to smectite and is not necessarily regularly ordered. There is no evidence for the higher temperature chlorite dehydroxylation within the assemblage – however, only 6 % of this sample is chlorite, and sedimentary chlorites have been found to dehydroxylate at lower temperatures (see Földvári, 2011), so it is likely that the chlorite dehydroxylation is concurrent with the clay mineral dehydroxylation in this case.

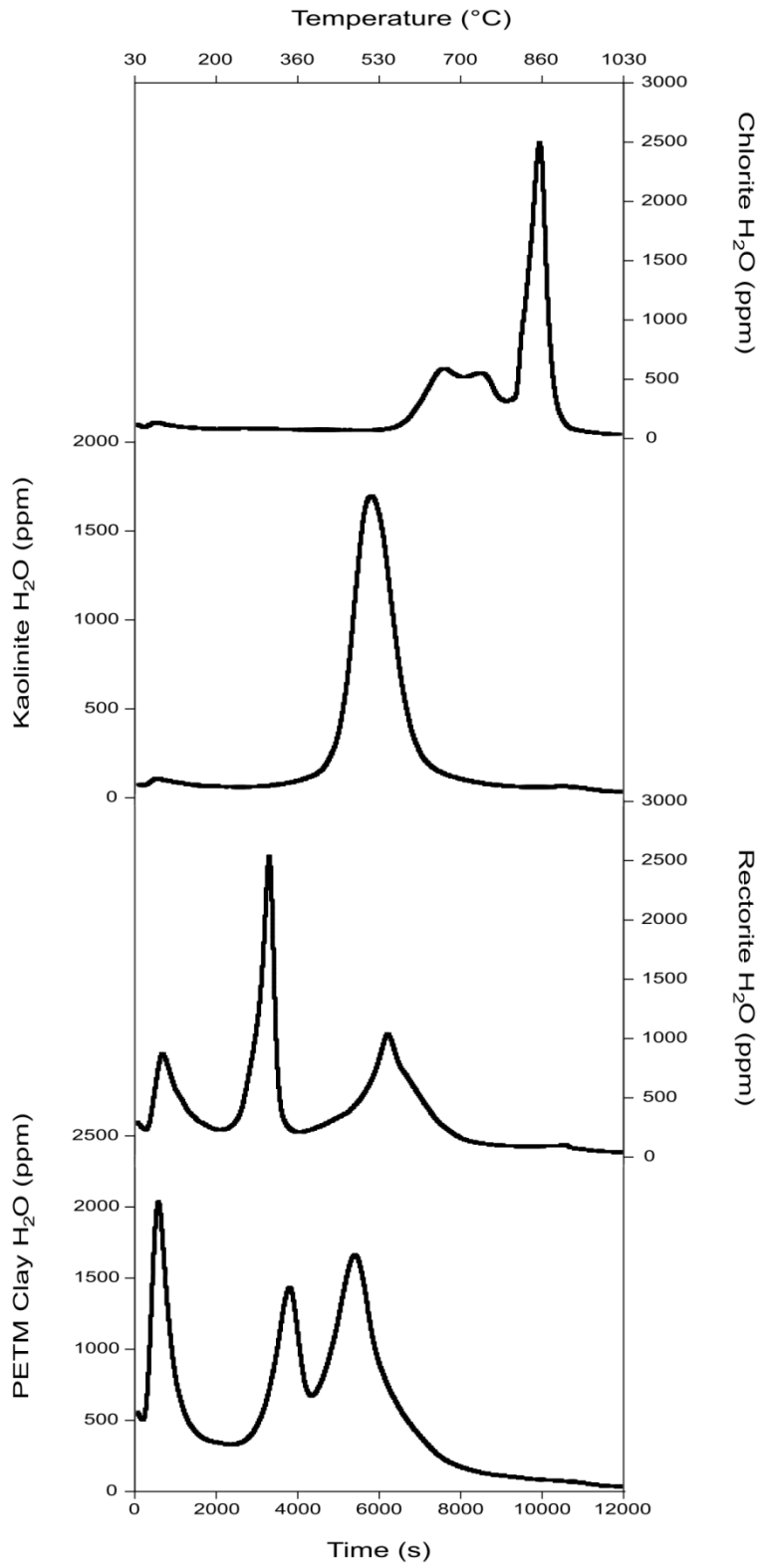

Figure 4.2. A comparison of the dehydration profiles of the PETM clay assemblage and pure standard samples of clay assemblage's constituent clays. These dehydration profiles were obtained by using a heating rate of 5 °C per minute between 30 °C and 1030 °C (e.g. so each 1800 second time period represents an increase of 150 °C).

To find the optimal heating program, a DSC curve (Figure 4.3) was measured at a constant heating rate (40 °C per minute), and isotherms were inserted where the DSC curve reached minima. This corresponds to temperatures at which dehydration and dehydroxylation are minimised for the clay assemblage (use of TG for this process where available would be a simpler method for determining the isotherm temperatures, but the TG was not functioning at time of measurement).

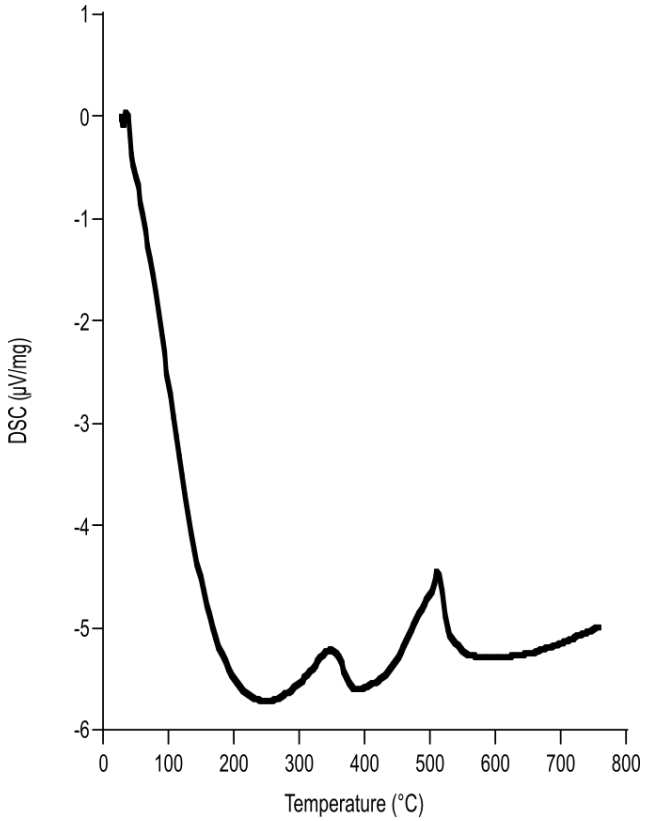

Figure 4.3. The DSC measurement of the PETM clay dehydration at a 40 °C per minute heating rate. The DSC curve minima at around 250 °C and 390 °C were chosen as the temperatures to insert isothermal steps between peaks, as these minima should represent times when the sample is using all absorbed heat to increase in temperature.

The optimal DTIA heating program was found to be: a 10 minute isotherm at 30 °C, a heating ramp to 250 °C, then a 12 minute isotherm, followed by a heating ramp to 390 °C, a further 12 minute isotherm at 390 °C, and a final heating ramp to 950 °C. A high final

temperature was chosen to ensure that any chlorite dehydroxylation peaks were not missed in samples containing a higher proportion of chlorite. Appropriate sample sizes were found by running an initial small portion (3-4 mg) of each sample through this process, and scaling the sample size as required to increase the hydroxyl peak height to 11,000-14,000 ppm water in the optical cavity of the Picarro 2130 analyzer.

The core samples were found to contain trace amounts of carbonate by XRD and so were treated with the 2 M sodium acetate/acetic acid buffer solution described above. I used 2 ml of buffer solution for these samples following the proportions suggested in Mseddi *et al.*, 2010, and assuming a carbonate concentration <5 %. A large excess of acid is undesirable, as it is may lead to an accelerated isotopic exchange.

4.4 Results

4.4.1 Clay Dehydration Experiments

The results of hydroxyl water measurement for all ten of the clays measured are shown in Table 4.4. The errors for these measurements vary significantly (from ± 0.04 ‰ to ± 3.82 ‰ for $\delta^{18}O$, and from ± 0.29 ‰ to ± 1.52 ‰ for δD, though most of the large errors are due to small sample size (excluding these samples, errors in measurement range from ± 0.04 ‰ to ± 0.92 ‰ for $\delta^{18}O$, average ± 0.39 ‰, and from ± 0.29 ‰ to ± 1.04 ‰ for δD, average ± 0.61 ‰). Two of the samples, nontronite and talc, have a large error simply because their first measurement vary significantly from subsequent measurements – this is likely a memory effect, and is discussed further under the individual clay results (see Table 4.6 for the results of individual nontronite and talc measurements showing the apparent memory effect – note that the talc measurement quoted in Table 4.4 is from a different measurement set). Excluding all of the samples with elevated errors, including the kaolinite measurement, errors are limited to ranges of ± 0.04 ‰ to ± 0.52 ‰ for $\delta^{18}O$, average ± 0.31 ‰, and ± 0.29 ‰ to ± 0.72 ‰ for δD, average ± 0.53 ‰). Table 4.5 shows the measurement of other water types in the clays where such measurements were made. The following sections will discuss the results from each clay individually in brief.

4.4.1.1 Kaolinite ($Al_2Si_2O_5(OH)_4$)

The hydroxyl isotopic composition of the Blackpool kaolinite was found to be $\delta^{18}O = 6.63 \pm 0.92$ ‰ and $\delta D = -62.15 \pm 0.67$ ‰. The amount of water given off during these measurements is approximately 0.95 µl when calibrating the integral of the Picarro water concentration measurements against gypsum samples (which have known water content by mass), so future measurements would ideally use slightly more sample. The dehydration profile seems to show a small increase in the background water level during heating before the hydroxyl measurement – it is unclear what the source of water is here, but it could be due to water being adsorbed onto the surface of the furnace when the system is exposed to air, which is then removed as the furnace temperature increases. The effect of this will be negligible, given how small the total increase in background water is compared to the peak sizes required for DTIA measurements.

Clay Hydroxyl	No. Repeats	H_2O	H_2O Error	δD / ‰	δD Error	$\delta^{18}O$ / ‰	$\delta^{18}O$ Error
Beidellite SBCa-1	4	3.69×10^6	4.11×10^4	–127.62	0.62	–9.61	0.52
Hectorite SHCa-1	4	1.92×10^6	1.12×10^4	–107.16	1.52	21.80	0.06
Kaolinite	4	3.28×10^6	3.81×10^4	–62.15	0.67	6.63	0.92
Montmorillonite Ethiudna	2	8.76×10^6	1.05×10^6	–93.56	0.29	18.43	0.48
Montmorillonite STx-1b	4	3.07×10^6	9.82×10^3	–41.60	0.57	13.42	0.13
Montmorillonite SWy-3	5	2.72×10^6	1.54×10^4	–116.91	0.72	3.20	0.36
Nontronite NAu-1	4	4.14×10^6	4.85×10^3	–90.29	1.04	0.99	0.32
Palygorskite PFl-1	4	2.48×10^5	4.01×10^3	–39.95	1.02	21.31	3.82
Rectorite RAr-1	4	3.83×10^6	1.85×10^5	–65.24	0.57	–3.77	0.32
Sepiolite SepSp-1	2	1.61×10^6	1.19×10^3	–60.80	1.22	17.75	0.55
Syn Talc	3	3.92×10^6	9.12×10^3	–67.11	0.39	–6.15	0.04

Table 4.4. A summary of the results of DTIA measurement of the hydroxyl water for the 11 measured clay minerals, showing the relative amount of water (found by integrating the CRDS water ppm signal), the δD and $\delta^{18}O$ values, and the errors for these measurements. Note that the very large error for palygorskite $\delta^{18}O$ is likely caused by the very low water amount.

Clay	Water Type	No. Repeats	H_2O	H_2O Error	δD / ‰	δD Error	$\delta^{18}O$ / ‰	$\delta^{18}O$ Error
Montmorillonite Ethiudna	Interlayer	2	1.34×10^7	1.78×10^6	–23.90	0.54	10.89	0.03
	Hydroxyl		8.76×10^6	1.05×10^6	–93.56	0.29	18.43	0.48
Montmorillonite STx-1b	Interlayer	4	9.57×10^6	2.36×10^5	–37.84	0.92	–2.98	0.43
	Hydroxyl		3.07×10^6	9.82×10^3	–41.60	0.57	13.42	0.13
Nontronite NAu-1	Potential Bound Water	4	9.28×10^5	3.09×10^4	–71.89	1.36	1.51	0.58
	Hydroxyl		4.14×10^6	4.85×10^3	–90.29	1.04	0.99	0.32
Palygorskite PFl-1	Bound Water I	4	1.77×10^6	1.56×10^4	–15.15	1.44	12.07	0.49
	Bound Water II		3.09×10^6	3.35×10^4	–23.08	0.90	14.07	0.45
	Hydroxyl		2.48×10^5	4.01×10^3	–39.95	1.02	21.31	3.82
Rectorite RAr-1	Interlayer	4	2.16×10^6	2.33×10^5	–44.38	2.83	5.29	0.41
	Potential Bound Water		1.98×10^6	4.42×10^4	–113.22	1.37	–4.87	0.19
	Hydroxyl		3.83×10^6	1.85×10^5	–65.24	0.57	–3.77	0.32
Sepiolite SepSp-1	Bound Water II	2	1.97×10^6	4.91×10^3	–63.18	1.42	15.69	0.36
	Hydroxyl		1.61×10^6	1.19×10^3	–60.80	1.22	17.75	0.55

Table 4.5. A comparison of isotopic composition of non-hydroxyl water to hydroxyl water for clays which have multiple water environments within their structure.

4.4.1.2 Montmorillonite ($(Na,Ca)_{0.33}(Al,Mg)_2(Si_4O_{10})(OH)_2 \cdot nH_2O$)

The hydroxyl group water was isolated in each case for the montmorillonite samples. Isotope measurements are generally accurate for the two montmorillonite standards (STx-1b and SWy-3), though the water amount measured is slightly lower than would be desired (3.46 x 10^6 is the peak size required for approximately 1 µl water). I found values of $\delta^{18}O = 13.42 \pm 0.13$ ‰ and $\delta D = -41.60 \pm 0.57$ ‰ for the STx-1b hydroxyl and values of $\delta^{18}O = 3.20 \pm 0.36$ ‰ and $\delta D = -116.91 \pm 0.72$ ‰ for the SWy-3 hydroxyl.

The montmorillonite Ethiudna sample, despite being measured with the background (something that was dropped as it generally increased the size of measurement errors and because peak height was not found to have a large effect on the results of measurement) had very small errors in the two measurements made. Although the dehydroxylation occurred over a larger, lower temperature range, there was still no trouble isolating the hydroxyl peak from the interlayer water dehydration peaks. The results of DTIA were $\delta^{18}O = 18.43 \pm 0.48$ ‰ and $\delta D = -93.56 \pm 0.29$ ‰ for the hydroxyl group and $\delta^{18}O = 10.89 \pm 0.03$ ‰ and $\delta D = -23.90 \pm 0.54$ ‰ for the interlayer water (shown together in Table 4.5).

4.4.1.3 Beidellite ($(Ca_{0.5},Na)_{0.3}Al_2(Si, Al)_4O_{10}(OH)_2 \cdot nH_2O$)

As with montmorillonite, separation of the interlayer water from the hydroxyl water was achieved without difficulty. Measurement gave $\delta^{18}O = -9.61 \pm 0.52$ ‰ and $\delta D = -127.62 \pm 0.62$ ‰ for the hydroxyl group.

4.4.1.4 Hectorite ($Na_{0.3}(Mg,Li)_3Si_4O_{10}(OH)_2$)

Given the limitations on sample size, it is unsurprising that the results for δD (–107.16 ± 1.52 ‰) have a much larger error than the results for $\delta^{18}O$ (21.80 ± 0.06 ‰), as water amount has a stronger effect on δD measurements. While we were not expecting to have to separate any water peaks for the hectorite sample, separation was straightforward for this unmixed clay.

4.4.1.5 Nontronite $(CaO_{0.5},Na)_{0.3}Fe^{3+}_2(Si,Al)_4O_{10}(OH)_2 \cdot nH_2O$

As shown in Table 4.6, there seems to be a more significant memory effect on the δD results for nontronite, but the use of a sacrificial sample would be sufficient to overcome the memory effect seen here. The result for hydroxyl $\delta^{18}O$ is 0.99 ± 0.32 ‰ and for hydroxyl δD is –90.29 ± 1.04 ‰, and the results for the bound water peak were found to be $\delta^{18}O$ = 1.51 ± 0.58 ‰ and δD = –71.89 ± 1.36 ‰, though again the bound water peak error is greatly affected by the faulty first measurement (when excluded, results become $\delta^{18}O$ = 1.23 ± 0.13 ‰ and δD = –72.51 ± 0.71 ‰, which are reasonable errors for a peak of only 0.28 µl of water). Results for both peaks are shown together in Table 4.6.

		Nontronite		Syn Talc	
		$\delta^{18}O$ / ‰	δD / ‰	$\delta^{18}O$ / ‰	δD / ‰
Measurement Number	1	1.40	–88.73	–3.54	–67.11
	2	0.84	–90.83	–6.10	–66.78
	3	1.04	–90.69	–6.14	–66.57
	4	0.66	–90.90	-	-
Total Including First Result	Total	0.99	–90.29	–5.26	–66.82
	Error	0.32	1.04	1.49	0.27
Total Excluding First Result	Total	0.94	–90.76	–6.12	–66.68
	Error	0.15	0.10	0.03	0.15

Table 4.6. The individual results of DTIA measurement of nontronite and synthetic talc dehydroxylation. Note that a large part of the error for these samples is due to the first measurement, suggesting some memory of the previous sample.

4.4.1.6 Palygorskite $((CaO_{0.5},Na)_{0.3}Fe^{3+}_2(Si,Al)_4O_{10}(OH)_2 \cdot nH_2O)$

Given that the palygorskite hydroxyl peak only contains 0.07 µl of water, it is meaningless to further analyse the hydroxyl peak – the large errors of the hydroxyl measurement are to be expected when the water amount is so much less than 1 µl. The dehydration profiles do however demonstrate that palygorskite samples can be analysed by DTIA, with each water type separated out into individual dehydration peaks. Measurements were made of the two bound water environments in the palygorskite sample (Table 4.5), finding the first bound

water peak to have an isotopic composition of $\delta^{18}O$ = 12.07 ± 0.49 ‰ and δD = –15.15 ± 1.44 ‰ (peak size 0.51 µl) and the second bound water peak to have an isotopic composition of $\delta^{18}O$ = 14.07 ± 0.45 ‰ and δD = –23.08 ± 0.90 ‰ (peak size 0.89 µl).

4.4.1.7 Rectorite ($(Na,Ca)Al_4((Si,Al)_8O_{20})(OH)_4 \cdot 2H_2O$)

The three water peaks were isolated and analysed for the rectorite sample (Table 4.5). Interestingly, for the rectorite sample, the second peak (potentially bound water or final interlayer water) is the most isotopically depleted water, which would not be expected if the relationship between the first and second peaks was purely kinetic. Results of DTIA for the hydroxyl peak were $\delta^{18}O$ = –3.77 ± 0.32 ‰ and δD = –65.24 ± 0.57 ‰, while results for the other water types have much larger δD errors due to low water amounts (0.57 µl and 0.62 µl for the potential bound water and interlayer water respectively). Results for the bound water are $\delta^{18}O$ = –4.87 ± 0.19 ‰ and δD = –113.22 ± 1.37 ‰, and results for the interlayer water are $\delta^{18}O$ = 5.29 ± 0.41 ‰ and δD = –44.38 ± 2.83 ‰.

4.4.1.8 Sepiolite ($Mg_4Si_6O_{15}(OH)_2 \cdot 6H_2O$)

The slower 5 °C per minute heating ramp for sepiolite shows that all water types can be separated for sepiolite, as for palygorskite. Errors are greater than would normally be expected because of insufficient sample size. The hydroxyl peak isotopic composition was found to be $\delta^{18}O$ = 17.75 ± 0.55 ‰ and δD = –60.80 ± 1.22 ‰, while the second bound water peak isotopic composition was found to be $\delta^{18}O$ = 15.69 ± 0.36 ‰ and δD = –63.18 ± 1.42 ‰.

4.4.1.9 Talc ($Mg_3Si_4O_{10}(OH)_2$)

Results from the initial measurement of talc are shown in Table 4.6, where it can be seen that the $\delta^{18}O$ result seems to show a memory effect for the first measurement. Following this, the results of DTIA experiments on synthetic talc using different crucible types are shown in Table 4.7. The Al_2O_3 crucible appears to show a very strong memory effect compared to the platinum-rhodium crucible. The experiment sets were carried out 18 days apart, so it is not the case that the first set of synthetic talc measurements (using an Al_2O_3 crucible) would have affected the second set of synthetic talc measurements (using a platinum-rhodium crucible).

The measurements of the synthetic talc using the most optimized method are $\delta^{18}O$ = –6.15 ± 0.04 ‰ and δD = –67.11 ± 1.39 ‰ (shown in Table 4.4).

		Al_2O_3 Crucible		Platinum-Rhodium Crucible	
		$\delta^{18}O$ / ‰	δD / ‰	$\delta^{18}O$ / ‰	δD / ‰
Measurement Number	1	2.67	–69.01	–3.94	–64.37
	2	–2.54	–65.51	–4.97	–63.93
	3	–4.10	–65.28	–5.33	–64.56
	4	–4.84	–65.14	–5.75	–64.33
	5	–5.33	–64.74	–5.58	–64.67
Total / ‰		–2.83	–65.94	–5.11	–64.37
Error		3.25	1.74	0.72	0.28

Table 4.7. The measurement-by-measurement results of DTIA on synthetic talc using two different crucible types to hold the sample during heating. The measurements using the aluminium oxide (Al_2O_3) crucible show a larger and more persistent memory effect than the measurements made with the platinum-rhodium crucible.

4.4.1.10 Chlorite ($(Mg,Fe)_3(Si,Al)_4O_{10}(OH)_2 \cdot (Mg,Fe)_3(OH)_6$)

The dehydration profile of our metamorphic chlorite against the rectorite, kaolinite and PETM clay dehydration profiles is shown in Figure 4.2. Comparing the chlorite to the individual pure clays, the metamorphic chlorite has a significantly higher dehydroxylation temperature than the other clays (where chlorite's main dehydroxylation peak starts at about 780 °C, with a smaller water loss starting at about 570 °C), suggesting that metamorphic chlorite, if present, should be separable from other smectite-type clays. Comparison to the PETM clay assemblage shows that no water peaks are found in the PETM clay dehydration profile at temperatures of metamorphic chlorite dehydroxylation.

4.4.2 Isotherm Length Experiments

While very little change in the hydroxyl isotopic composition was seen over short isotherm lengths, significant isotopic exchange occurred at two hours and more at greater isotherm lengths (Figure 4.4), with measured hydroxyl isotopic composition tending towards atmospheric values (–11 to –14 ‰ for $\delta^{18}O$, and –110 to –130 ‰ for δD). Over 60 hours, the measured hydroxyl isotopic composition changed by –9.85 ‰ for $\delta^{18}O$ and by –83.22 ‰ for δD.

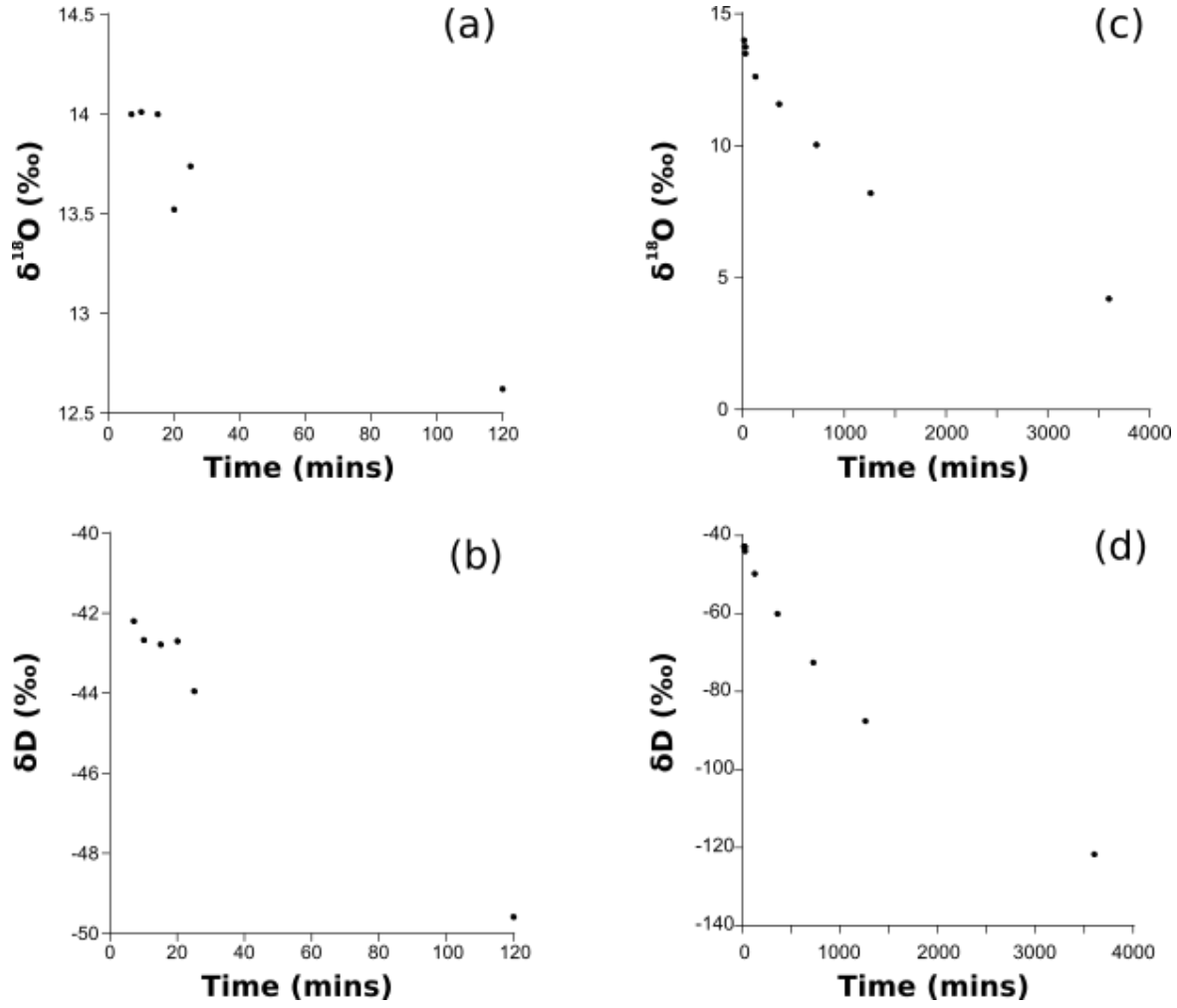

Figure 4.4. Impact of extended isothermal steps before hydroxyl isotopic measurement. The first two graphs, a and b, are an expansion of the 0 to 2 hour range, where a significant change is seen between 25 minutes and two hours. The final two graphs, c and d, show all of the results from 0 to 60 hours.

4.4.3 Mixed Clay Experiments

The total measured hydroxyl waters for the mixed clay samples have similar isotopic compositions to the expected values (shown together in Table 4.8). This suggests that there is no isotopic exchange between the emitted water and the clay structural oxygen during the dehydroxylation.

I was unable to separate the kaolinite and montmorillonite hydroxyl peaks using different heating programs because of the overlapping temperatures of the dehydroxylation for each clay. The dehydration profiles of a 10 °C per minute run and a standard measurement run are shown in Figure 4.5.

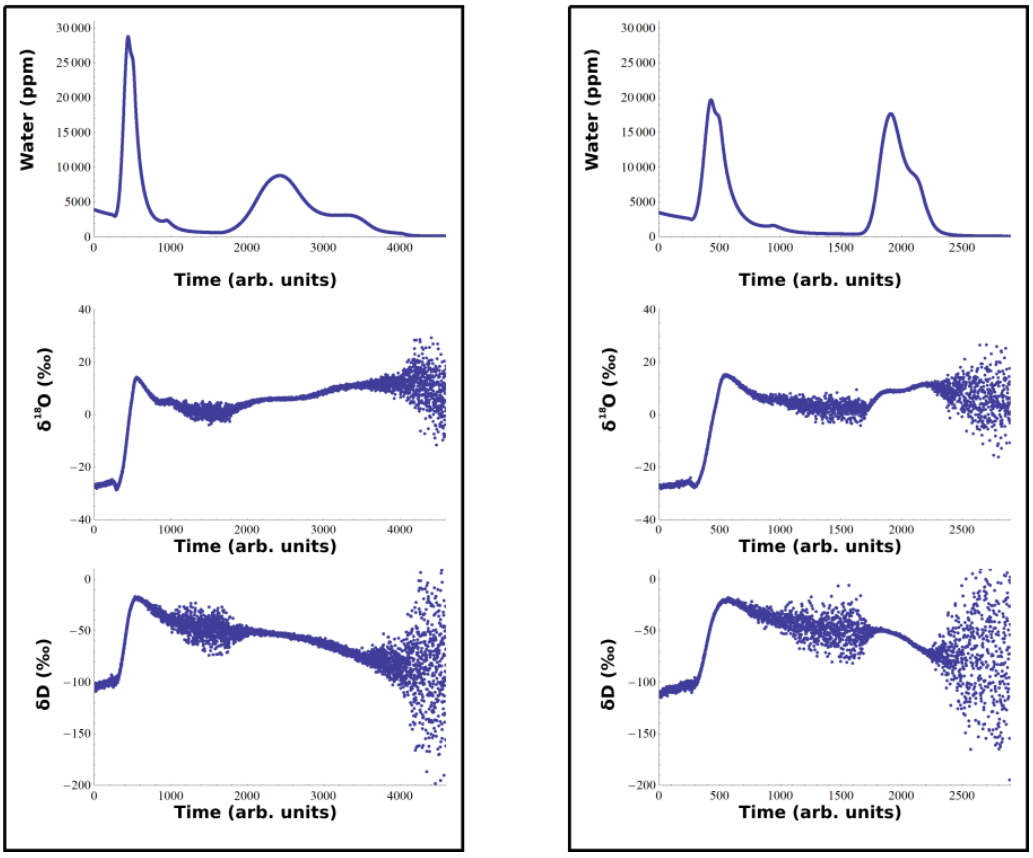

Figure 4.5. The heating profiles of the mixed kaolinite and montmorillonite samples at two different ramp rates. The left panel uses a heating rate of 10 °C per minute, resulting in a much broader dehydroxylation peak, but not separating the kaolinite and montmorillonite dehydroxylations. The right panel uses a heating rate of 40 °C per minute.

Sample	Kaolinite / %	Water from Kaolinite / %	Measured				Expected			
			δD / ‰	δD Error	$\delta^{18}O$ / ‰	$\delta^{18}O$ Error	δD / ‰	δD Error	$\delta^{18}O$ / ‰	$\delta^{18}O$ Error
Kaolinite	100	100	–62.15	0.67	6.63	0.92	-	-	-	-
Montmorillonite STx-1b	0	0	–41.60	0.57	13.42	0.13	-	-	-	-
Montmorillonite Kaolinite Mix 1	21.2	54	–53.61	0.12	10.48	0.40	–52.74	0.45	9.74	0.50
Montmorillonite Kaolinite Mix 2	31.2	67	–55.05	0.16	9.27	0.10	–55.29	0.49	8.90	0.62
Montmorillonite Kaolinite Mix 3	39.5	74	–56.35	0.24	8.83	0.29	–56.85	0.52	8.38	0.69

Table 4.8. Comparison of DTIA measurements of pure kaolinite and montmorillonite to samples containing a mixture of both kaolinite and montmorillonite in different ratios. The predicted values for the isotopic compositions of the hydroxyl peak of the mixtures is close to the values measured in each case, being within one standard deviation of the prediction error for mixes 2 and 3.

Attempts to separate out the hydroxyl peaks in analysis were unsuccessful. Initially, I integrated smaller parts of the kaolinite dehydroxylation peak, integrating only the area from the peak start to either the peak maximum, or the point halfway between the peak start and peak maximum. However, comparison of the values obtained in this way for the kaolinite mixed with montmorillonite against unmixed kaolinite (see Table 4.9) shows that even the initial part of the dehydroxylation peak is affected by the presence of other clays. The effect is much stronger for hydrogen isotope measurements, which is consistent with the hydrogen of the hydroxyl group being more exchangeable. In particular, the δD values recorded from the first half and first quarter of the peaks are almost the same for the mixed clay, whereas for the single pure clay there is a large difference between the δD for the first half of the peak and the δD for the first quarter of the peak. Similar results were observed even when the heating rate was lowered to 20 °C per minute. I also tried modelling the dehydroxylation, but while the water concentration profile measured by the Picarro can be modelled very accurately as a combination of two Gaussian peaks (Figure 4.6), it was unclear how the $\delta^{18}O$ and δD signals could be modelled for peak deconvolution.

Clay	Water Type	No. Repeats	H_2O	δD / ‰	$\delta^{18}O$ / ‰
Kaolinite Unmixed	First 1/2 of Peak	3	1.67×10^6	–62.20	6.07
	First 1/4 of Peak		2.26×10^5	–73.11	2.53
Kaolinite Mixed (20 % Kaolinite)	First 1/2 of Peak	3	1.60×10^6	–46.94	7.79
	First 1/4 of Peak		2.06×10^5	–46.57	3.92
Kaolinite Mixed (40 % Kaolinite)	First 1/2 of Peak	3	1.83×10^6	–50.35	7.62
	First 1/4 of Peak		1.91×10^5	–50.45	3.97

Table 4.9. Comparison of the results from DTIA measurements of pure kaolinite and mixed clay samples containing kaolinite and montmorillonite, where only first fraction of the hydroxyl peak is included in the calculation of the hydroxyl isotopic composition. While the total amount of water captured by selecting fractions of the peak from the peak maxima is similar, the isotopic compositions of those fractions are not of similar values. At the same time, the mixed clays give similar results for the first half and quarter fractions, while the pure kaolinite does not.

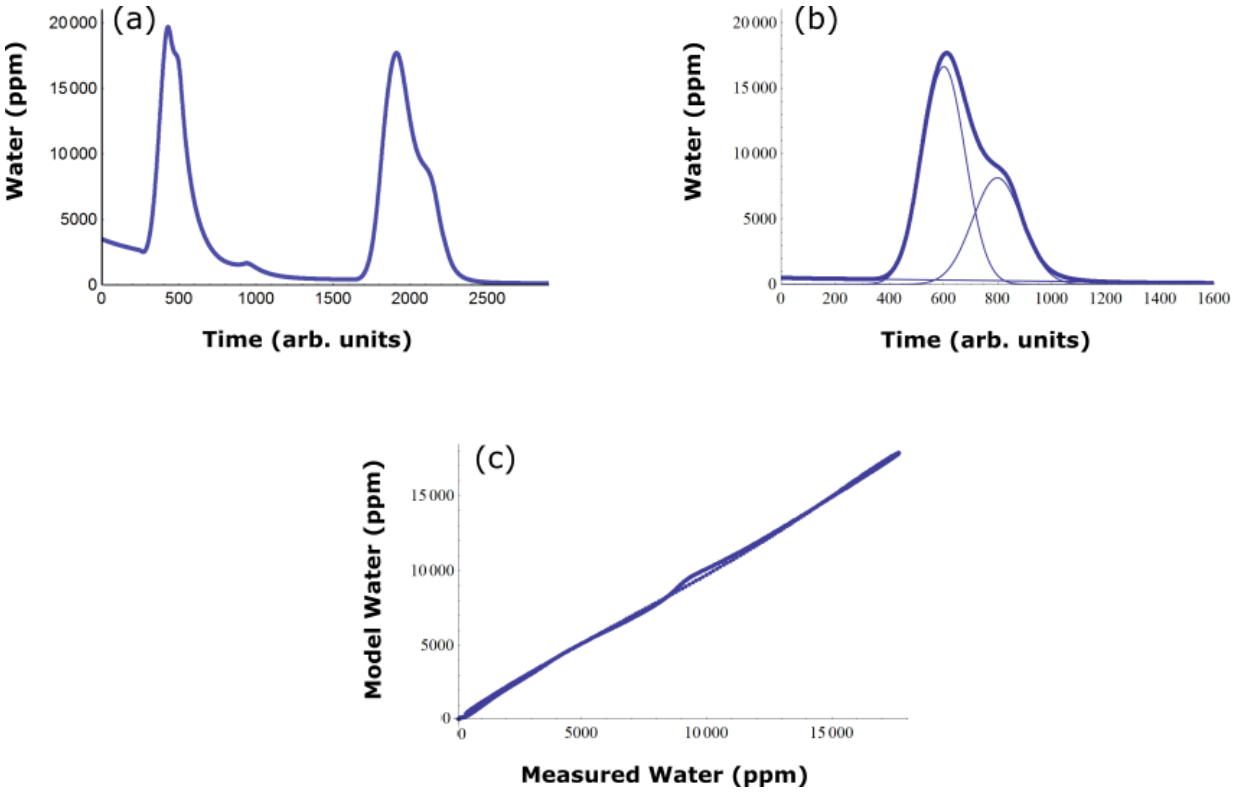

Figure 4.6. A series of graphs showing the accuracy with which the mixed clay dehydroxylation peak can be modelled as a combination of two Gaussian peaks and a linear background. The first graph, a, shows the total dehydration profile. The second graph, b, focuses on the dehydroxylation peak, and shows the component parts of the model – the two individual Gaussian peaks and linear background (thin blue lines), as is the modelled dehydration profile (the sum of the component parts), beneath the dehydration profile (thick blue line) – no deviation between the modelled dehydration profile and the actual profile is seen. The final graph, c, shows the water concentration values of the model against the measured water concentration values (thick blue line), and a 1:1 line (thin blue line).

4.4.4 Carbonate Removal

Measurements of the isotopic composition of the acid-treated kaolinite sample, alongside results for untreated kaolinite, are found in Table 4.10. I found no significant change in the $\delta^{18}O$ or δD signal after acid treatment. FTIR showed that the carbonate had been successfully removed (see Figure 4.7). This demonstrates that the chosen acid treatment is appropriate for carbonate removal when measuring clay hydroxyl water.

	Untreated Kaolinite	Offline-Measured Kaolinite	Kaolinite after acid treatment
No. Repeats	4	5	3
H_2O	3.28×10^6	-	3.55×10^6
H_2O Error	3.81×10^4	-	1.97×10^4
δD / ‰	–62.15	–62.57	–62.48
δD Error	0.67	3.70	0.23
$\delta^{18}O$ / ‰	6.63	5.80	5.97
$\delta^{18}O$ Error	0.92	0.55	0.07

Table 4.10. Comparison of DTIA measurement of kaolinite after carbonate removal treatment (acid treatment) compared to DTIA measurement and offline measurement of untreated kaolinite. The results are all within one standard deviation of each other, suggesting that acid treatment did not affect the isotopic composition of the hydroxyl water.

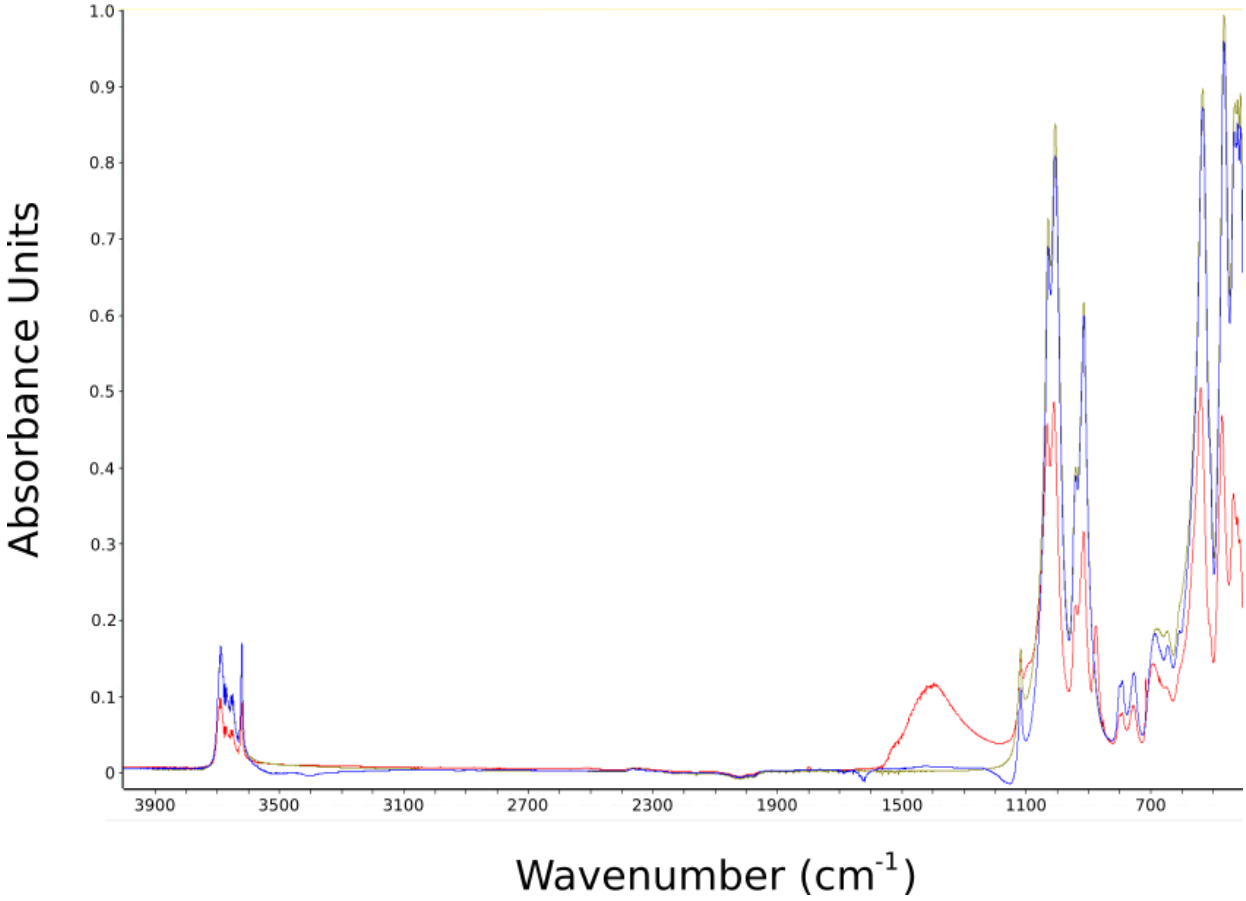

Figure 4.7. FTIR measurements of a kaolinite sample (green), the same kaolinite with added carbonate (red), and the same sample after acid treatment to remove carbonate (blue). The carbonate peak at 1400 cm^{-1} has been removed completely.

4.4.5 Clay Exchange Experiment

Results from the 23 month experiment where montmorillonite STx-1b was submerged in water with $\delta^{18}O$ and δD of –6.21 ‰ and –43.87 ‰ respectively are compared to untreated montmorillonite STx-1b results in Table 5.4.viii. We can see that the δD values of the water-immersed montmorillonite are significantly different to the δD of the untreated montmorillonite – the submerged montmorillonite is isotopically depleted in hydrogen in both the interlayer and hydroxyl water.

Water Type	Isotope Type	Montmorillonite STx-1b untreated		Montmorillonite STx-1b submerged	
		Value	Error	Value	Error
Interlayer Water	$\delta^{18}O$ / ‰	–2.98	0.43	–3.67	2.17
	δD / ‰	–37.84	0.92	–47.17	3.89
Hydroxyl Water	$\delta^{18}O$ / ‰	13.42	0.13	13.03	0.55
	δD / ‰	–41.60	0.57	–50.50	1.45

Table 4.11. Comparison of DTIA measurements of untreated montmorillonite STx-1b and montmorillonite STx-1b after submersion in water for 23 months. The interlayer and hydroxyl water δD values of the exchange-experiment montmorillonite shows increased errors, and both are shifted away from the δD value of the untreated montmorillonite. However, the $\delta^{18}O$ remains unchanged.

The oxygen isotopes do not show the same behaviour. There appears to be no change in the hydroxyl $\delta^{18}O$ in the submerged montmorillonite. It is difficult to tell if there is a change in the interlayer water, due to the large error in measurement.

It is worth noting that the errors for the isotopic measurements of the submerged sample are higher than seen for other clays when using DTIA, in particular for the interlayer water and hydroxyl hydrogen. This seems to be caused by some inconsistency or memory effect across sample measurement – successive measurements of the submerged samples show unidirectional changes in the isotopic composition measured (Table 4.12).

Additionally, the clay seems to have begun reacting over the 23 month time period. Figure 4.8 compares the dehydration profiles of the untreated and submerged montmorillonites – a small portion of the 23-month treated sample begins dehydroxylation early, showing a small dehydroxylation peak shoulder in the dehydration profile. This could in part explain the

memory effect seen in the results, if the sample, after spending 23 months submerged, reacted further under air.

Montmorillonite Sample	Water Type	Isotope Type	Measurement Number			
			1	2	3	4
Untreated	Interlayer Water	δD / ‰	–36.60	–38.21	–37.76	–38.78
		$\delta^{18}O$ / ‰	–2.38	–3.14	–3.00	–3.38
	Hydroxyl Water	δD / ‰	–42.44	–41.18	–41.43	–41.35
		$\delta^{18}O$ / ‰	13.56	13.34	13.50	13.29
Submerged	Interlayer Water	δD / ‰	–51.3	–49.45	–45.08	–42.83
		$\delta^{18}O$ / ‰	–5.85	–5.12	–2.38	–1.31
	Hydroxyl Water	δD / ‰	–52.08	–52.31	–50.36	–49.26
		$\delta^{18}O$ / ‰	12.25	13.43	13.02	13.40

Table 4.12. Measurement-by-measurement results of the exchange montmorillonite sample, compared to untreated montmorillonite. The submerged sample shows a strong `memory effect` like trend in the interlayer water isotopic compositions. This is significantly less strong in the hydroxyl water, but the hydroxyl hydrogen results do show a slight directional trend across measurements.

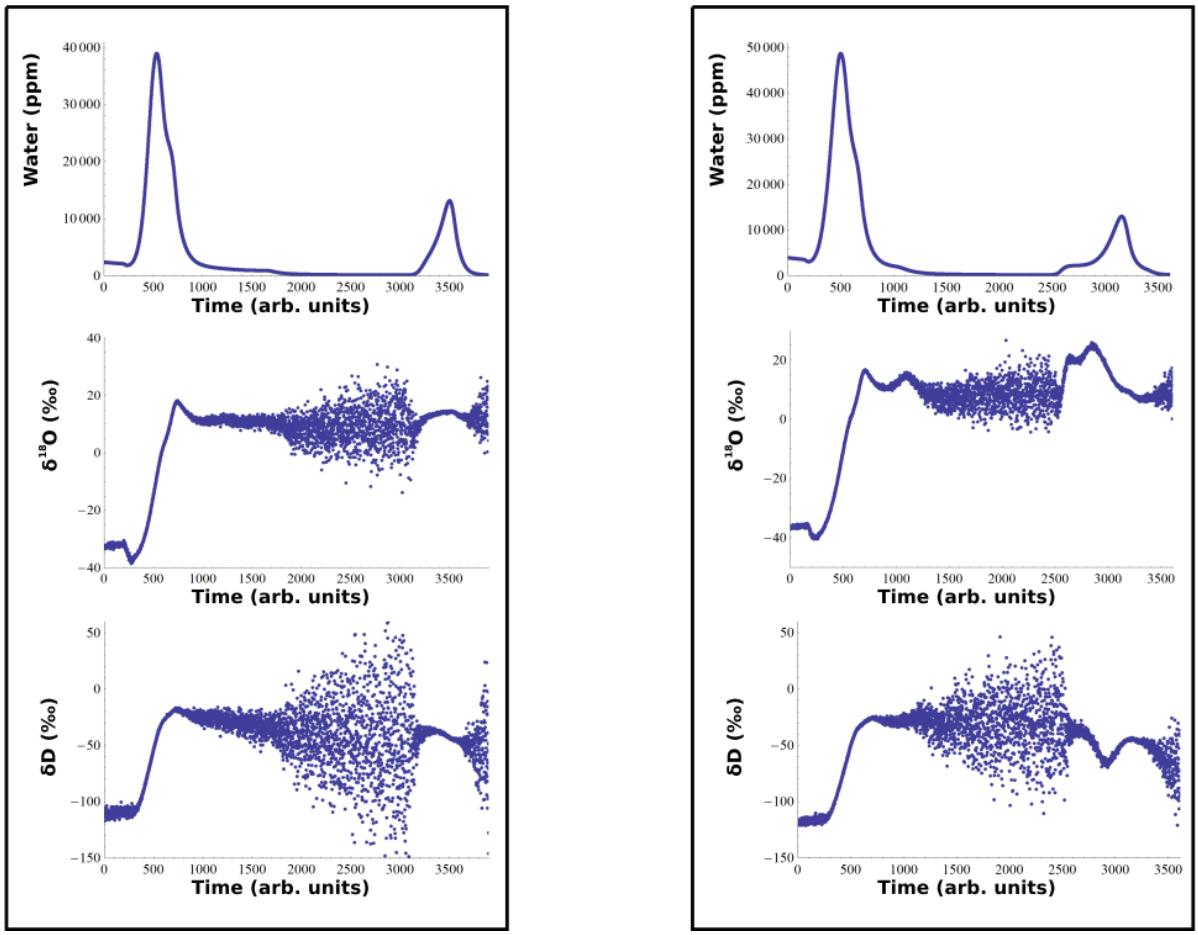

Figure 4.8. A comparison of the dehydration profiles of untreated montmorillonite (left) and montmorillonite that had been submerged in water for 23 months (right). The untreated montmorillonite has a narrower dehydroxylation peak, while the water-treated montmorillonite dehydroxylation peak starts at a lower temperature with a broad shoulder.

4.4.6 PETM Clay Measurement

As shown in Figure 4.9 for two PETM clay samples of differing clay composition, the three dehydration peaks can be separated into individual sharp peaks, enabling the isotopic composition of each to be measured accurately. No differentiation between the component clay hydroxyl waters can be seen within the final dehydroxylation peak, so no attempt was made to deconvolve the OH peak. The results of the PETM clay measurements are discussed in Chapter 5.

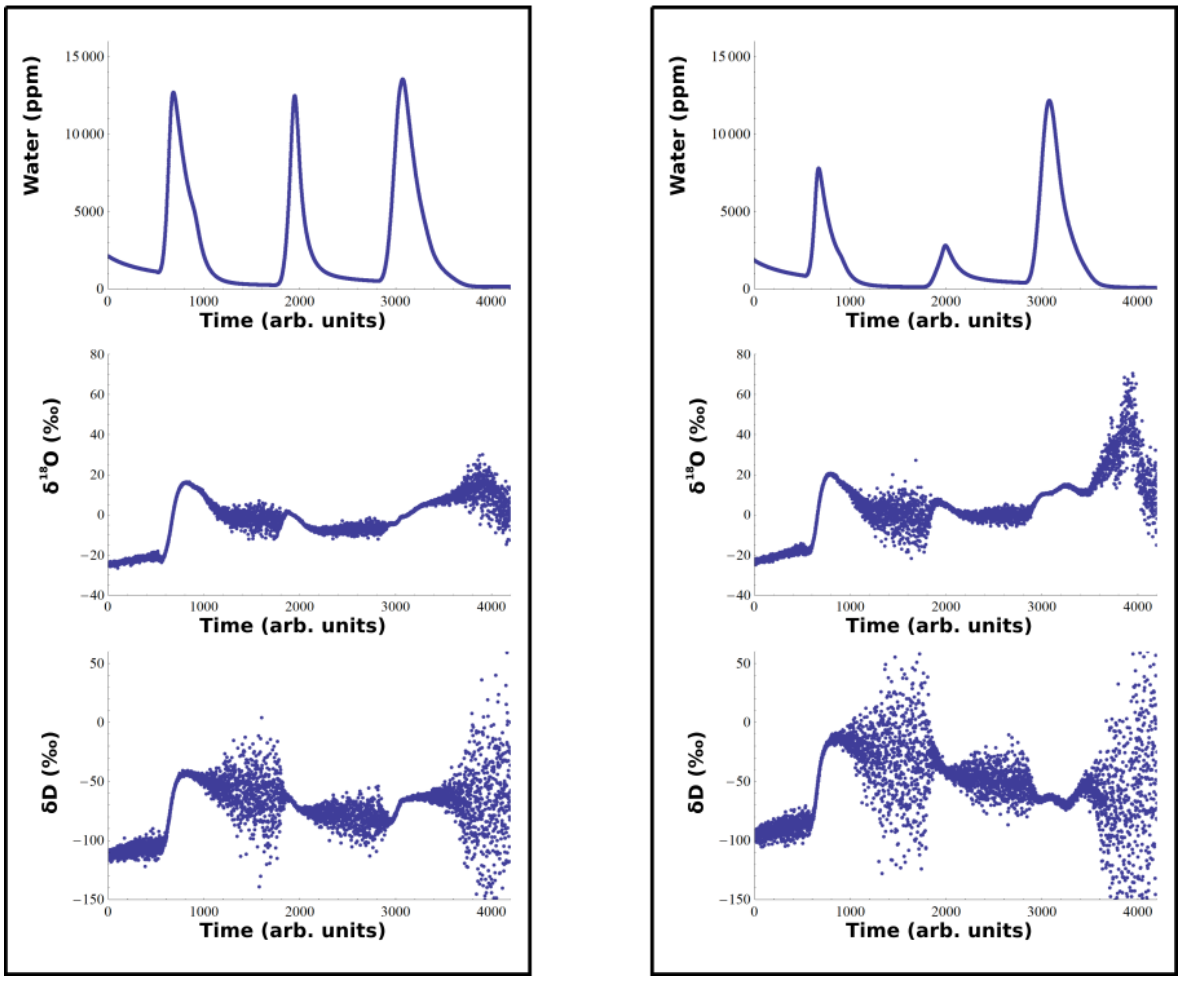

Figure 4.9. A comparison of the final measured dehydration profiles of two PETM samples from depths: a) 2613.48 m, and b) 2616.34 m. The first and second peaks likely reflect exchangeable interlayer water. The second peak varies in size across the samples, being between 12-51 % of the size of the third peak, and thus is too small for accurate isotopic measurements. Including the second peak as part of the hydroxyl peak in isotope analysis leads to only small changes in reported values, and does not change the overall hydroxyl isotope trends; given this, and the fact that the second peak is removed at lower temperatures than one would expect dehydroxylation to occur at for any of the clays present, it is safe to ignore the second peak when calculating the hydroxyl isotopic compositions of the samples (even though the origin of the peak is not known).

4.5 Discussion

4.5.1 Clay Dehydration Experiments

The results demonstrate that the isotopic composition of clay hydroxyl groups can in isolation be measured accurately using DTIA. While not all measurements were carried out to a high precision, as noted with the talc later, the larger errors arising from having initial measurements not match subsequent measurements can be lessened through use of a platinum-rhodium crucible, and can also be overcome by running an extra sample and ignoring the first result for the most accurate measurements. At the same time, errors are still comparable to recent isotopic studies of clay minerals (e.g. Yang *et al.*, 2017, where uncertainties were estimated at ± 3 ‰ for δD and ± 0.3 ‰ for $\delta^{18}O$). It is possible that a more rigorous cleaning method is required for the crucibles between measurements – perhaps sonication followed by heating to a high temperature to drive off excess water would reduce errors slightly.

4.5.1.1 Kaolinite ($Al_2Si_2O_5(OH)_4$)

Kaolinite DTIA measurements are simple to carry out, as the structure of kaolinite does not contain any interlayer water or structural water, only hydroxyl groups, with the possibility of some water absorbed on the surface of the clay. As such, isothermal steps may seem of lesser importance, as it is likely that background water levels will return to low amounts before the temperatures for dehydroxylation are reached. However, they are still worth including in case of isotopic exchange between atmospheric water and the kaolinite hydroxyl in a hot furnace, or possible exchange reactions between oxygen in the air, and the kaolinite structure and released water.

As these were the first measurements carried out for dehydroxylation experiments, errors are somewhat high for kaolinite. Repeat measurements using current methods (slightly more sample, faster ramp rates and shorter isotherms at higher temperatures) would improve the accuracy and approach the errors for other clays (as in fact seen in the acid treatment experiments). As discussed in Chapter 2, DTIA measurements agree with other offline

measurements of the kaolinite hydroxyl isotopic composition, and with previous measurements of the kaolinite hydroxyl δD (Sheppard, 1977).

4.5.1.2 Montmorillonite ($(Na,Ca)_{0.33}(Al,Mg)_2(Si_4O_{10})(OH)_2 \cdot nH_2O$)

The montmorillonite measurements serve to show that both clay standards and more heavily eroded clays, such as the Ethiudna montmorillonite, whose broad dehydroxylation was characteristic of a degraded smectite, can be measured by DTIA. It is not known whether the erosion of the Ethiudna montmorillonite had an effect on the isotopic composition of the hydroxyl group, as it was not possible to measure samples of the same origin which were less heavily eroded. It has previously been suggested that clay hydroxyl hydrogen isotopically exchanges as part of the transport process during the weathering of clays (Lawrence and Taylor, 1972), but the study is inconclusive, and I am unaware of further work on this topic.

4.5.1.3 Nontronite ($CaO_{0.5},Na)_{0.3}Fe^{3+}{}_2(Si,Al)_4O_{10}(OH)_2 \cdot nH_2O$

It is unclear why the nontronite sample showed a memory effect, while most other samples did not. Unlike the synthetic talc, it does not dehydroxylate at an especially high temperature. It is possible that it is related to the prior sepiolite measurement (where δD is ≈ 30 ‰ lower than for nontronite).

4.5.1.4 Palygorskite ($(CaO_{0.5},Na)_{0.3}Fe^{3+}{}_2(Si,Al)_4O_{10}(OH)_2 \cdot nH_2O$)

No particularly interesting results pertaining to palygorskite were found by our preliminary measurements. However, given that the dehydration of bound water in palygorskite is likely due to structural changes (as known for sepiolite), it is possible that a detailed study on a number of palygorskite and sepiolite studies using the difference in isotopic composition between the bound water peaks could tell us about the sites from which water is removed last, and the kinetics of the dehydration from these sites. If the separation of bound water into the two peaks upon dehydration was purely kinetic, we would expect the second bound water peak removed at higher temperatures to have heavier isotopes for both hydrogen and oxygen, which is not seen in our results for palygorskite (with the caveat that the first bound water peak has a low water content).

4.5.1.5 Rectorite ($(Na,Ca)Al_4((Si,Al)_8O_{20})(OH)_4 \cdot 2H_2O$)

The origin of the second dehydration peak between 220-340 °C does not appear to be discussed in the literature of clay thermal analysis. The temperature range appears too low to be due to a dehydroxylation process (clay mineral dehydroxylation typically starts at temperatures higher than 400 °C (Smykatz-Kloss, 2003), though dehydroxylations beginning at temperatures as low as 340 °C and 350 °C have been reported for gibbsite (Smykatz-Kloss, 2003) and iron-rich illites (Murad and Wagner, 1995), respectively – note that the iron-rich illite dehydroxylation was centred around the much higher temperature of 565 °C). Determining the origin of this peak is of interest, given that it appears at slightly higher temperatures in the PETM clays (which contain a significant portion of illite-smectite, though not necessarily in a 1:1 dioctahedral smectite to dioctahedral mica ratio), and given that different types of illite-smectite are very common in clay mixtures which have formed from or undergone some hydrous alteration.

4.5.1.6 Talc ($Mg_3Si_4O_{10}(OH)_2$)

The cause of talc having a much stronger memory effect than the other samples is likely due to the high temperature of its dehydroxylation. Higher temperatures would be expected to increase the rate of exchange, so if exchange is occurring with oxygen-containing crucibles, it should occur fastest for the synthetic talc samples. This is observed in experiments carried out by Koehler and Wassenaar (2012), though it is unclear whether they are seeing exchange with molecular oxygen from the dry air carrier gas only, or both exchange between molecular oxygen and released water and between materials used in the furnace (quartz in this case) and released water. Certainly the study demonstrates the importance of using dry nitrogen as a carrier gas, and combined with our results from using the aluminium oxide crucibles, it seems likely that both types of exchange occur, and hence that using a crucible type that does not contain oxygen is important for high temperature DTIA measurements.

4.5.2 Isotherm Length Experiments

The results of these experiments demonstrate the need to keep isothermal steps as short as possible, while still maintaining peak separation, rather than removing interlayer and bound water over extended dehydration periods, as has been done in previous studies attempting to

measure clay hydroxyl isotopic composition (for examples see: Bell and Ihinger, 2000; Gong and Chen, 2007; Bauer and Vennemann, 2014). However, it is important to note that previous studies isolated the clay hydroxyl group by dehydrating interlayer water at lower temperatures and often under vacuum, so it is unlikely that any exchange effects will have been nearly as prominent in these studies as they were in the results of my experiments – although we cannot discount the possibility of exchange between hydroxyl oxygen and the clay bulk oxygen, which my results do not give conclusive evidence for or against. The results most importantly show that small isotherms do not change the results of measurement, meaning that even if it is possible that the theoretically optimum measurement would dehydrate unwanted water using vacuum over a short time period, it is in practice unnecessary for DTIA measurements.

4.5.3 Mixed Clay Experiments

The results of the mixed clay experiments are very important for the theoretical utility of DTIA when examining geological samples containing mixed clays. If the expected values had not matched the measured values, meaning that the presence of other clays affected the hydroxyl measurement of the total hydroxyl water, it would have suggested that even single clays experience exchange between the structural bulk oxygen and the hydroxyl oxygen when heated. As this is not the case, it seems that clay hydroxyl measurement can indeed be used to measure distinct signals. The results also suggest that the dehydration of interlayer water does not facilitate exchange between interlayer water and hydroxyl water, as the total hydroxyl composition does not move towards the isotopic composition of the montmorillonite STx-1b interlayer water. Finally, the results clearly demonstrate that the hydroxyl groups of mixtures of clays can be accurately measured by DTIA, even if individual hydroxyl peaks cannot be isolated.

The results of the partial peak analysis also have interesting implications for DTIA. Either the added material is causing the dehydroxylation to proceed through a different mechanism, so have a different isotopic profile, which seems unlikely, or at high temperatures we are seeing some amount of exchange between the hydroxyl group hydrogen of the two clays. The change in $\delta^{18}O$ when comparing the mixed clay to pure kaolinite likely arises from the failure to isolate water from only kaolinite, even when considering the first quarter peak of the dehydroxylation. This is consistent with the mixed first half peak and first quarter peak

values for $\delta^{18}O$ being closer to the values for kaolinite than to the values for montmorillonite STx-1b. The same is not true for the δD values, suggesting that more is occurring than simply the failure to isolate only kaolinite hydroxyl-derived water.

4.5.4 Carbonate Removal

The importance is carbonate removal is clear from our experiments, and treatment with weak acid appears to be an effective solution for carbonate removal, removing all carbonate without affecting the hydroxyl isotopic composition. However, there are some downsides to using a water-based decarbonation method. In particular, any interlayer water in the clay sample is likely to partially exchange over the course of the acid treatment, so even if local water had been preserved in the clay sample, it would not be possible to accurately measure the isotopic composition of that water after acid treatment. Moreover, dolomite is not able to be removed through use of a weak acid, but treatment by strong acids (such as HCl) is damaging to clay samples, and HCl in particular was found to cause partial dissolution of the synthetic talc sample. At this stage, it seems that removal of dolomite is reliant on physical separation methods, such as use of a flotation cell.

4.5.5 Clay Exchange Experiment

The clay exchange experiment highlights limitations of exchange studies when it comes to examining clay isotopic composition, rather than directly informing us of the likelihood of isotopic exchange in clays. The possibility of a smectite clay (montmorillonite) reacting over the course of two years was not one I anticipated when choosing the test sample. Further exchange experiments are clearly indicated. However, it would be of great interest to know if these clay-alteration reactions lead to a change in the hydroxyl isotopic composition, as this would have implications for the information recovered from altered clays, specifically whether altered clays preserve information about the alteration conditions, or about the original conditions the clay formed in before alteration. As a montmorillonite was chosen for the exchange experiment, it is unclear if the change to the dehydroxylation profile was due to the start of a transition to an illite-smectite clay, or whether it is due to the montmorillonite degrading from cis-vacant to trans-vacant, hence lowering the dehydroxylation temperature (Cuadros and Altaner, 1998; Emmerich and Kahr, 2001).

The isotope results themselves fit with other published research. In particular, long-term water exchange experiments carried out on the hydroxyl groups of volcanic ash found that only the hydrogen isotopic composition changed over a period of 20 months, even when carried out at elevated temperatures of 70 °C (Nolan and Bindeman, 2013). As such, we would expect clay hydroxyl groups to similarly only exchange hydrogen isotopes, which is what our preliminary experiments seem to indicate. The depletion seen in the submerged sample would be consistent with equilibrium isotopic exchange between the sample and submersion water; although there is no published value for αD_{OH} for montmorillonite, if we assume that it is of a similar magnitude to other smectites (kaolinite and illite-smectite, where at 30 °C αD_{OH} is equal to –31.64 and –54.73 respectively), then we would expect montmorillonite δD to reach equilibrium with the submersion water between –99 and –74 ‰. This is significantly more depleted than the measured δD, suggesting that if exchange is the cause of the shift, then the montmorillonite sample is not close to equilibrium with the submersion water.

Prior research has been carried out specifically on the exchangeability of clay hydroxyl isotopes, but it is important to note that the prior mentioned limitations of my experiments seem to apply to other studies of clay hydroxyl isotopic exchange. Clays have found use as suitable burial material for nuclear waste, and as such experiments have been carried out to investigate the capacity of clays to absorb tritium isotopes (e.g. Lytovchenko *et al.*, 2005; López-Galindo *et al.*, 2008), where, in contrast to older research (e.g. Moun and Rosenqvist, 1958), they found that water liberated from clays at higher temperatures (in the dehydroxylation region) is affected by hydrogen-tritium exchange. However, it is difficult to compare changes in the number of tritium atoms to large scale changes to δD, as tritium concentrations are unknown (but typically very small), and the exact methods used for the dehydration, and subsequent trapping, of clay interlayer and hydroxyl water are not clear. Moreover, while the finding that tritium exchanges after short periods of time is not affected by the possibility of clay reaction, experimental results for the longer experiments do not take the possibility into account. Earlier research into isotopic exchange by O'Neil and Kharaka (1976) suggested that at temperatures over 100 °C (and up to 350 °C) both hydrogen and oxygen could exchange with solutions over periods of two years, with hydrogen exchange occurring at a much faster rate, and with exchange occurring much faster when facilitated by interlayer water. However, results from high temperatures are not applicable to all natural clay samples, and again the water separation achieved in these experiments is not perfect.

The authors do however note that over 350 °C significant clay reactions occur, which do not appear to affect the $\delta^{18}O$ values significantly – this is certainly of further interest.

Outside of laboratory-based exchange experiments, some evidence for hydroxyl hydrogen isotope exchange in kaolinite has been found in ancient North American kaolinites (Lawrence and Meaux, 1993), though for some kaolinites this appears to have occurred only during burial and uplift in the early Cenozoic. For other kaolinites, the causes of δD values not reflecting the meteoric mother water δD values are unclear.

4.5.6 PETM Clay Measurement

When examining the PETM clay measurements, it is slightly unsatisfactory that the second peak is only assigned by comparison to component clays, without a good understanding of what that second peak represents in the component clay. However, the amount of water in the second peak is generally very small in the samples, such that even if the analysis includes the second peak, only small changes to the magnitudes of results ensue, rather than any changes in the overall trend. For discussion of the results, see Chapter 5.

4.6 Conclusion

Measurements of pure clays demonstrate that accurate measurements of the hydroxyl groups of clay minerals are achievable for a number of different clays using DTIA, using a significantly less labour intensive process than previous methods for isotope measurement. The errors in measurement are reasonable, and broadly consistent with those published in recent isotopic studies, though in general δD measurements are more accurate for DTIA, while $\delta^{18}O$ measurements are of similar accuracy. It would be of potential further interest to test the types of heating steps used in the broader literature on clay water isotope analysis, to determine if holding clays at temperatures between 150-300 °C under vacuum leads to isotopic exchange, as seen in our long isotherm experiments. Further examination of mixed clays, and how peaks might be separated analytically by modelling of the measured δD and $\delta^{18}O$ curves in addition to modelling the water concentration curve, would also be of use in natural sample cases where peak separation cannot be fully achieved through the use of DTIA. Additionally, while only carbonate was dealt with as a major contaminant in this chapter, geological samples often contain major proportions of non-clay minerals prior to physical separation. As physical separation of clay minerals is labour intensive, quantifying the effect of non-clay mineral contamination on DTIA accuracy would also be highly useful for assessing what degree of sample separation is required.

However, the most important area of clay isotope measurement that requires further work is the potential of clay mineral hydroxyl groups to isotopically exchange while in contact with water, and how reactions with the water might affect the measured isotopic composition of the final altered clay. This is crucial for knowing what information diagenetic clays retain for palaeoclimatic analysis – that is to say, whether information from the original formation environment of the precursor clay is retained, or if information from the environment under which diagenesis occurs is retained.

5 Enhanced Paleocene-Eocene Thermal Maximum Hydrology Inferred from Clay Hydroxyl Isotopes

Note on Authorship

The results and much of the rest of this chapter have been published as the paper 'Clay hydroxyl isotopes show an enhanced hydrological cycle during the Paleocene-Eocene Thermal Maximum' in *Nature Communications*. I am the primary author of this paper. The chapter includes some results from experiments carried out by co-authors:

- preparation of the 4 μm clay fraction
- measurements of clay bulk oxygen isotopes

Walters, G. L., Kemp, S. J., Hemingway, J. D., Johnston, D. T., & Hodell, D.A. (2022). Clay hydroxyl isotopes show an enhanced hydrologic cycle during the Paleocene-Eocene Thermal Maximum. Nature Communications, 13, 7885. doi:10.1038/s41467-022-35545-2

5.1 Abstract

The Paleocene-Eocene Thermal Maximum (PETM) was an abrupt global warming event associated with a large injection of carbon into the ocean-atmosphere system, as evidenced by a diagnostic carbon isotope excursion (CIE). Evidence also suggests substantial hydrologic perturbations, but details have been hampered by a lack of appropriate proxies. To address this shortcoming, the isotope composition of hydroxyl groups (OH^-) in clay minerals from a highly expanded PETM section in the North Sea Basin were isolated and measured, together with their bulk oxygen isotope composition. At this location, hydroxyl O- and H-isotopes are shown to be less influenced than bulk values by clay compositional changes due to mixing and/or inherited signals and thus better track hydrologic variability. Clay OH^- hydrogen-isotope values (δ^2H_{OH}) are found to decrease slowly prior to the PETM and then abruptly by ~8 ‰ at the CIE onset. Coincident with an increase in relative kaolinite content, this indicates increased rainfall and weathering and implies an enhanced hydrologic cycle

response to global warming, particularly during the early stages of the PETM. Subsequently, δ^2H_{OH} returns to pre-PETM values well before the end of the CIE, suggesting hydrologic changes in the North Sea were short-lived relative to carbon-cycle perturbations.

5.2 Introduction

The Paleocene-Eocene Thermal Maximum (PETM) represents an intense global warming event that occurred approximately 55.5 Ma (Kennett and Stott, 1991; Thomas *et al.*, 2002; Zachos *et al.*, 2003; Sluijs *et al.*, 2006; Westerhold *et al.*, 2017; for summary, see McInerney and Wing, 2011). While the exact cause of the PETM remains uncertain, several diagnostic markers exist in the geological record, including a prominent carbon isotope excursion (CIE) of approximately 3-4 ‰ at the PETM onset and widespread dissolution of marine carbonates (Kennett and Stott, 1991; Thomas *et al.*, 2002; McInerney and Wing, 2011). This carbon injection led to average global temperature increases of 4-5 °C (Kennett and Stott, 1991; Thomas *et al.*, 2002; Sluijs *et al.*, 2006), oceanographic changes including deoxygenation and acidification leading to mass benthic extinctions (Schmidt *et al.*, 2018), and perturbations in the hydrologic cycle (Carmichael *et al.*, 2017).

The global hydrologic cycle is thought to have changed during the PETM relative to today, but large regional variability likely existed (for summary, see Carmichael *et al.*, 2017). Palynological and biomarker isotope studies suggest sustained increases in terrestrial runoff, both in the tropics (e.g. Venezuela; Jaramillo *et al.*, 2010) and in high-latitude regions (e.g. Arctic Spitsbergen (Harding *et al.*, 2011), New Zealand (Crouch *et al.*, 2003), North Sea (Kender *et al.*, 2012), and Arctic Ocean (Pagani *et al.*, 2006)). In contrast, sedimentological, palynological, and palaeosol data imply either increasing aridity (e.g. southern Rocky Mountains (Bowen and Bowen, 2008) and Tanzania (Handley *et al.*, 2008)) or strong seasonality and extreme rainfall events in the subtropics to lower mid-latitudes (e.g. Spanish Pyrenees (Schmitz and Pujalte, 2007) and Normandy (Garel *et al.*, 2013)). Despite these general trends, large uncertainty persists in our quantitative understanding of PETM hydrologic cycle and the timing of these changes relative to the CIE.

Improving constraints on the PETM hydrologic cycle is of particular relevance for ongoing and future climate change. Anthropogenic warming is predicted to exceed 2 °C by the end of this century even under the stabilisation (RCP6.0) greenhouse gas scenario (Stocker *et al.*, 2013). Such warming will likely increase hydrologic-cycle intensity, thus exacerbating environmental stress (Trenberth *et al.*, 2003; Dai, 2006). Current models suggest an enhanced hydrologic cycle with elevated precipitation driven by higher evaporation rates

(Houghton *et al.*, 2001; Held and Soden, 2006; Seager *et al.*, 2010), a pattern which already may be beginning to emerge. However, while spatial changes in total precipitation amount can be modelled accurately, climate models are not yet precise enough to predict spatial variations in the frequency, seasonality, intensity or type of precipitation (Dai, 2006; Sun *et al.*, 2006). Testing whether current climate models can simulate the observed hydrologic responses to temperature during the PETM will aid in assessing future hydrological projections in response to global warming.

Large variations in clay mineralogy are recorded in sediments deposited over the PETM in response to changing climate conditions. A major unresolved observation of the PETM is that many mid- to high-latitude sections record a conspicuous increase in the deposition of kaolinite (e.g. Gibson et al., 1993, 2000; Robert and Kennett, 1994; Bolle et al., 2000; Kelly et al., 2005; Dypvik et al., 2011; Soliman et al., 2011; John et al., 2012; Khozyem et al., 2013; Bornemann et al., 2014; Chen et al., 2016). Kaolinite is a clay mineral that is generally assumed to form predominantly by intense weathering in humid tropical climates (White and Brantley, 1995; Thiry, 2000; Egger *et al.*, 2002). The origin and significance of PETM kaolinite deposition is controversial, because it could result from either: (i) increased chemical weathering and kaolinite formation under warmer climate and elevated year-round precipitation (Robert and Kennett, 1994; Gawenda *et al.*, 1999; Bolle and Adatte, 2001; Clechenko, 2007), or (ii) enhanced mobilization, physical transport, and exhumation of previously weathered material (e.g. laterite soils) during strong seasonal rainfall events (Thiry, 2000; John *et al.*, 2012; Kemp *et al.*, 2016; Carmichael *et al.*, 2018). While the former interpretation of increased chemical weathering is consistent with a direct negative silicate-weathering feedback to elevated temperatures (Walker *et al.*, 1981), the latter of increased physical weathering provides a less direct feedback and may indicate a decoupling between climate and weathering intensity. The two processes are not mutually exclusive and evidence exists that both may have occurred at the time of the PETM in different settings.

To provide such constraints, online DTIA was used to measure the isotopic composition of clay hydroxyl groups from an expanded PETM section in the Sele Formation, North Sea (well 22/10a-4 (57°44′8.47″N; 1°50′26.59″E; up to ~500 m water depth); Figure 5.1; Kender *et al.*, 2012; Kemp *et al.*, 2016). During the early Palaeogene, the North Sea was a restricted marine basin, bounded by Scotland to the north, Greenland to the west and the Fenno-Scandian Shield to the east. The basin contains a highly expanded Paleocene-Eocene

transition sequence, uninterrupted but for minor erosion at the base of thin turbidite sandstones (Kender *et al.*, 2012). Terrigenous input was high during the Palaeogene and thought to be derived primarily from the Scotland Faeroe-Shetland landmass (Knox, 1998), making this an ideal location to study mid-latitude PETM hydrologic variability. Furthermore, by isolating and measuring the hydrogen and oxygen isotope composition of clay hydroxyl groups ($\delta^{2}H_{OH}$ and $\delta^{18}O_{OH}$) in addition to bulk clay $\delta^{18}O$ ($\delta^{18}O_{bulk}$), the approach used aims to avoid potential biases by clay end-member mixing and/or inherited isotopic compositions (John *et al.*, 2012). The record is thus expected to robustly track PETM hydrologic variability.

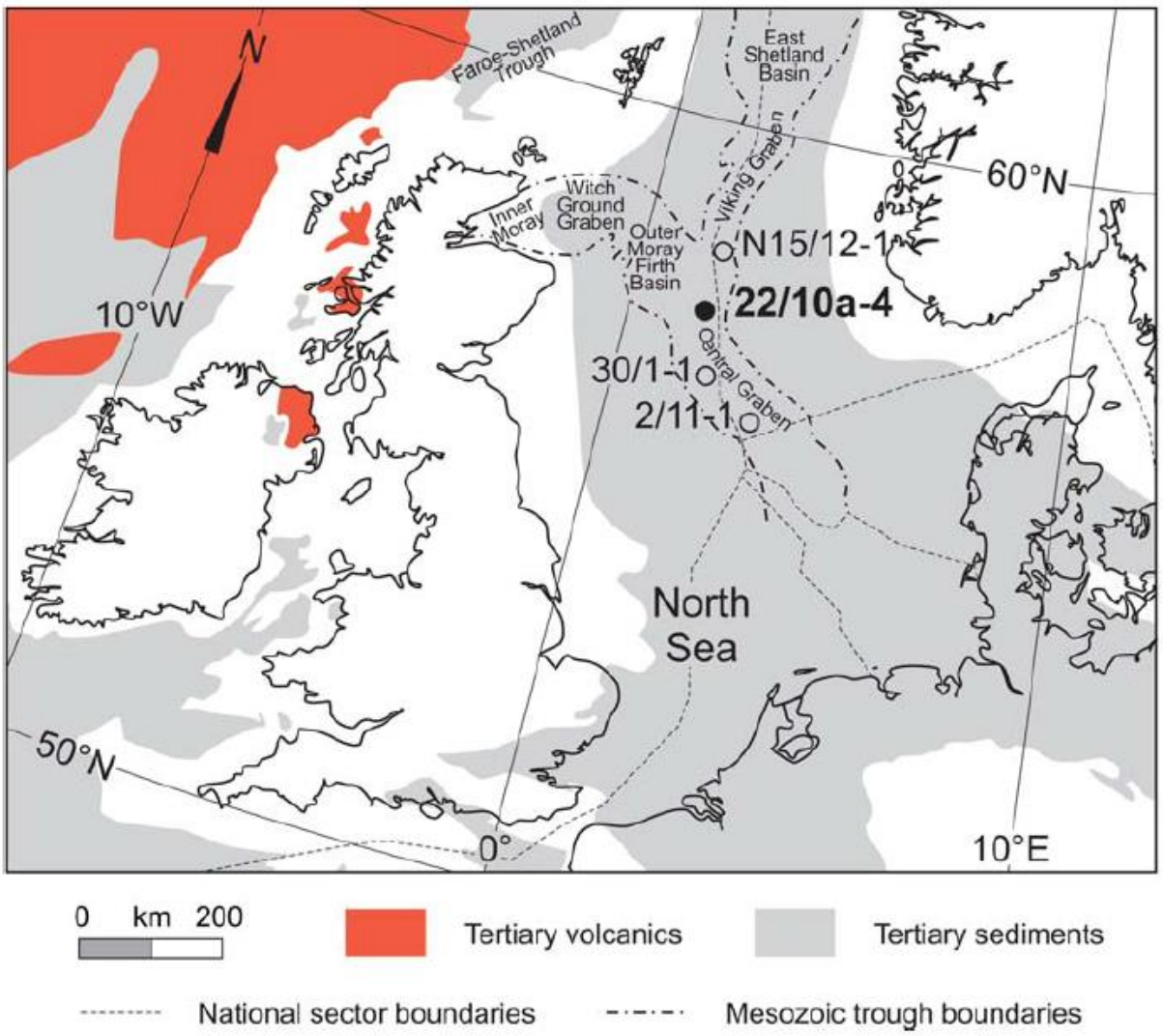

Figure 5.1. Map of the North Sea Basin, showing the location of well 22/10a-4 and the surrounding geological features and Palaeogene deposits. Figure 5.1 is reproduced from Kemp, S., Ellis, M., Mounteney, I., & Kender, S. (2016). Palaeoclimatic implications of high-resolution clay mineral assemblages preceding and across the onset of the Paleocene–Eocene Thermal Maximum, North Sea Basin. Clay Minerals, 51(5), 793-813. © The Mineralogical Society of Great Britain and Ireland 2016, published by Cambridge University Press, reproduced with permission.

5.3 Materials and Methods

5.3.1 Materials

Measurements of 22 samples consisting of separated <4 μm size fractions of sediment samples across the PETM from the Sele Formation were made in this research, taken from well 22/10a-4 (57°44′8.47″N; 1°50′26.59″E; up to ~500 m water depth; Figure 5.1) located in the central North Sea. Samples of the same <4 μm size fractions were used previously for a clay mineralogical study (Kemp *et al.*, 2016).

5.3.2 Methods

5.3.2.1 Sample Preparation and Measurement – Hydroxyl Isotopes

Details of the initial preparation and isolation of the <4 μm samples are given by Kemp *et al.*, 2016. Details of further preparation for DTIA measurement and the specifics of the DTIA measurements are given in Chapter 4.

Three to four DTIA measurements were taken at each depth (at 2610.82 m, only two measurements could be taken, due to having limited sample). Errors (1 σ) were calculated from the standard deviation of the measurements at each depth.

5.3.2.2 Sample Analysis – Hydroxyl Isotopes

To calculate the fractionation factor corrected δ^2H values from the hydroxyl δ^2H, which should represent the approximate mother water hydrogen isotopic composition, a number of assumptions are required. Not all clays have hydroxyl fractionation factors reported in the literature, so it must be assumed that the hydroxyl water was derived from a mixture of illite-smectite and kaolinite only. The proportion of hydroxyl water that each clay mineral would contribute to the total hydroxyl water is then calculated, by comparing the proportions of each clay in the assemblage to the relative weight percentage of hydroxyl in the clay chemical formulae, assuming a typical clay elemental composition. For illite-smectite, it is assumed that changes to the percentage composition of illite, $K_{0.65}Al_{2.65}Si_{3.35}O_{10}(OH)_2$, and

montmorillonite, $Na_{0.1}Ca_{0.23}Al_2Si_4O_{10}(OH)_2(H_2O)_{11.66}$ (assuming the montmorillonite is 36.1 % water by weight), do not affect the fractionation factor, but do change the proportion of hydroxyl isotope contributed. The mother water values were then estimated by applying the fractionation factors weighted by the water amounts contributed by each clay:

$$\delta^2\mathrm{H_{mw}} = \delta\mathrm{D_{OH}} - [1000 \ln \alpha^2\mathrm{H_{kaolinite}} \times f_H H_2O_{kaolinite} + 1000 \ln \alpha^2\mathrm{H_{illite-smectite}} \times (1 - f_H) H_2O_{\mathrm{illite-smectite}}]$$

where:

$$f_H = \frac{\%_{kaolinite} \times \%_{OH\ in\ kaolinite}}{(\%_{kaolinite} \times \%_{OH\ in\ kaolinite} + \%_{illiite-smectite} \times \%_{OH\ in\ illite-smectite})}$$

$\alpha^2\mathrm{H_{mineral}}$ is the water-mineral hydrogen fractionation factor, and $\delta^2\mathrm{H_{mw}}$ is the estimated mother water value for δ^2H. Hydrogen fractionation factors at 30 °C are taken from Gilg and Sheppard, 1996, and Hyeong and Capuano, 2004, for kaolinite and illite-smectite respectively. The $\delta^2\mathrm{H_{mw}}$ is also estimated assuming compositions of 100 % kaolinite and 100 % illite-smectite, to account for the spread of possible values for $\delta^2\mathrm{H_{mw}}$ in lieu of error calculations (where the largest error is caused by not having fractionation factors for an average of ~25 % of the hydroxyl isotope contribution).

No accompanying measured values for hydroxyl oxygen fractionation in clays exist in the literature. As such, it was not possible to carry out this analysis for hydroxyl oxygen. Fractionation factors for bulk oxygen do exist; however, the samples contain considerable amounts of quartz of unknown provenance (up to 31 %). For such an analysis to be useful, the quartz would have to be separated from the clay fraction, or the oxygen contribution of the quartz otherwise constrained.

It is worth noting that, with accurate fractionation factors and quartz constraints, the hydroxyl oxygen data (or bulk oxygen data, assuming that the hydroxyl and bulk signals originate from the same mother water) and hydroxyl hydrogen data could be combined to find the formation temperature of a hydroxylated mineral. For example, the fractionation factors detailed in Sheppard and Gilg (1996) for bulk oxygen have a dependence on T^{-2}, and the hydrogen fractionation factor in Hyeong and Capuano (2004) has a dependence on T^{-1}. As such, the fractionation factors in the mother water calculations can be substituted for expressions

dependent on temperature, leaving the mother water isotopic composition and the temperatures as unknowns. The mother water δD and $\delta^{18}O$ are linked, however, by the global meteoric water line (GMWL) – as such, we can treat the deuterium and oxygen equations as simultaneous equations, and can eliminate the mother water isotopic composition to find an expression dependent only on measured values and temperature. In practice, without these fractionation factors and quartz constraints, the values found from this method using the bulk oxygen data do not appear to mirror reasonable temperatures (ranging from –73 to 35 °C).

Mineral	Reference	1000 ln α (Hydroxyl Hydrogen) at 30 °C
Kaolinite	Gilg and Sheppard (1996)	–31.64
Illite-smectite	Hyeong and Capuano (2004)	–54.73

Table 5.1. The hydroxyl hydrogen fractionation factors used in this research.

5.3.2.3 Sample Preparation and Measurement – Bulk Oxygen Isotopes

Samples were first treated with 1 M hydrochloric acid (HCl) at a greater than 40:1 liquid to solid ratio for four hours to remove carbonates. This is unsuitable for hydroxyl δD measurements as it leads to hydrogen isotope exchange, but it does not cause problems for bulk oxygen measurements. Samples were then treated with 30 % hydrogen peroxide (H_2O_2) for 48 hours at room temperature to remove organic matter, again at a greater than 40:1 liquid to solid ratio, and were subsequently centrifuged, decanted, and rinsed three times with 18.1 MΩ Milli-Q water to remove residual H_2O_2. HCl and H_2O_2 treatments are shown to negligibly impact bulk $\delta^{18}O$ values for a kaolinite standard material, supporting the use of these methods (raw $\delta^{18}O$ = 21.6 ± 0.6 ‰, n = 2; HCl treated $\delta^{18}O$ = 22.5 ± 0.5 ‰, n = 2; H_2O_2 treated $\delta^{18}O$ = 20.5 ± 0.7 ‰, n = 9).

Following this, samples were dried overnight at 65 °C in a vacuum oven, loaded into a 21-well laser fluorination tray and dried for a further 72 hours at 65 °C in a vacuum oven. This tray was then inserted into a laser fluorination chamber, heated to ~65 °C under vacuum for ~6 hours, and allowed to cool to room temperature before being reacted with 40 T fluorine gas (F_2) for 15 hours to remove any remaining hydration water ("pre-fluorination"). Pre-fluorination product O_2 was then removed under vacuum. To analyze each sample, the chamber was again charged with 40 T F_2 gas and same material was reacted by use of a 50 W CO_2 laser (Teledyne) following Sharp, 1992; laser power was initially low to prevent sputtering and was gradually increased to ~10 % until no visible sample residue remained. Fluorinated compounds were then removed by liquid nitrogen, residual F_2 gas was passivated by KBr salt held at 200 °C, and O_2 gas was purified by passage through a 3m long gas chromatography column packed with 5 Å molecular sieve as described in Cowie and Johnston, 2016.

Analyte O_2 gas was measured on a ThermoFischer Scientific MAT 253 isotope ratio mass spectrometer (IRMS) operated in dual inlet mode; for each sample, gas was analyzed in 4-acquisition blocks of 10 cycles each and averaged. Resulting $\delta^{18}O$ and $\Delta'^{17}O$ values were corrected to the 2-point calibration SMOW/SLAP scale following Schoenemann *et al.*, 2013, by directly fluorinating and analyzing VSMOW-2 and SLAP-2 standard material using a CoF_3 reactor as described in Barkan and Luz, 2005. Uncertainty was taken as the difference between replicate sample aliquots.

5.4 Results

To track PETM onset and recovery, all clay isotope results are described relative to the bulk organic matter $\delta^{13}C$ record from the same section (Kender *et al.*, 2012). In the late Paleocene prior to the PETM, the $\delta^{13}C$ signal remains relatively constant at –25 ± 1 ‰ VPDB (Methods; Figure 5.2 a). The CIE onset in this section is located between 2614.3 and 2613.5 m (Kender *et al.*, 2012; Kemp *et al.*, 2016), with a rapid $\delta^{13}C$ decrease to –30 ± 1 ‰ VPDB at 2612.0 m. Carbon isotope values remain low (–30.7 ± 0.3 ‰) until at least 2605.0 m; post-PETM $\delta^{13}C$ recovery has not been captured with the available data but must occur higher in this section.

Throughout the section, the clay mineral assemblage comprises a mixture of kaolinite, illite, illite-smectite (I-S) and chlorite (Kemp *et al.*, 2016). Illite (13-23 %) and I-S (44-54 %) dominate in the base of the section (2634.0 to 2620.0 m), with chlorite content also at its highest in this interval (7-10 %; Figure 5.3). In contrast, kaolinite concentrations are low during this period (1-4 %), but begin to increase at 2620.0 m and rise irregularly to a maximum of 44 % just after the CIE onset at 2613.5 m; this is mirrored by a decrease in I-S concentration to 19 % (Figure 5.3 a,b). Following this peak, between 2612.0 and 2608.0 m kaolinite, illite and chlorite concentrations decline to 6-32 %, 9-20 % and 1-3 %, respectively, whereas I-S recovers to 27-52 % (mirroring the pattern in kaolinite concentrations). In the upper-most section between 2608.0 and 2596.0 m, I-S again dominates (53-68 %), but illite (10-16 %) and chlorite (1-3 %) are less abundant than in the base of the section (Figure 5.3 c,d), whereas kaolinite content remains higher (12-24 %) than before PETM onset.

Measured δ^2H_{OH} values decrease gradually by 13.7 ± 0.6 ‰ over the 15 m leading up to the CIE onset, reaching –67.8 ± 0.3 ‰ VSMOW at 2613.5 m (Methods; Figure 5.2 b). The CIE onset at 2613.5 m is followed by an abrupt δ^2H_{OH} decrease of 8.1 ± 0.4 ‰; δ^2H_{OH} decreases further throughout the early CIE, culminating in a minimum value of –87.0 ± 0.2 ‰ VSMOW at 2611.6 m. This δ^2H_{OH} excursion occurs only between 2613.5 and 2608.7 m, with δ^2H_{OH} values returning to the pre-PETM baseline at 2606.4 m, well before the end of the CIE (Figure 5.2 b; Kender *et al.*, 2012). In total, δ^2H_{OH} spans a range of 34.1 ± 0.3 ‰ (27.6 ± 0.3 ‰ if the one-point minimum is excluded). Furthermore, the observed δ^2H_{OH} excursion is coincident with both an increased abundance of low-salinity dinoflagellate cysts excluding *Apectodinium*, and of *Apectodinium* itself (a genus abundant during the PETM and possibly

associated with enhanced terrestrial runoff (Crouch *et al.*, 2003); see Frieling and Sluijs, 2018, for further discussion of the origin of recorded PETM *Apectodinium* abundances) (Figure 5.2 b,c,d; Kender *et al.*, 2012). The strong correlation between dinoflagellate assemblages and δ^2H_{OH} is particularly apparent between 2612.8 and 2608.7 m, which marks the lowest observed δ^2H_{OH} values and greatest abundance of low-salinity dinoflagellate cysts excluding *Apectodinium* (and of *Apectodinium*).

In contrast to δ^2H_{OH}, resulting $\delta^{18}O_{OH}$ changes appear to more closely track events in clay composition and $\delta^{13}C$ variability (Figure 5.2 e), but overall correlation with clay oxygen contents is weak (e.g. for kaolinite, the strongest correlation, $r^2 = 0.46$; *p*-value < 0.01; $n = 22$). At the base of the section, $\delta^{18}O_{OH}$ averages 3.2 ± 0.3 ‰ VSMOW but quickly increases to 8.7 ± 0.2 to 10.7 ± 0.2 ‰ VSMOW (omitting a one-point minimum of 1.38 ± 0.13 ‰ VSMOW at 2617.4 m, which corresponds to a kaolinite content maximum and I-S content minimum; Figure 5.3 a,b). At the CIE onset, $\delta^{18}O_{OH}$ values again decrease by 10.2 ± 0.2 ‰ to 0.42 ± 0.04 ‰ VSMOW and remain stable between -0.7 ± 0.2 ‰ and 3.7 ± 0.2 ‰ VSMOW for the remainder of the record.

Similar to $\delta^{18}O_{OH}$, bulk clay $\delta^{18}O$ values are positively correlated with I-S oxygen content ($r^2 = 0.30$; *p*-value = 0.01; $n = 22$). Both $\delta^{18}O_{OH}$ and $\delta^{18}O_{bulk}$ are also negatively correlated with kaolinite oxygen contribution, with $\delta^{18}O_{bulk}$ shows a much stronger correlation ($r^2 = 0.83$; *p*-value < 0.01; $n = 22$; Figure 5.2 f, 5.3 b,c). In addition, the magnitude of $\delta^{18}O_{OH}$ variability (11.3 ± 0.3 ‰) is much greater than that for $\delta^{18}O_{bulk}$ (3.7 ± 0.8 ‰; Figure 5.2 e,f). Agreement between the $\delta^{18}O_{bulk}$ and $\delta^{18}O_{OH}$ trends is weak ($r^2 = 0.45$; *p*-value < 0.01; $n = 22$). Prior to the PETM, $\delta^{18}O_{bulk}$ averages 18.6 ± 0.5 ‰ VSMOW at 2634 m and increases to 19.7 ± 0.6 ‰ VSMOW at 2623.3 m; however, these high values are not maintained until the CIE onset. Rather, $\delta^{18}O_{bulk}$ decreases to 17.4 ± 0.7 ‰ VSMOW between 2621.2 m and 2617.4 m, then recovers to 18.7 ± 0.3 ‰ VSMOW at 2616.3 m before rapidly decreasing to 16.0 ± 0.6 ‰ VSMOW at the CIE onset at 2612.8 m. Unlike $\delta^{18}O_{OH}$, $\delta^{18}O_{bulk}$ begins to recover after the CIE onset – increasing to 19.6 ± 1.2 ‰ VSMOW at 2608.7 m – before decreasing to 17.5 ± 0.4 ‰ VSMOW at the top of the section.

Finally, we estimate the hydrogen-isotope composition of clay mineral (neo)formation mother water ($\delta^2H_{OH\text{-}MW}$) using mineral-specific ^2H fractionation factors (Gilg and Sheppard, 1996, and Hyeong and Capuano, 2004, for kaolinite and illite-smectite respectively)

combined with measured δ^2H_{OH} and clay mineral content trends (Figure 5.3 e). Resulting $\delta^2H_{OH\text{-}MW}$ closely tracks the measured δ^2H_{OH} signal (r^2 = 0.90; *p*-value < 0.01; *n* = 22). Absolute values are significantly less negative (ranging from –2.5 ‰ to –50.9 ‰ VSMOW) and exhibit larger variability (48.5 ‰) relative to δ^2H_{OH} (34.1 ± 0.3 ‰), as the most enriched δ^2H_{OH} values correspond to depths with higher I-S concentrations, while the most depleted δ^2H_{OH} values correspond to depths with higher kaolinite concentrations, despite kaolinite having a larger fractionation factor.

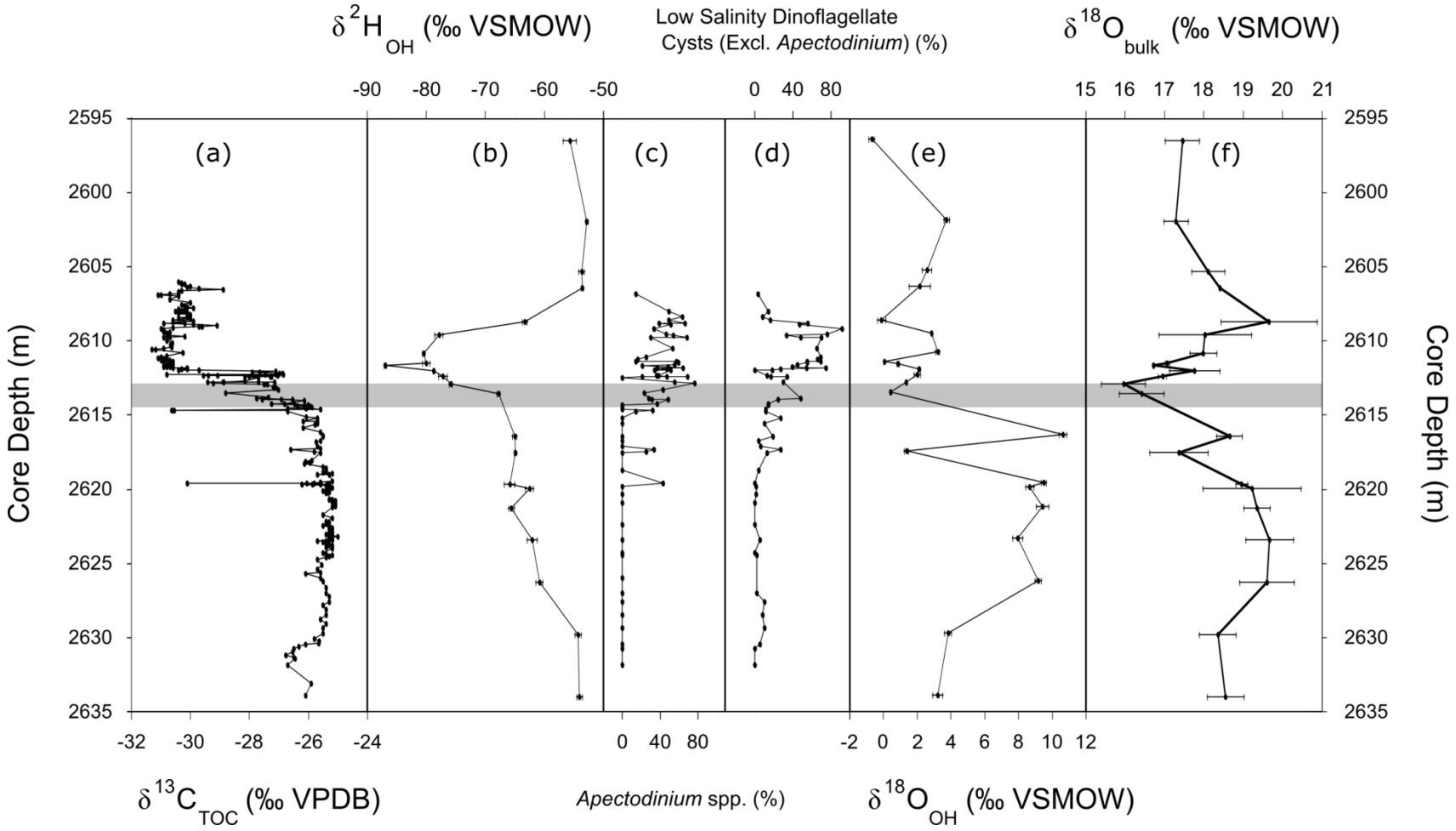

Figure 5.2. Comparison of the major trends across the onset of the PETM versus depth in the core from well 22/10a-4. The onset of the CIE is shown by the light grey bar. (a) $\delta^{13}C$ of total organic carbon (TOC) (Kender *et al*., 2012); (b) clay hydroxyl $\delta^{2}H_{OH}$; (c) percentage of the dinoflagellate *Apectodinium* spp. (Kender *et al*., 2012); (d) percentage of low salinity dinoflagellate cysts excluding *Apectodinium* (Kender *et al*., 2012); (e) clay hydroxyl $\delta^{18}O_{OH}$; and (f) the bulk clay $\delta^{18}O_{bulk}$. Error bars for (b), (e) and (f) are ±1 σ analytical uncertainty.

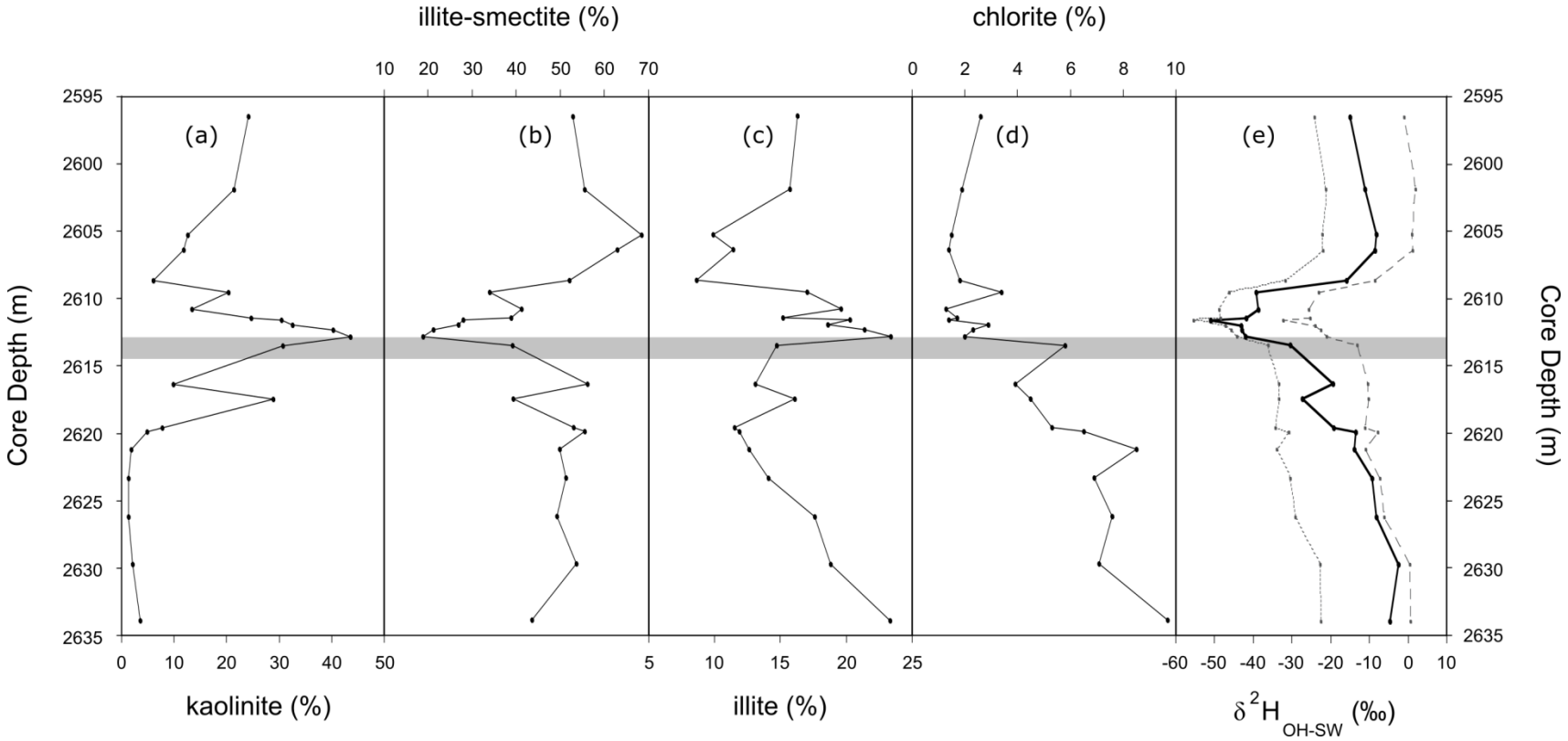

Figure 5.3. Comparison of the relative percentage of the component clays (note that panels use different scales) and reconstructed clay mineral formation source water versus depth in the core from well 22/10a-4. The onset of the Carbon Isotope Excursion (CIE) is shown by the light grey bar. (a) kaolinite; (b) illite-smectite; (c) illite; and (d) chlorite in the <4 μm size fraction from well 22/10a-4 (Kemp *et al.*, 2016) and (e) the reconstructed clay mineral (neo)formation mother water δ^2H ($\delta^2H_{OH\text{-}MW}$). Also shown in (e) are end-members assuming 100 % kaolinite (dotted grey line) or 100 % illite-smectite (dashed grey line). Reconstructions are calculated using empirical fractionation factors from Gilg and Sheppard, 1996, and Hyeong and Capuano, 2018, respectively. These end-member values are expected to encompass the range of possible $\delta^2H_{OH\text{-}MW}$ values for a given time point.

Mineral	R^2 correlation of isotope contribution		
	$\delta^{18}O_{bulk}$	$\delta^{18}O_{OH}$	$\delta^{2}H_{OH}$
Chlorite	**0.281**	**0.446**	0.157
Illite	**0.194**	0.110	0.005
Illite-smectite	**0.305**	**0.323**	**0.482**
Illite (total)	0.042	**0.340**	**0.511**
Kaolinite	**0.833**	**0.456**	**0.380**
Quartz	**0.483**	-	-
Smectite	**0.460**	**0.248**	**0.187**

Table 5.2. Correlation coefficients between the amount of oxygen or hydrogen contributed by the component mineral (i.e. mineral relative abundances scaled by structural or hydroxyl weight %) and the recorded $\delta^{18}O_{bulk}$, $\delta^{18}O_{OH}$ or $\delta^{2}H_{OH}$ (ordinary least squares). Calculations for illite (total) include the illite component of I-S. Calculations for smectite refer to the smectite component of I-S. Correlations which are significant at a 95 % confidence interval are in bold (p-value < 0.05).

5.5 Discussion

The origin of the pervasive increase in PETM kaolinite deposition is debated. Early studies interpreted this trend as reflecting contemporaneous PETM kaolinite formation, indicating increased pedogenesis and weathering under a warm, humid climate with an intensified hydrologic cycle (Robert and Kennett, 1994; Gawenda *et al.*, 1999; Bolle and Adatte, 2001; Clechenko *et al.*, 2007). More recent studies considered the time required for regolith kaolinization – with estimates on the order of one Ma (Thiry, 2000) – and suggested this signal instead represents increased erosion and exhumation of previously deposited kaolinite that formed well before the PETM (John *et al.*, 2012; Kemp *et al.*, 2016; Carmichael *et al.*, 2018). However, such long timescales refer to the formation of kaolinite from unweathered bedrock but do not necessarily apply to the kaolinization of pre-existing clays in soil profiles. The transformation in soils of 2:1 type phyllosilicates (e.g. smectite and illite) into 1:1 types (e.g. kaolinite) has been found to occur on the order of 100 days under laboratory conditions at 150 °C (Ryan and Huertas, 2013), and significant kaolinization of smectites can occur over a 5-10 ka period under tropical weathering conditions (Ryan and Huertas, 2009).

5.5.1 Implications of Bulk and Hydroxyl Isotopes on Clay Origin

Clay oxygen isotopes provide information about possible mineral sources and their genesis. As such, bulk oxygen measurements of PETM-age clays have been analysed previously; for example, from the Bass River section on the New Jersey margin, which similarly contains a mineral assemblage of smectite, illite, kaolinite and quartz (John *et al.*, 2012). In that study, a strong correlation was observed between smectite and $\delta^{18}O_{bulk}$ (r^2 = 0.96) and between kaolinite and $\delta^{18}O_{bulk}$ (r^2 = 0.88). This suggested that $\delta^{18}O_{bulk}$ variability resulted from compositional changes in the proportion of kaolinite and smectite – each with constant $\delta^{18}O_{bulk}$ values – rather than changes to the $\delta^{18}O_{bulk}$ of the individual clay minerals across the PETM. Applying a similar analysis to the $\delta^{18}O_{bulk}$ measurements of this research, only kaolinite is found to show a similarly strong correlation (r^2 = 0.83) with $\delta^{18}O_{bulk}$ (Table 5.2). This implies that kaolinite across the section has a fairly constant $\delta^{18}O_{bulk}$ value, suggesting that kaolinite $\delta^{18}O_{bulk}$ does not necessarily capture isotopic changes across the PETM; this could be the result of kaolinite erosion from a pre-existing source, or from kaolinization of

existing soil profiles (where $\delta^{18}O_{bulk}$ will only be partially affected by the addition of hydroxyl groups).

By contrast, the relative amounts of oxygen contributed by smectite, illite, quartz and chlorite components do not strongly correlate with $\delta^{18}O_{bulk}$, $\delta^{18}O_{OH}$, or $\delta^{2}H_{OH}$, with r^2 values never exceeding 0.52 (Table 5.2). Kaolinite content – which contributes up to 75 % of the oxygen and hydrogen for the hydroxyl measurements – also shows poor correlation to $\delta^{18}O_{OH}$ and $\delta^{2}H_{OH}$, suggesting that the variation in the hydroxyl isotopes over the section is not driven by changes in the clay-sized mineral proportions.

Therefore strong clay compositional effects are not observed in the section studied here. In fact, the $\delta^{2}H_{OH\text{-}SW}$ variability increases when measured isotopic values are corrected for clay composition (i.e. by mineral-specific fractionation factors), suggesting a greater change in source water isotopic composition than is actually measured. Furthermore, the measured $\delta^{2}H_{OH\text{-}SW}$ decrease (48.5 ‰) is consistent with *n*-alkane $\delta^{2}H$ data from the same region (the Normandy Vasterival section), where a decrease of 60 ‰ was measured across the early PETM (Garel *et al.*, 2013). The observed changes in $\delta^{2}H_{OH}$ are thus best explained by the formation and alteration of clays during the PETM, rather than by the erosion of pre-existing deposits.

In order for kaolinite formation to capture changing source water isotopic composition across the PETM, it must have formed via a faster mechanism than regolith kaolinization (as regolith kaolinization is estimated to take longer than the duration of the PETM (Thiry, 2000)). It is therefore suggested that kaolinite was formed by the transformation of 2:1-type phyllosilicate clays (e.g. smectite and illite) into 1:1-type clays (e.g. kaolinite) within soil profiles. This kaolinization process of smectitic precursors leads to the addition of new hydroxyl groups – which will isotopically reflect meteoric water – and has been shown to occur under warm, humid conditions at rates sufficiently fast to capture changes in rainfall isotope composition across the PETM (Dudek *et al.*, 2006; Cuadros *et al.*, 2009).

If, as argued above, clay formation and alteration during the PETM is the major contributor to $\delta^{2}H_{OH}$ in this section, then the effect of temperature on $\delta^{2}H_{OH}$ must also be considered, as temperatures in the North Sea region increased over the PETM. Current models for clay hydroxyl group H-isotope fractionation factors ($^{2H}\alpha_{OH}$) predict values less than one (Gilg and

Sheppard, 1996; Hyeong and Capuano, 2004), meaning that clay hydroxyl group H-isotopes are depleted relative to the hydroxyl group source water. Less isotopic fractionation occurs at higher temperatures, so temperature increases would therefore be expected to result in higher δ^2H_{OH} values over the CIE in contrast to the observed lower values.

The δ^2H_{OH} signal may be somewhat biased towards marine values by post-depositional isotopic exchange; however, in contrast to exposed terrestrial clays, there is little evidence for hydrogen isotopic exchange in deep-sea buried clays over ~3 Ma outside of the <0.1 μm fraction (Yeh and Epstein, 1978), so significant hydroxyl exchange is unlikely.

5.5.2 Palaeohydrologic Implications of δ^2H_{OH}

Taking into account the weak or insignificant correlations between measured isotope values and clay mineral proportions, and the inverse relationship between temperature and $^{2H}\alpha_{OH}$, the hydroxyl isotope record is interpreted as capturing changes in the isotopic composition of the source water. Although the decrease in δ^2H_{OH} at the PETM onset is the largest observed change, both the measured δ^2H_{OH} and the calculated $\delta^2H_{OH\text{-}SW}$ show a clear trend towards more negative values in the period leading up to the PETM onset. This trend towards more negative δ^2H_{OH} values precedes the CIE, suggesting that hydrologic changes during the PETM were not solely a result of changes in the carbon cycle. The pre-PETM decrease in δ^2H_{OH} may instead reflect increased terrestrial input to the North Sea, as sea level in the basin was lowered by ~100 m during this time (Knox, 1996). However, there is additional palynological evidence from a close-by North Sea well, where significant changes to vegetation were documented prior to the CIE, implying the pre-PETM decrease in δ^2H_{OH} does reflect hydrologic changes which predate the CIE (Eldrett *et al.*, 2014).

The 8 ‰ VSMOW decrease in δ^2H_{OH} at the onset of the PETM is interpreted to reflect a decrease in the δ^2H_{OH} of rainfall. The mechanism proposed to cause this δ^2H_{OH} decrease is the amount effect (Dansgaard, 1964) – an observed negative correlation between monthly mean rainwater isotope composition and the total amount of precipitation, typically seen in the tropics at low elevation due to increased precipitation intensity in those regions. Increased PETM precipitation amount is further evidenced in this section by the concurrency of the δ^2H_{OH} excursion and the increased abundances of the low-salinity-tolerant dinoflagellate

cysts (and *Apectodinium*), implying that δ^2H_{OH} accurately reflects the δ^2H of rainfall during the PETM.

The measured δ^2H_{OH} decrease during the PETM may reflect high intensity precipitation events where rainfall is depleted in ^{18}O and ^{2}H; for example, those resulting from tropical cyclone activity (Müller *et al.*, 2020). TEX_{86}-derived sea-surface temperatures for the North Sea suggest a temperature increase of at least ~10 °C across the CIE onset with temperatures exceeding 30 °C (Stokke *et al.*, 2020). Such high temperatures exceed the tropical convective threshold (Folkins and Braun, 2003), and may have contributed to the high rainfall intensity. The δ^2H_{OH} results are consistent with previous interpretations that global warming during the PETM caused an intensified hydrologic cycle and northward migration of storm tracks (Pagani *et al.*, 2006; Kender *et al.*, 2012; Carmichael *et al.*, 2018).

The δ^2H_{OH} values return to their pre-PETM baseline before the CIE termination, suggesting that increased rainfall intensity around the North Sea was short-lived; this too is consistent with prior δ^2H measurements from the region, where short-lived increases in seasonality have been inferred from *n*-alkane δ^2H in the Normandy Vasterival section (Garel *et al.*, 2013).

Similar hydrological behaviour during the CIE is suggested by mineralogical data from the Fur section in Denmark, where the total clay fraction, clay mineral proportions, and the clay chemical index of alteration return to pre-PETM values before the end of the CIE (Stokke *et al.*, 2021). Lithium isotopic composition measurements from the Fur section similarly show an excursion at the PETM onset before beginning to return to pre-PETM isotopic values during the CIE (Pogge von Strandmann *et al.*, 2021). However, relative changes in proxies around the CIE onset differ in the Fur section compared to those reported in this research – in particular, only the total clay fraction seems to increase before the CIE onset, and kaolinite in this section is mostly present after the CIE onset. The Fur section is less expanded over the start of the PETM (i.e. the Stolleklint clay layer), suggesting that early hydrological changes may not have been fully captured.

Also of note is that the 8 ‰ VSMOW decrease in δ^2H_{OH} at the PETM onset appears to precede the CIE in the North Sea Basin section. This may offer further evidence that hydrologic changes during the PETM were not a result of carbon excursion. However, the CIE onset recorded in this section is complex and potentially influenced by multiple

confounding factors, including variable mixing of different carbon sources at time of deposition (where carbon sources could be either marine or terrestrial, and may or may not reflect newly sequestered carbon; Lyons *et al.*, 2019), and possible variability caused by a pre-onset carbon isotope excursion, which has been recorded in other sections (Babila *et al.*, 2022), though is not present in this section's measured record.

This research uses the newly developed differential thermal isotope analysis (DTIA) method to report clay δ^2H_{OH} across the PETM. Clay hydroxyl isotopic composition is not a well-developed area of research; future work will benefit from better constraints on hydrogen isotopic fractionation factors for clay hydroxyl groups ($^{2H}\alpha_{OH}$). There currently exist a limited number of $^{2H}\alpha_{OH}$ values in the literature (Gilg and Sheppard, 1996; Hyeong and Capuano, 2004), and reported values assume that fractionation is not influenced by variations in chemical composition (i.e. the interlayer metal ions present) or mineralogical composition (i.e. the ratio of illite to smectite within I-S). New $^{2H}\alpha_{OH}$ estimates for a suite of clay minerals under environmentally relevant conditions are needed to more accurately correct for changing clay composition and estimates of palaeo-precipitation δ^2H variability. Similar clay isotope measurements should be made in other PETM sections to determine whether the δ^2H_{OH} values reported here indicate pervasive hydroclimate changes at the PETM onset or was driven by local effects in the North Sea Basin. Future studies must be careful to evaluate the effects of changing clay composition on the $\delta^{18}O_{bulk}$, $\delta^{18}O_{OH}$ and δ^2H_{OH} before an environmental interpretation is proffered.

5.6 Conclusions

A recently-developed method for measuring δ^2H and $\delta^{18}O$ of the hydroxyl group in clay minerals has been applied to reconstruct past hydrological changes during the PETM. A large decrease in δ^2H_{OH} coinciding with the CIE is observed, which is interpreted to reflect increased precipitation – possibly resulting from increased tropical cyclone activity – in response to global warming during the PETM. This interpretation is supported by concomitant increases in the abundances of low-salinity dinoflagellates (Kender *et al.*, 2012), indicating increased runoff to the North Sea Basin. Hydrologic changes are short-lived relative to the CIE, as evidenced by δ^2H_{OH} values and low-salinity-tolerant dinoflagellate abundances returning to pre-PETM values before recovery of the carbon cycle. Taken together, these results imply increased kaolinization, silicate weathering intensity, and hence humidity, in response to warming events in a greenhouse world. Comparing these and future PETM clay δ^2H_{OH} measurements to predictions from isotopically enabled models offers the promise of quantitative reconstructions of palaeo-hydrologic conditions that can enhance our understanding of hydrology and pedology in a warming world.

Clay hydroxyl group isotopes are a largely untapped proxy, which can greatly improve our understanding of clay provenances and palaeoclimates across any geological event that included prominent clay deposition. Further measurements of PETM sections are warranted, to understand whether the changes seen in the North Sea Basin are local to the North Sea Basin or reflect changing conditions across wider areas of Europe – which is of particular interest, given recent extreme precipitation events in Europe. At the same time, further research into the fractionation factors of clay hydroxyl groups is warranted; the current clay hydroxyl isotope interpretation is limited to clay hydroxyl hydrogen, because there are no reliable fractionation factors for clay hydroxyl oxygen isotopes. Given the GMWL relationship between precipitation δ^2H and $\delta^{18}O$, understanding the source of hydroxyl oxygen, and being able to quantify the $\delta^{18}O$ of that source using accurate fractionation factors, would add further confidence to interpretations of δ^2H and $\delta^{18}O_{bulk}$ data.

6 Conclusions

6.1 Summary

In this thesis, I have described the development of the online DTIA method, an experimental procedure which can isolate different types of mineral hydration water (e.g. adsorbed water, interlayer water, structural water, hydroxyl groups) by temperature and measure the oxygen and hydrogen isotopic composition of each water type. I have further described the results of investigations made using the DTIA method. I have showed that the extra information provided by the online measurement of mineral hydration water oxygen and hydrogen isotopic composition is meaningful, revealing more about dehydration mechanics and mineral formation environments than current offline measurement techniques.

In Chapter 2, I presented an overview of the DTIA method, including descriptions of the experimental setup, the methodological and analytical procedures, and the validity of results acquired using DTIA. The high precision and accuracy of the DTIA method was demonstrated through the comparison of gypsum water isotopic composition measurements by DTIA and by a conventional offline water extraction method followed by CRDS analysis. In addition, the ability of DTIA to accurately measure water oxygen and hydrogen isotopic composition at high temperatures was showcased, alongside the ability to separate different water types when making DTIA measurements of clay minerals.

In Chapter 3, I demonstrated through the use of DTIA that the gypsum two peak dehydration (across the gypsum → bassanite → anhydrite transitions) is primarily driven by kinetic factors during dehydration, rather than by differences in gypsum water bonding environment; in particular, sample grain size and the partial pressure of water present in the gypsum dehydration environment were both shown to have a large effect on the dehydration reaction pathway, and hence on whether a bassanite-dominated phase forms during the dehydration. It was thus shown that the gypsum two peak dehydration is not of interest for palaeoclimatic studies. The results of experiments for finding the oxygen and hydrogen fractionation factors for hydration water in bassanite were also presented; however, these attempts to determine accurate experimental fractionation factors were unsuccessful.

In Chapter 4, I demonstrated that the DTIA method can be applied to a wide range of clay minerals, including kaolinite and both calcium-rich and sodium-rich montmorillonite samples, separating out the multiple types of water frequently present in clay minerals (adsorbed water, interlayer water, zeolitic water, hydroxyl groups) and measuring them individually. This was supported by DTIA experiments carried out on mixtures of known individual clays, which found that the measured hydroxyl oxygen and hydrogen isotopic compositions of the mixture were equivalent to the expected isotopic compositions calculated by summing the individual clay fractions. The importance of the non-destructive removal of carbonate from clay samples before DTIA measurement was also demonstrated. Finally, some limitations in clay water isotope exchange experiments were highlighted through an attempted isotope exchange experiment.

In Chapter 5, I applied the online DTIA method to a well-characterised set of mixed clay samples buried in the North Sea Basin during the Paleocene-Eocene Thermal Maximum (PETM), in order to investigate whether further information about palaeoclimatic changes during the PETM could be learnt from the clay hydroxyl group isotope record. Results indicated that rainfall intensity and weathering increased during the early stages of the PETM, implying an enhanced hydrologic cycle response to global warming. The measured clay hydroxyl group oxygen and hydrogen isotopic compositions were compared to bulk clay oxygen isotopic composition as measured by mass spectrometry, as well as other climate proxies such as clay composition, the isotopic composition of total organic carbon and the count of dinoflagellate cysts. In particular, clay hydroxyl group hydrogen results were found to be consistent with other proxies measured at the site of study, while clay hydroxyl oxygen could not be used to calculate source water isotopic compositions, due to a lack of reliable values for clay hydroxyl group oxygen fractionation factors in the literature. This is the first application of online DTIA to a palaeoclimate study, and its success indicates that DTIA should be applied more widely to studies of the palaeoclimate conditions under which geological deposits form.

Overall, this research has significantly developed a new method for the analysis of mineral hydration water oxygen and hydrogen isotopic composition. While some further work is still required to characterise which geological settings the DTIA method is valid in (e.g. understanding in which settings hydration water isotopic composition is likely to reflect source water isotopic composition at the time of mineral formation, and in which settings

mineral hydration water is likely to have undergone isotopic exchange or to have changed isotopic composition due to mineral alteration), it has been demonstrated that DTIA is a useful tool for palaeoclimate reconstruction, which can greatly improve our understanding of clay provenances and can help enhance our understanding of past climate conditions – and hence improve our ability to predict future climate conditions.

6.2 Future Research

The culmination of this thesis' work in developing the DTIA method is the demonstration of the DTIA method on a set of clay samples dating to the PETM. This is the first study of its kind; as such, there are many directions for future research. In particular, clay hydroxyl group isotopes are a largely untapped proxy; DTIA could be used to determine palaeo-hydrologic conditions during a number of significant geological events where layers of hydrated clay have been deposited, such as the Cretaceous–Palaeogene (K-Pg) boundary, or the PETM.

Following on the research from this thesis, it would be of great interest to record changes in clay hydroxyl group isotopic composition across the PETM both from other sections around the North Sea, and more widely; this would allow the determination of whether the hydrologic changes seen in my study of the North Sea Basin are local to the North Sea Basin, or reflect changing conditions across wider areas of Europe. It would also help to answer questions around the origin of the PETM kaolinite; where it is not clear how much of the kaolinite deposited during the PETM originated from the erosion of existing kaolinite deposits, and how much kaolinite was produced during the PETM by the kaolinization of soil profiles.

However, to use DTIA at its full potential, studies have to be able to make use of both hydroxyl hydrogen isotopic composition and hydroxyl oxygen isotopic composition. Clay hydroxyl isotopic composition is not a well-developed area of research, and in particular, knowledge of clay hydroxyl oxygen isotopic fractionation is very limited, with no reliable published fractionation factors for clay hydroxyl oxygen. This means it is extremely difficult to interpret the results of hydroxyl oxygen isotopic composition measurement. It is also unclear whether isotopic fractionation between clay hydroxyl groups and source water is

dependent on clay mineral chemical composition (i.e. the interlayer metal ions present) or mineralogical composition (i.e. the ratio of illite to smectite within I-S). Having accurate fractionation factors for both hydroxyl oxygen and hydroxyl hydrogen would allow for much more accurate estimation of clay mineral source water. Moreover, as both clay hydroxyl oxygen fractionation and clay hydroxyl hydrogen fractionation will depend on temperature, and source water will in most cases follow the Global Meteoric Water Line (GMWL), it is possible that clay hydroxyl group isotopes could be used as a palaeo-thermometer; much more research is required to determine this.

More work is also required to understand the behaviour of hydration water hydroxyl isotopic composition over time in different geological settings, with a particular emphasis not only on isotopic exchange, but also on the mechanics of clay alteration, and how hydroxyl groups are added or removed from clay minerals during alteration, and the effect that this alteration has on both the hydroxyl group isotopic composition and the bulk oxygen isotopic composition. This would greatly increase the confidence in studies using hydration water isotopic composition to establish mineral provenance, and would help establish in which types of environments DTIA should be used.

Finally, although some work was done in this thesis to characterise the effect of sample contamination with carbonates, natural samples frequently contain non-carbonate organic compounds. The effect of this contamination on measurement accuracy is thought to be small, but this effect has not been investigated in depth. Developing methods for more general organic compound removal which do not affect clay hydroxyl group isotopic composition would increase the reliability of the DTIA method. Failing this, further characterisation of the amount of organic carbon required in a sample to see significant inaccuracies in clay hydroxyl group isotopic composition measurements, and at which temperatures organics are likely to affect CRDS measurement of oxygen and hydrogen isotopic composition, would similarly increase the accuracy of conclusions drawn from the results of DTIA studies.

References

Affolter, S., Fleitmann, D., & Leuenberger, M. (2014). New online method for water isotope analysis of speleothem fluid inclusions using laser absorption spectroscopy (WS-CRDS). Climate of the Past, 10(4), 1291–1304. doi:10.5194/cp-10-1291-2014

Alvarez, L. W., Alvarez, W., Asaro, F., & Michel, H. V. (1980). Extraterrestrial Cause for the Cretaceous-Tertiary Extinction. Science, 208(4448), 1095–1108. doi:10.1126/science.208.4448.1095

Amjad, Z. (1988). Calcium sulfate dihydrate (gypsum) scale formation on heat exchanger surfaces: The influence of scale inhibitors. Journal of Colloid and Interface Science, 123(2), 523–536. doi:10.1016/0021-9797(88)90274-3

Arienzo, M. M., Swart, P. K., & Vonhof, H. B. (2013). Measurement of $\delta^{18}O$ and $\delta^{2}H$ values of fluid inclusion water in speleothems using cavity ring-down spectroscopy compared with isotope ratio mass spectrometry. Rapid Communications in Mass Spectrometry, 27(23), 2616–2624. doi:10.1002/rcm.6723

Atoji, M., & Rundle, R. E. (1958). Neutron Diffraction Study of Gypsum, $CaSO_4 2H_2O$. The Journal of Chemical Physics, 29(6), 1306–1311. doi:10.1063/1.1744713

Babila, T. L., Penman, D. E., Standish, C. D., Doubrawa, M., Bralower, T. J., Robinson, M. M., Self-Trail, J. M., Speijer, R. P., Stassen, P., Foster, G. L., & Zachos, J. C. (2022). Surface ocean warming and acidification driven by rapid carbon release precedes Paleocene-Eocene Thermal Maximum. Science Advances, 8(11), eabg1025. doi:10.1126/sciadv.abg1025

Barkan, E., & Luz, B. (2005). High precision measurements of $^{17}O/^{16}O$ and $^{18}O/^{16}O$ ratios in H_2O. Rapid Communications in Mass Spectrometry, 19(24), 3737–3742. doi:10.1002/rcm.2250

Bauer, K. K., & Vennemann, T. W. (2014). Analytical methods for the measurement of hydrogen isotope composition and water content in clay minerals by TC/EA. Chemical Geology, 363, 229–240. doi:10.1016/j.chemgeo.2013.10.039

Bauer, K. K., Vennemann, T. W., & Gilg, H. A. (2016). Stable isotope composition of bentonites from the Swiss and Bavarian Freshwater Molasse as a proxy for paleoprecipitation. Palaeogeography, Palaeoclimatology, Palaeoecology, 455, 53–64. doi:10.1016/j.palaeo.2016.02.002

Bauska, T. K., Walters, G., Gázquez, F., & Hodell, D. A. (2017). Online Differential Thermal Isotope Analysis of Hydration Water in Minerals by Cavity Ringdown Laser Spectroscopy. Analytical Chemistry, 90(1), 752–759. doi:10.1021/acs.analchem.7b03136

Bell, D. R., & Ihinger, P. D. (2000). The isotopic composition of hydrogen in nominally anhydrous mantle minerals. Geochimica et Cosmochimica Acta, 64(12), 2109–2118. doi:10.1016/s0016-7037(99)00440-8

Bidwell, J. I., Jepson, W.B., & Toms, G. L. (1970). The interaction of kaolinite with polyphosphate and polyacrylate in aqueous solutions – some preliminary results. Clay Minerals, 8(4), 445–459. doi:10.1180/claymin.1970.008.4.07

Bohor, B. F., Triplehorn, D. M., Nichols, D. J., & Millard, H. T. (1987). Dinosaurs, spherules, and the “magic” layer: A new K-T boundary clay site in Wyoming. Geology, 15(10), 896. doi:10.1130/0091-7613(1987)15<896:dsatml>2.0.co;2

Bolle, M.-P., Pardo, A., Adatte, T., Tantawy, A. A., Hinrichs, K.-U., Von Salis, K., & Burns, S. (2000). Climatic evolution on the southern and northern margins of the Tethys from the Paleocene to the early Eocene. GFF, 122(1), 31–32. doi:10.1080/11035890001221031

Bolle, M.-P., & Adatte, T. (2001). Palaeocene- early Eocene climatic evolution in the Tethyan realm: clay mineral evidence. Clay Minerals, 36(02), 249–261. doi:10.1180/000985501750177979

Bornemann, A., Norris, R. D., Lyman, J. A., D'haenens, S., Groeneveld, J., Röhl, U., Farley, K. A., Speijer, R. P. (2014). Persistent environmental change after the Paleocene–Eocene Thermal Maximum in the eastern North Atlantic. Earth and Planetary Science Letters, 394, 70–81. doi:10.1016/j.epsl.2014.03.017

Bowen, G. J., & Bowen, B. B. (2008). Mechanisms of PETM global change constrained by a new record from central Utah. Geology, 36(5), 379. doi:10.1130/g24597a.1

Brand, W. A., Tegtmeyer, A. R., & Hilkert, A. (1994). Compound-specific isotope analysis: extending toward and. Organic Geochemistry, 21(6-7), 585–594. doi:10.1016/0146-6380(94)90004-3

Caballero, E., & Jiménez de Cisneros, C. (2018). Oxygen Isotopic Fractionation in the Kaolinite-Water System during the Synthetic Process. Journal of Minerals and Materials Characterization and Engineering, 6, 507–516. doi:10.4236/jmmce.2018.64036

Carmichael, M. J., Inglis, G. N., Badger, M. P. S., Naafs, B. D. A., Behrooz, L., Remmelzwaal, S., Monteiro, F. M., Rohrssen. M., Farnsworth. A., Buss. H. L., Dickson. A. J., Valdes. P. J., Lunt. D. J., & Pancost, R. D. (2017). Hydrological and associated biogeochemical consequences of rapid global warming during the Paleocene-Eocene Thermal Maximum. Global and Planetary Change, 157, 114–138. doi:10.1016/j.gloplacha.2017.07.014

Carmichael, M. J., Pancost, R. D., & Lunt, D. J. (2018). Changes in the occurrence of extreme precipitation events at the Paleocene–Eocene thermal maximum. Earth and Planetary Science Letters, 501, 24–36. doi:10.1016/j.epsl.2018.08.005

Chamberlain, C., Poage, M., Craw, D., & Reynolds, R. (1999). Topographic development of the Southern Alps recorded by the isotopic composition of authigenic clay minerals, South Island, New Zealand. Chemical Geology, 155(3-4), 279–294. doi:10.1016/s0009-2541(98)00165-x

Chen, Z., Ding, Z., Yang, S., Zhang, C., & Wang, X. (2016). Increased precipitation and weathering across the Paleocene-Eocene Thermal Maximum in central China. Geochemistry, Geophysics, Geosystems, 17(6), 2286–2297. doi:10.1002/2016gc006333

Christensen, A. N., Olesen, M., Cerenius, Y., & Jensen, T. R. (2008). Formation and Transformation of Five Different Phases in the $CaSO_4$−H_2O System: Crystal Structure of the Subhydrate β-$CaSO_4 \cdot 0.5H_2O$ and Soluble Anhydrite $CaSO_4$. Chemistry of Materials, 20(6), 2124–2132. doi:10.1021/cm7027542

Clayton, R. N., & Mayeda, T. K. (1963). The use of bromine pentafluoride in the extraction of oxygen from oxides and silicates for isotopic analysis. Geochimica et Cosmochimica Acta, 27(1), 43–52. doi:10.1016/0016-7037(63)90071-1

Clechenko, E. R., Kelly, D. C., Harrington, G. J., & Stiles, C. A. (2007). Terrestrial records of a regional weathering profile at the Paleocene-Eocene boundary in the Williston Basin of North Dakota. Geological Society of America Bulletin, 119(3-4), 428–442. doi:10.1130/b26010.1

Cole, W. F., & Lancucki, C. J. (1974). A refinement of the crystal structure of gypsum $CaSO_4.2H_2O$. Acta Crystallographica Section B Structural Crystallography and Crystal Chemistry, 30(4), 921–929. doi:10.1107/s0567740874004055

Compton, J.S., Conrad, M.E., Vennemann, T. W. (1999) Stable isotope evolution of volcanic ash layers during diagenesis of the Miocene Monterey formation, California. Clays and Clay Minerals, Vol. 47, No. I, 84-95. doi:10.1346/CCMN.1999.0470109

Conley, R. F., & Bundy, W. M. (1958). Mechanism of gypsification. Geochimica et Cosmochimica Acta, 15(1-2), 57–72. doi:10.1016/0016-7037(58)90010-3

Coplen, T.B. (1995). New IUPAC guidelines for the reporting of stable hydrogen, carbon, and oxygen isotope-ratio data. Journal of Research of the National Institute of Standards and Technology, 100(3), 285. doi:10.6028/jres.100.021

Cowie, B. R., & Johnston, D. T. (2016). High-precision measurement and standard calibration of triple oxygen isotopic compositions ($\delta^{18}O$, $\Delta'^{17}O$) of sulfate by F_2 laser fluorination. Chemical Geology, 440, 50-59. doi:10.1016/j.chemgeo.2016.07.003

Craig, H. (1961). Standard for Reporting Concentrations of Deuterium and Oxygen-18 in Natural Waters. Science, 133(3467), 1833–1834. doi:10.1126/science.133.3467.1833

Crouch, E. M., Dickens, G. R., Brinkhuis, H., Aubry, M.-P., Hollis, C. J., Rogers, K. M., & Visscher, H. (2003). The Apectodinium acme and terrestrial discharge during the Paleocene–Eocene thermal maximum: new palynological, geochemical and calcareous nannoplankton observations at Tawanui, New Zealand. Palaeogeography, Palaeoclimatology, Palaeoecology, 194(4), 387–403. doi:10.1016/s0031-0182(03)00334-1

Cuadros, J., & Altaner, S. P. (1998). Characterization of mixed-layer illite-smectite from bentonites using microscopic, chemical, and X-ray methods; constraints on the smectite-to-illite transformation mechanism. American Mineralogist, 83(7-8), 762–774. doi:10.2138/am-1998-7-808

Cuadros, J., Nieto, F., & Wing-Dudek, T. (2009). Crystal-chemical changes of mixed-layer kaolinite-smectite with progressive kaolinization, as investigated by TEM-AEM and HRTEM. Clays and Clay Minerals, 57(6), 742–750. doi:10.1346/ccmn.2009.0570607

Dai, A. (2006). Precipitation Characteristics in Eighteen Coupled Climate Models. Journal of Climate, 19(18), 4605–4630. doi:10.1175/jcli3884.1

Dansgaard, W. (1964). Stable isotopes in precipitation. Tellus, 16(4), 436–468. doi:10.3402/tellusa.v16i4.8993

Dole, M. (1935). The relative atomic weight of oxygen in water and in air. Journal of the American Chemical Society, 57(12), 2731–2731. doi:10.1021/ja01315a511

Dudek, T., Cuadros, J., & Fiore, S. (2006). Interstratified kaolinite-smectite: Nature of the layers and mechanism of smectite kaolinization. American Mineralogist, 91(1), 159–170. doi:10.2138/am.2006.1897

Dypvik, H., Riber, L., Burca, F., Rüther, D., Jargvoll, D., Nagy, J., & Jochmann, M. (2011). The Paleocene–Eocene thermal maximum (PETM) in Svalbard — clay mineral and geochemical signals. Palaeogeography, Palaeoclimatology, Palaeoecology, 302(3-4), 156–169. doi:10.1016/j.palaeo.2010.12.025

Egger, H., Homayoun, M., & Schnabel, W. (2002). Tectonic and climatic control of Paleogene sedimentation in the Rhenodanubian Flysch basin (Eastern Alps, Austria). Sedimentary Geology, 152(3-4), 247–262. doi:10.1016/s0037-0738(02)00072-6

Eiler, J. M., & Kitchen, N. (2001). Hydrogen-isotope analysis of nanomole (picoliter) quantities of H 2 O. Geochimica et Cosmochimica Acta, 65(24), 4467–4479. doi:10.1016/s0016-7037(01)00723-2

Eldrett, J.S., Greenwood, D.R., Polling, M., Brinkhuis, H., and Sluijs, A. (2914). A seasonality trigger for carbon injection at the Paleocene–Eocene Thermal Maximum. Climate of the Past, 10(2), 759–769. doi: 10.5194/cp-10-759-2014

Emmerich, K., & Kahr, G. (2001). The cis- and trans-vacant variety of a montmorillonite: an attempt to create a model smectite. Applied Clay Science, 20(3), 119–127. doi:10.1016/S0169-1317(01)00065-5

Eslinger, E. V., & Yeh, H.-W. (1981). Mineralogy, O^{18}/O^{16} and D/H ratios of clay-rich sediments from Deep Sea Drilling Project site 180, Aleutian Trench. Clay and Clay Minerals, 29(4), 309–315. doi:10.1346/CCMN.1981.0290409

Evans, N. P., Turchyn, A. V., Gázquez, F., Bontognali, T. R. R., Chapman, H. J., & Hodell, D. A. (2015). Coupled measurements of $\delta^{18}O$ and δ D of hydration water and salinity of fluid inclusions in gypsum from the Messinian Yesares Member, Sorbas Basin (SE Spain). Earth and Planetary Science Letters, 430, 499–510. doi:10.1016/j.epsl.2015.07.071

Evans, N. P., Bauska, T. K., Gázquez-Sánchez, F., Brenner, M., Curtis, J. H., & Hodell, D. A. (2018). Quantification of drought during the collapse of the classic Maya civilization. Science, 361(6401), 498–501. doi:10.1126/science.aas9871

Földvári, M. Handbook of Thermogravimetric System of Minerals and Its Use in Geological Practice; Occasional Papers of the Geological Institute of Hungary; Geological Institute of Hungary: Budapest, 2011; Vol. 213.

Folkins, I., & Braun, C. (2003). Tropical Rainfall and Boundary Layer Moist Entropy, Journal of Climate, 16(11), 1807-1820. doi:10.1175/1520-0442(2003)016<1807:TRABLM>2.0.CO;2

Fontes, J. Ch. and Gonfiantini, R. (1967). Fractionnement isotopique del'hydrogene dans l'eau de crystallisation du gypse. Comptes Rendues, Academie des Sciences de Paris, Series D, 265, 4–6.

Friedman, I., & Smith, R. L. (1958). The deuterium content of water in some volcanic glasses. Geochimica et Cosmochimica Acta, 15(3), 218–228. doi:10.1016/0016-7037(58)90059-0

Frieling, J., & Sluijs, A. (2018). Towards quantitative environmental reconstructions from ancient non-analogue microfossil assemblages: Ecological preferences of Paleocene – Eocene dinoflagellates. Earth-Science Reviews, 185, 956–973. doi:10.1016/j.earscirev.2018.08.014.

Fusseis, F., Schrank, C., Liu, J., Karrech, A., Llana-Fúnez, S., Xiao, X., & Regenauer-Lieb, K. (2012). Pore formation during dehydration of a polycrystalline gypsum sample observed and quantified in a time-series synchrotron X-ray micro-tomography experiment. Solid Earth, 3(1), 71–86. doi:10.5194/se-3-71-2012

Garel, S., Schnyder, J., Jacob, J., Dupuis, C., Boussafir, M., Le Milbeau, C., Storme, J.Y., Iakovleva, A.I., Yans, J., Baudin, F., Flehoc, C., Quesnel, F., Fléhoc, C., Quesnel, F., Flehoc, C., Quesnel, F., Fléhoc, C., Quesnel, F. (2013). Paleohydrological and paleoenvironmental changes recorded in terrestrial sediments of the Paleocene–Eocene boundary (Normandy, France). Palaeogeography, Palaeoclimatology, Palaeoecology, 376, 184–199. doi:10.1016/j.palaeo.2013.02.035

Gázquez, F., Calaforra, J.-M., Stoll, H., Sanna, L., Forti, P., Lauritzen, S.-E., Delgado, A., Rull, F., Martínez-Frías, J. (2013). Isotope and trace element evolution of the naica aquifer (Chihuahua, Mexico) over the past 60,000 yr revealed by speleothems. Quaternary Research, 80(03), 510–521. doi:10.1016/j.yqres.2013.09.004

Gázquez, F., Mather, I., Rolfe, J., Evans, N. P., Herwartz, D., Staubwasser, M., & Hodell, D. A. (2015). Simultaneous analysis of $^{17}O/^{16}O$, $^{18}O/^{16}O$ and $^{2}H/^{1}H$ of gypsum hydration water by cavity ring-down laser spectroscopy. Rapid Communications in Mass Spectrometry, 29(21), 1997–2006. doi:10.1002/rcm.7312

Gázquez, F., Evans, N. P., & Hodell, D. A. (2017). Precise and accurate isotope fractionation factors ($\alpha^{17}O$, $\alpha^{18}O$ and αD) for water and $CaSO_4{\cdot}2H_2O$ (gypsum). Geochimica et Cosmochimica Acta, 198, 259–270. doi:10.1016/j.gca.2016.11.001

Gawenda, P., Winkler, W., Schmitz, B., & Adatte, T. (1999). Climate and bioproductivity control on carbonate turbidite sedimentation (Paleocene to earliest Eocene, Gulf of Biscay, Zumaia, Spain). Journal of Sedimentary Research, 69(6), 1253–1261. doi:10.2110/jsr.69.1253

Gemery, P. A., Trolier, M., & White, J. W. C. (1996). Oxygen isotope exchange between carbon dioxide and water following atmospheric sampling using glass flasks. Journal of Geophysical Research: Atmospheres, 101(D9), 14415–14420. doi:10.1029/96jd00053

Gendrin, A. (2005). Sulfates in Martian Layered Terrains: The OMEGA/Mars Express View. Science, 307(5715), 1587–1591. doi:10.1126/science.1109087

Giauque, W. F., & Johnston, H. L. (1929a). An isotope of oxygen, mass 18. Nature, 123, 318. doi:10.1038/123318c0

Giauque, W. F., & Johnston, H. L. (1929b). An isotope of oxygen, mass 17, in the Earth's atmosphere. Journal of the American Chemical Society, 51(12), 3528-3534. doi:10.1021/ja01387a004

Gibson, T. G., Bybell, L. M., & Owens, J. P. (1993). Latest Paleocene lithologic and biotic events in neritic deposits of southwestern New Jersey. Paleoceanography, 8(4), 495–514. doi:10.1029/93pa01367

Gibson, T. G., Bybell, L. M., & Mason, D. B. (2000). Stratigraphic and climatic implications of clay mineral changes around the Paleocene/Eocene boundary of the northeastern US margin. Sedimentary Geology, 134(1-2), 65–92. doi:10.1016/s0037-0738(00)00014-2

Gilg, H. A., & Sheppard, S. M. F. (1996). Hydrogen isotope fractionation between kaolinite and water revisited. Geochimica et Cosmochimica Acta, 60(3), 529–533. doi:10.1016/0016-7037(95)00417-3

Gonfiantini, R., & Fontes, J. C. (1963). Oxygen Isotopic Fractionation in the Water of Crystallization of Gypsum. Nature, 200(4907), 644–646. doi:10.1038/200644a0

Gong, B., Zheng, Y.-F., & Chen, R.-X. (2007). An online method combining a thermal conversion elemental analyzer with isotope ratio mass spectrometry for the determination of hydrogen isotope composition and water concentration in geological samples. Rapid Communications in Mass Spectrometry, 21(8), 1386–1392. doi:10.1002/rcm.2973

Grauel, A.-L., Hodell, D. A., & Bernasconi, S. M. (2016). Quantitative estimates of tropical temperature change in lowland Central America during the last 42 ka. Earth and Planetary Science Letters, 438, 37–46. doi:10.1016/j.epsl.2016.01.001

Handley, L., Pearson, P. N., McMillan, I. K., & Pancost, R. D. (2008). Large terrestrial and marine carbon and hydrogen isotope excursions in a new Paleocene/Eocene boundary section from Tanzania. Earth and Planetary Science Letters, 275(1-2), 17–25. doi:10.1016/j.epsl.2008.07.030

Harding, I. C., Charles, A. J., Marshall, J. E. A., Pälike, H., Roberts, A. P., Wilson, P. A., Jarvis, E., Thorne, R., Morris, E., Moremon, R., Pearce, R., Akbari, S. (2011). Sea-level and salinity fluctuations during the Paleocene–Eocene thermal maximum in Arctic Spitsbergen. Earth and Planetary Science Letters, 303(1-2), 97–107. doi:10.1016/j.epsl.2010.12.043

Hariya, Y., & Tsutsumi, M. (1981). Hydrogen isotopic composition of MnO(OH) minerals from manganese oxide and massive sulfide (Kuroko) deposits in Japan. Contributions to Mineralogy and Petrology, 77(3), 256–261. doi:10.1007/bf00373540

Hassanipak, A. A., & Eslinger, E. (1985). Mineralogy, crystallinity, O18/O16, and D/H of Georgia Kaolins. Clay and Clay Minerals, 33(2), 99-106. doi:10.1346/CCMN.1985.0330203

Held, I. M., & Soden, B. J. (2006). Robust Responses of the Hydrological Cycle to Global Warming. Journal of Climate, 19(21), 5686–5699. doi:10.1175/jcli3990.1

Hodell, D. A., Turchyn, A. V., Wiseman, C. J., Escobar, J., Curtis, J. H., Brenner, M., Gilli, A., Mueller, A. D., Anselmetti, F., Aritzegui, D. and Brown, E. T. (2012). Late Glacial temperature and precipitation changes in the lowland Neotropics by tandem measurement of $\delta^{18}O$ in biogenic carbonate and gypsum hydration water. Geochimica et Cosmochimica Acta, 77, 352–368. doi:10.1016/j.gca.2011.11.026

Horita, J., & Wesolowski, D. J. (1994). Liquid-vapor fractionation of oxygen and hydrogen isotopes of water from the freezing to the critical temperature. Geochimica et Cosmochimica Acta, 58(16), 3425–3437. doi:10.1016/0016-7037(94)90096-5

Houghton, J & Ding, Y & Griggs, D & Noguer, Maria & Linden, P. & Dat, X & Maskell, K & Johnson, C. (2001). Contribution of Working Group I to the Second Assessment Report of the Intergovernmental Panel on Climate Change. WMO/UNEP.

Hyeong, K., & Capuano, R. M. (2004). Hydrogen isotope fractionation factor for mixed-layer illite/smectite at 60° to 150°C: New data from the northeast Texas Gulf Coast. Geochimica et Cosmochimica Acta, 68(7), 1529–1543. doi:10.1016/j.gca.2003.10.002

IPCC, 2013: Climate Change 2013: The Physical Science Basis. Contribution of Working Group I to the Fifth Assessment Report of the Intergovernmental Panel on Climate Change [Stocker, T.F., D. Qin, G.-K. Plattner, M. Tignor, S.K. Allen, J. Boschung, A. Nauels, Y. Xia, V. Bex and P.M. Midgley (eds.)]. Cambridge University Press, Cambridge, United Kingdom and New York, NY, USA, 1535 pp, doi:10.1017/CBO9781107415324

Jacques, S. D. M., González-Saborido, A., Leynaud, O., Bensted, J., Tyrer, M., Greaves, R. I. W., & Barnes, P. (2009). Structural evolution during the dehydration of gypsum materials. Mineralogical Magazine, 73(03), 421–432. doi:10.1180/minmag.2009.073.3.421

Jaramillo, C., Ochoa, D., Contreras, L., Pagani, M., Carvajal-Ortiz, H., Pratt, L. M., Krishnan, S., Cardona, A., Romero, M., Quiroz, L., Rodriguez, G., Rueda, M. J., de la Parra, F., Morón, A., Green, W., Bayona, G., Montes, C., Quintero, O., Ramirez, R., Mora, G., Schouten, S., Bermudez, H., Navarrete, Rosa., Parra, F., Alvarán, M., Osorno, J., Crowley, J. L., Valencia, V., Vervoort, J. (2010). Effects of Rapid Global Warming at the Paleocene-Eocene Boundary on Neotropical Vegetation. Science, 330(6006), 957–961. doi:10.1126/science.1193833

John, C. M., Banerjee, N. R., Longstaffe, F. J., Sica, C., Law, K. R., & Zachos, J. C. (2012). Clay assemblage and oxygen isotopic constraints on the weathering response to the Paleocene-Eocene thermal maximum, east coast of North America. Geology, 40(7), 591–594. doi:10.1130/g32785.1

Kelly, D. C., Zachos, J. C., Bralower, T. J., & Schellenberg, S. A. (2005). Enhanced terrestrial weathering/runoff and surface ocean carbonate production during the recovery stages of the Paleocene-Eocene thermal maximum. Paleoceanography, 20(4). doi:10.1029/2005pa001163

Kemp, S. J., Ellis, M. A., Mounteney, I., & Kender, S. (2016). Palaeoclimatic implications of high-resolution clay mineral assemblages preceding and across the onset of the Palaeocene–Eocene Thermal Maximum, North Sea Basin. Clay Minerals, 51(05), 793–813. doi:10.1180/claymin.2016.051.5.08

Kender, S., Stephenson, M.H., Riding, J.B., Leng, M.J., Knox, R.W.O'B., Peck, V.L., Kendrick, C.P., Ellis, M.A., Vane, C.H. & Jamieson, R. (2012). Marine and terrestrial environmental changes in NW Europe preceding carbon release at the Paleocene–Eocene transition. Earth and Planetary Science Letters, 353-354, 108–120. doi:10.1016/j.epsl.2012.08.011

Kennett, J., Stott, L. (1991). Abrupt deep-sea warming, palaeoceanographic changes and benthic extinctions at the end of the Palaeocene. Nature 353, 225–229. doi:10.1038/353225a0

Khademi, H., Mermut, A. R., & Krouse, H. R. (1997). Isotopic composition of gypsum hydration water in selected landforms from central Iran. Chemical Geology, 138(3-4), 245–255. doi:10.1016/s0009-2541(97)00017-x

Khalil, A. A. A. (1982). Kinetics of gypsum dehydration. Thermochimica Acta, 55(2), 201–208. doi:10.1016/0040-6031(82)85154-x

Khozyem, H., Adatte, T., Spangenberg, J. E., Tantawy, A. A., & Keller, G. (2013). Palaeoenvironmental and climatic changes during the Palaeocene–Eocene Thermal Maximum (PETM) at the Wadi Nukhul Section, Sinai, Egypt. Journal of the Geological Society, 170(2), 341–352. doi:10.1144/jgs2012-046

Kieffer, S. W. (1982). Thermodynamics and lattice vibrations of minerals: 5. Applications to phase equilibria, isotopic fractionation, and high-pressure thermodynamic properties. Reviews of Geophysics, 20(4), 827. doi:10.1029/rg020i004p00827

Kiyohiro, T., & Otsuka, R. (1989). Dehydration mechanism of bound water in sepiolite. Thermochimica Acta, 147(1), 127–138. doi:10.1016/0040-6031(89)85169-x

Klopregge, J.T., Breukelaar, J., Geus, J. W., & Jansen, B. H. (1994). Characterization of Mg-saponites synthesized from gels containing amounts of Na^{+}, K^{+}, Rb^{+} , Ca^{2+}, Ba^{2+}, or Ce^{4+} equivalent to the CEC of the saponite. Clays and Clay Minerals, 42(1), 18–22.

Knauth, L. P., & Epstein, S. (1976). Hydrogen and oxygen isotope ratios in nodular and bedded cherts. Geochimica et Cosmochimica Acta, 40(9), 1095–1108. doi:10.1016/0016-7037(76)90051-x

Knauth, L. P., & Epstein, S. (1982). The nature of water in hydrous silica. American Mineralogist, 67(5-6), 510– 520.

Knox, R. W. O. (1996). Correlation of the early Paleogene in northwest Europe: an overview. Geological Society, London, Special Publications, 101(1), 1–11. doi:10.1144/gsl.sp.1996.101.01.01

Knox, R.W.O'B. (1998). The tectonic and volcanic history of the North Atlantic region during the Paleocene–Eocene transition: Implications for NW European and global biotic events, in Aubrey, M.P., Lucas, S.G., and Berggren, W.A., eds., Late Paleocene–Early Eocene climatic and biotic events in the marine and terrestrial records: New York, Columbia University Press, p. 91–102.

Koehler, G., & Wassenaar, L. I. (2012). Determination of the Hydrogen Isotopic Compositions of Organic Materials and Hydrous Minerals Using Thermal Combustion Laser Spectroscopy. Analytical Chemistry, 84(8), 3640–3645. doi:10.1021/ac3000489

Langevin, Y. (2005). Sulfates in the North Polar Region of Mars Detected by OMEGA/Mars Express. Science, 307(5715), 1584–1586. doi:10.1126/science.1109091

Lawrence, J. R., & Taylor, H. P. (1972). Hydrogen and oxygen isotope systematics in weathering profiles. Geochimica et Cosmochimica Acta, 36(12), 1377–1393. doi:10.1016/0016-7037(72)90068-3

Lawrence, J. R., & Meaux, J. R. (1993). The Stable Isotopic Composition of Ancient Kaolinites of North America. Geophysical Monograph Series, 249–261. doi:10.1029/gm078p0249

Li, J., Li, M., Fang, X., Zhang, G., Zhang, W., & Liu, X. (2017). Isotopic composition of gypsum hydration water in deep Core SG-1, western Qaidam basin (NE Tibetan Plateau), implications for paleoclimatic evolution. Global and Planetary Change, 155, 70–77. doi:10.1016/j.gloplacha.2017.06.006

Liu, K.-K., & Epstein, S. (1984). The hydrogen isotope fractionation between kaolinite and water. Chemical Geology, 46(4), 335–350. doi:10.1016/0009-2541(84)90176-1

Liu, T., Artacho, E., Gázquez, F., Walters, G., & Hodell, D. (2018). Prediction of Equilibrium Isotopic Fractionation of the Gypsum/Bassanite/Water System using First-Principles Calculations. Geochimica et Cosmochimica Acta. doi:10.1016/j.gca.2018.08.045

López-Galindo, A., Hach-Alí, P. F., Pushkarev, A. V., Lytovchenko, A. S., Baker, J. H., & Pushkarova, R. A. (2008). Tritium redistribution between water and clay minerals. Applied Clay Science, 39(3-4), 151–159. doi:10.1016/j.clay.2007.06.005

Lou, W., Guan, B., & Wu, Z. (2010). Dehydration behavior of FGD gypsum by simultaneous TG and DSC analysis. Journal of Thermal Analysis and Calorimetry, 104(2), 661–669. doi:10.1007/s10973-010-1100-6

Lupker, M., France-Lanord, C., Galy, V., Lavé, J., Gaillardet, J., Gajurel, A. P., Guilmetter, C., Rahman M., Singh, S. K., Sinha, R. (2012). Predominant floodplain over mountain weathering of Himalayan sediments (Ganga basin). Geochimica et Cosmochimica Acta, 84, 410–432. doi:10.1016/j.gca.2012.02.001

Lyons, L.L., Baczynski, A. A., Babila, T. L., Bralower, T. J., Hajek, E. A., Kump, L. R., Polites, E. G., Self-Trail, J. M., Trampush, S. M., Vornlocher, J. R., Zachos, J. C., & Freeman, K. H. (2019). Palaeocene–Eocene Thermal Maximum prolonged by fossil carbon oxidation. Nature Geoscience, 12, 54-60. doi:10.1038/s41561-018-0277-3

Lytovchenko, A. S., Pushkarev, A.V., Fenoll Hach-Ali, P., López-Galindo, A., Baker, J. H., Pushkarova, R. A. (2005) Assessment of the potential ability of phyllosilicates to accumulate and retain tritium in structural OH-groups. Mineralogical Journal, 27 (2), 59-65. ISSN: 2519-2396.

Majoube, M. (1971). Fractionnement en oxygene-18 et en deuterium entre l'eau et sa vapeur. Journal de Chimie Physique, 68, 1423- 1436. doi:10.1051/jcp/1971681423

Manian, S. H., Urey, H. C., & Bleakney, W. (1934). An investigation of the relative abundance of the oxygen isotopes O16:O18 in stone meteorites. Journal of the American Chemical Society, 56(12), 2601–2609. doi:10.1021/ja01327a020

Matsuo, S., Friedman, I., & Smith, G. I. (1972). Studies of quaternary saline lakes—I. Hydrogen isotope fractionation in saline minerals. Geochimica et Cosmochimica Acta, 36(4), 427–435. doi:10.1016/0016-7037(72)90033-6

McInerney, F. A., & Wing, S. L. (2011). The Paleocene-Eocene Thermal Maximum: A Perturbation of Carbon Cycle, Climate, and Biosphere with Implications for the Future. Annual Review of Earth and Planetary Sciences, 39(1), 489–516. doi:10.1146/annurev-earth-040610-133431

Méheut, M., Lazzeri, M., Balan, E., & Mauri, F. (2007). Equilibrium isotopic fractionation in the kaolinite, quartz, water system: Prediction from first-principles density-functional theory. Geochimica et Cosmochimica Acta, 71(13), 3170–3181. doi:10.1016/j.gca.2007.04.012

Méheut, M., & Schauble, E. A. (2014). Silicon isotope fractionation in silicate minerals: Insights from first-principles models of phyllosilicates, albite and pyrope. Geochimica et Cosmochimica Acta, 134, 137–154. doi:10.1016/j.gca.2014.02.014

Mix, H. T., & Chamberlain, C. P. (2014). Stable isotope records of hydrologic change and paleotemperature from smectite in Cenozoic western North America. Geochimica et Cosmochimica Acta, 141, 532–546. doi:10.1016/j.gca.2014.07.008

Mook, W. M. E. 2001. Environmental Isotopes in the Hydrological Cycle. Principles and Applications. UNESCO/IAEA Series

Moum, J., & Rosenqvist, I. T. (1958). Hydrogen (protium)-deuterium exchange in clays. Geochimica et Cosmochimica Acta, 14(3), 250–252. doi:10.1016/0016-7037(58)90084-x

Mseddi, H., Mammou, A. B., & Oueslati, W. (2010). Methodology for the extraction of carbonate-bound trace metals from carbonate-rich soils: application to Lakhouat soils, Tunis, Tunisia, Chemical Speciation & Bioavailability, 22:3, 165-170. doi:10.3184/095422910X12827488554310

Müller, T., Friesen, J., Weise, S. M., Al Abri, O., Bait Said, A. B. A., & Michelsen, N. (2020). Stable isotope composition of Cyclone Mekunu rainfall, Southern Oman. Water Resources Research, 56(12), e2020WR027644. doi:10.1029/2020WR027644

Murad, E., & Wagner, U. (1996). The thermal behaviour of an Fe-rich illite. Clay Minerals, 31(1), 45–52. doi:10.1180/claymin.1996.031.1.04

Noe Dobrea, E. Z., Wray, J. J., Calef, F. J., Parker, T. J., & Murchie, S. L. (2012). Hydrated minerals on Endeavour Crater's rim and interior, and surrounding plains: New insights from CRISM data. Geophysical Research Letters, 39(23). doi:10.1029/2012gl053180

Nolan, G. S., & Bindeman, I. N. (2013). Experimental investigation of rates and mechanisms of isotope exchange (O, H) between volcanic ash and isotopically-labeled water. Geochimica et Cosmochimica Acta, 111, 5–27. doi:10.1016/j.gca.2013.01.020

O'Neil, J. R., & Taylor, H. P. (1969). Oxygen isotope equilibrium between muscovite and water. Journal of Geophysical Research, 74(25), 6012–6022. doi:10.1029/jb074i025p06012

O'Neil, J. R., & Kharaka, Y. K. (1976). Hydrogen and oxygen isotope exchange reactions between clay minerals and water. Geochimica et Cosmochimica Acta, 40(2), 241–246. doi:10.1016/0016-7037(76)90181-2

Pagani, M., Pedentchouk, N., Huber, M., Sluijs, A., Schouten, S., Brinkhuis, H., Damste, J.S.S., Dickens, G.R., & Expedition 302 Scientists. (2006). Arctic hydrology during global warming at the Palaeocene/Eocene thermal maximum. Nature, 442(7103), 671–675. doi:10.1038/nature05043

Paulik, F., Paulik, J., & Arnold, M. (1992). Thermal decomposition of gypsum. Thermochimica Acta, 200, 195–204. doi:10.1016/0040-6031(92)85115-c

Pedersen, B. F., & Semmingsen, D. (1982). Neutron diffraction refinement of the structure of gypsum, $CaSO_4.2H_2O$. Acta Crystallographica Section B Structural Crystallography and Crystal Chemistry, 38(4), 1074–1077. doi:10.1107/s0567740882004993

Playà, E., Recio, C., & Mitchell, J. (2005). Extraction of gypsum hydration water for oxygen isotopic analysis by the guanidine hydrochloride reaction method. Chemical Geology, 217(1-2), 89–96. doi:10.1016/j.chemgeo.2004.12.005

Pogge von Strandmann, P. A. E., Jones, M. T., Joshua West, A., Murphy, M. J., Stokke, E. W., Tarbuck, G., Wilson, D. J., Pearce, C. R., & Schmidt, D. N. (2021). Lithium isotope evidence for enhanced weathering and erosion during the Paleocene-Eocene Thermal Maximum. Science Advances, 7(42), eabh4224. doi: 10.1126/sciadv.abh4224

Prieto-Taboada, N., Gómez-Laserna, O., Martínez-Arkarazo, I., Olazabal, M. Á., & Madariaga, J. M. (2014). Raman Spectra of the Different Phases in the $CaSO_4$–H_2O System. Analytical Chemistry, 86(20), 10131–10137. doi:10.1021/ac501932f

Rapin, W., Meslin, P.-Y., Maurice, S., Vaniman, D., Nachon, M., Mangold, N., Schröder, S., Gasnault, O., Forni, O., Wiens, R. C., Martínez, G.M., Cousin, A., Sautter, V., Lasue, J., Rampe, E. B., Archer, D. (2016). Hydration state of calcium sulfates in Gale crater, Mars: Identification of bassanite veins. Earth and Planetary Science Letters, 452, 197–205. doi:10.1016/j.epsl.2016.07.045

Rivkin, A. S., Volquardsen, E. L., & Clark, B. E. (2006). The surface composition of Ceres: Discovery of carbonates and iron-rich clays. Icarus, 185(2), 563–567. doi:10.1016/j.icarus.2006.08.022

Robert, C., & Kennett, J. P. (1994). Antarctic subtropical humid episode at the Paleocene-Eocene boundary: Clay-mineral evidence. Geology, 22(3), 211. doi:10.1130/0091-7613(1994)022<0211:asheat>2.3.co;2

Robertson, K., & Bish, D. (2013). Constraints on the distribution of $CaSO_4 \cdot nH_2O$ phases on Mars and implications for their contribution to the hydrological cycle. Icarus, 223(1), 407–417. doi:10.1016/j.icarus.2012.10.028

Ryan, P.C., & Huertas, F. J. (2009). The temporal evolution of pedogenic Fe-smectite to Fe-kaolin via interstratified kaolin-smectite in a moist tropical soil chronosequence. Geoderma, 151(1-2), 1–15. doi:10.1016/j.geoderma.2009.03.010

Ryan, P.C. , & Huertas, F. J. (2013). Reaction Pathways of Clay Minerals in Tropical Soils: Insights from Kaolinite-Smectite Synthesis Experiments. *Clays Clay Miner.*, **61**, 303–318. doi:10.1346/CCMN.2013.0610410

Savin, S. M., & Epstein, S. (1970a). The oxygen and hydrogen isotope geochemistry of clay minerals. Geochimica et Cosmochimica Acta, 34(1), 25–42. doi:10.1016/0016-7037(70)90149-3

Savin, S. M., & Epstein, S. (1970b). The oyxgen and hydrogen isotope geochemistry of ocean sediments and shales. Geochimica et Cosmochimica Acta, 34(1), 43–63. doi:10.1016/0016-7037(70)90150-x

Savin, S. M., & Hsieh, J. C. (1998). The hydrogen and oxygen isotope geochemistry of pedogenic clay minerals: principles and theoretical background. Geoderma, 82(1-3), 227–253. doi:10.1016/s0016-7061(97)00103-1

Savin S.M., & Lee M. (1988). Isotopic studies of phyllosilicates, in: Bailey, S.W., eds., Hydrous Phyllosilicates (Exclusive of Micas): Reviews in Mineralogy and Geochemistry, 19, Mineralogical Society of America, Washington, D.C., p189-223. doi:10.1515/9781501508998-012

Schmidt, D. N., Thomas, E., Authier, E., Saunders, D., & Ridgewell, A. (2018). Strategies in times of crisis – insights into the benthic foraminiferal record of the Palaeocene-Eocene Thermal Maximum. Philosophical Transactions of the Royal Society A-Mathematical Physical and Engineering Sciences, 376 (2130), 20170328. doi:10.1098/rsta.2017.0328

Schmitz, B., & Pujalte, V. (2007). Abrupt increase in seasonal extreme precipitation at the Paleocene-Eocene boundary. Geology, 35(3), 215. doi:10.1130/g23261a.1

Schoenemann, S.W., Schauer, A. J., & Steig, E. J. (2013). Measurement of SLAP2 and GISP $\delta^{17}O$ and proposed VSMOW-SLAP normalization for $\delta^{17}O$ and $^{17}O_{excess}$. Rapid Communications in Mass Spectrometry, 27(5), 582-590. doi:10.1002/rcm.6486

Seager, R., Naik, N., & Vecchi, G. A. (2010). Thermodynamic and Dynamic Mechanisms for Large-Scale Changes in the Hydrological Cycle in Response to Global Warming*. Journal of Climate, 23(17), 4651–4668. doi:10.1175/2010jcli3655.1

Sharp, Z. D. (1992). In situ laser microprobe techniques for stable isotope analysis. Chemical Geology, 101(1-2), 3-19. doi:10.1016/0009-2541(92)90199-F

Sharp, Z. D., Atudorei, V., & Durakiewicz, T. (2001). A rapid method for determination of hydrogen and oxygen isotope ratios from water and hydrous minerals. Chemical Geology, 178(1-4), 197–210. doi:10.1016/s0009-2541(01)00262-5

Sheppard, S. M. F. (1977). The Cornubian batholith, SW England: D/H and $^{18}O/^{16}O$ studies of kaolinite and other alteration minerals. Journal of the Geological Society; 133 (6): 573–591. doi:10.1144/gsjgs.133.6.0573

Sluijs, A., Schouten, S., Pagani, M., Woltering, M., Brinkhuis, H., Damsté, J. S. S., Dickens, G. R., Huber, M., Reichart, G.-J., Stein, R., Matthiessen, J., Lourens, L. J., Pedentchouk, N., Backman, J., & Moran, K. (2006). Subtropical Arctic Ocean temperatures during the Palaeocene/Eocene thermal maximum. Nature, 441(7093), 610–613. doi:10.1038/nature04668

Smykatz-Kloss, W., Heide, K., & Klinke, W. (2003). Applications of Thermal Methods in the Geosciences. Handbook of Thermal Analysis and Calorimetry, 451–593. doi:10.1016/s1573-4374(03)80015-8

Sofer, Z. (1978). Isotopic composition of hydration water in gypsum. Geochimica et Cosmochimica Acta, 42(8), 1141–1149. doi:10.1016/0016-7037(78)90109-6

Soliman, M. F., Aubry, M.-P., Schmitz, B., & Sherrell, R. M. (2011). Enhanced coastal paleoproductivity and nutrient supply in Upper Egypt during the Paleocene/Eocene Thermal Maximum (PETM): Mineralogical and geochemical evidence. Palaeogeography, Palaeoclimatology, Palaeoecology, 310(3-4), 365–377. doi:10.1016/j.palaeo.2011.07.027

Stokke, E.W., Jones, M. T., Tierney, J. E., Svensen, H. H., & Whiteside, J. H. (2020). Temperature changes across the Paleocene-Eocene Thermal Maximum – a new high-resolution TEX86 temperature record from the Eastern North Sea Basin. Earth and Planetary Science Letters, 544, 116388. doi:10.1016/j.epsl.2020.116388

Stokke, E. W., Jones, M. T., Riber, L., Haflidason, H., Midtkandal, I., Schultz, B. P., & Svensen, H. H. (2021). Rapid and sustained environmental responses to global warming: the Paleocene–Eocene Thermal Maximum in the eastern North Sea. Climate of the Past, 17, 1989–2013. doi: 10.5194/cp-17-1989-2021

Sun, Y., Solomon, S., Dai, A., & Portmann, R. W. (2006). How Often Does It Rain? Journal of Climate, 19(6), 916–934. doi:10.1175/jcli3672.1

Suzuoki, T., & Epstein, S. (1976). Hydrogen isotope fractionation between OH-bearing minerals and water. Geochimica et Cosmochimica Acta, 40(10), 1229–1240. doi:10.1016/0016-7037(76)90158-7

Taylor, H. P., & Epstein, S. (1962). Relationship between O^{18}/O^{16} ratios in coexisting minerals of igneous and metamorphic rocks. Geological Society of America Bulletin, 73(4), 461. doi:10.1130/0016-7606(1962)73[461:rboric]2.0.co;2

Tessier, A., Campbell, P. G. C., & Bisson, M. (1979). Sequential extraction procedure for the speciation of particulate trace metals. Analytical Chemistry, 51(7), 844–851. doi:10.1021/ac50043a017

Thiry, M. (2000). Palaeoclimatic interpretation of clay minerals in marine deposits: an outlook from the continental origin. Earth-Science Reviews, 49(1-4), 201–221. doi:10.1016/s0012-8252(99)00054-9

Thomas, D. J., Zachos, J. C., Bralower, T. J., Thomas, E., & Bohaty, S. (2002). Warming the fuel for the fire: Evidence for the thermal dissociation of methane hydrate during the Paleocene-Eocene thermal maximum. Geology, 30(12), 1067. doi:10.1130/0091-7613(2002)030<1067:wtfftf>2.0.co;2

Torii, K., & Iwasaki, T. (1987). Synthesis of hectorite. Clay Science, 7(1), 1-16. doi:10.11362/jcssjclayscience1960.7.1

Trenberth, K. E., Dai, A., Rasmussen, R. M., & Parsons, D. B. (2003). The Changing Character of Precipitation. Bulletin of the American Meteorological Society, 84(9), 1205–1218. doi:10.1175/bams-84-9-1205

Uemura, R., Nakamoto, M., Asami, R., Mishima, S., Gibo, M., Masaka, K., Jin-Ping, C., Wu, C.-C. Chang, Y.-W., & Shen, C.-C. (2016). Precise oxygen and hydrogen isotope determination in nanoliter quantities of speleothem inclusion water by cavity ring-down spectroscopic techniques. Geochimica et Cosmochimica Acta, 172, 159–176. doi:10.1016/j.gca.2015.09.017

Urey, H.C., Brickwedde, F. G., & Murphy, G. M. (1932). A hydrogen isotope of mass 2. Physical Review, 39, 164-165. doi:10.1103/PhysRev.39.164

Vaniman, D. T., Bish, D. L., Chipera, S. J. (2009). Bassanite on Mars. Lunar Planet. Sci. Conf. 40, abstract 1654

Vitali, F., Longstaffe, F. J., Bird, M. I., Gage, K. L., & Caldwell, W. G. E. (2001). Hydrogen-isotope fractionation in aluminum hydroxides: Synthesis products versus natural samples from bauxites. Geochimica et Cosmochimica Acta, 65(9), 1391–1398. doi:10.1016/s0016-7037(00)00604-9

Vitali, F., Longstaffe, F. J., McCarthy, P. J., Plint, A. G., & Caldwell, W. G. E. (2002). Stable isotopic investigation of clay minerals and pedogenesis in an interfluve paleosol from the Cenomanian Dunvegan Formation, N.E. British Columbia, Canada. Chemical Geology, 192(3-4), 269–287. doi:10.1016/s0009-2541(02)00225-5

Walker, J. C. G., Hays, P. B., & Kasting, J.F. (1981). A negative feedback mechanism for the long-term stabilization of Earth’s surface temperature. Journal of Geophysical Research. Oceans, 86, 9776–9782. doi:10.1029/JC086iC10p09776

Westerhold, T., Röhl, U., Frederichs, T., Agnini, C., Raffi, I., Zachos, J. C., & Wilkens, R. H. (2017). Astronomical calibration of the Ypresian timescale: implications for seafloor spreading rates and the chaotic behavior of the solar system. Climate of the Past, 13, 1129-1152. doi:10.5194/cp-13-1129-2017

White A.F. & Brantley S.L. (1995). Chemical weathering rates of silicate minerals; an overview, in White, A. F., and Brantley S. F., eds., Chemical Weathering of Silicate Minerals: Reviews in Mineralogy and Geochemistry, 31, Mineralogical Society of America, Washington, D.C., p. 1–22.

Wilson, M. R., Kyser, T. K., Mehnert, H. H., & Hoeve, J. (1987). Changes in the H-O-Ar isotope composition of clays during retrograde alteration. Geochimica et Cosmochimica Acta, 51(4), 869–878. doi:10.1016/0016-7037(87)90100-1

Wray, J. J., E. Z. Noe Dobrea, R. E. Arvidson, S. M. Wiseman, S. W. Squyres, A. S. McEwen, J. F. Mustard, & S. L. Murchie (2009). Phyllosilicates and sulfates at Endeavour Crater, Meridiani Planum, Mars, Geophysical Research Letters, 36, L21201, doi:10.1029/2009GL040734

Wray, J. J., Squyres, S. W., Roach, L. H., Bishop, J. L., Mustard, J. F., & Noe Dobrea, E. Z. (2010). Identification of the Ca-sulfate bassanite in Mawrth Vallis, Mars. Icarus, 209(2), 416–421. doi:10.1016/j.icarus.2010.06.001

Yang, C., Yang, S., & Su, N. (2016). Stable hydrogen and oxygen isotopes in mineral-bound water and the indication for chemical weathering intensity. Chemical Geology, 441, 14–23. doi:10.1016/j.chemgeo.2016.08.015

Yeh, H.-W., & Epstein, S. (1978). Hydrogen isotope exchange between clay minerals and sea water. Geochimica et Cosmochimica Acta, 42(1), 140–143. doi:10.1016/0016-7037(78)90224-7

Yeh, H.-W., & Eslinger, E. V. (1986). Oxygen isotopes and the extent of diagenesis of clay minerals during sedimentation and burial in the sea. Clays and Clay Minerals, 34(4), 403-406. doi:10.1346/CCMN.1986.0340407

Yeh, H.-F., Lin, H.-I., Lee, C.-H., Hsu, K.-C., & Wu, C.-S. (2014). Identifying Seasonal Groundwater Recharge Using Environmental Stable Isotopes. Water, 6(10), 2849–2861. doi:10.3390/w6102849

Zachos, J. C., Wara, M. W., Bohaty, S., Delaney, M. L., Petrizzo, M. R., Brill, A., Bralower, T. J., & Premoli-Silva, I. (2003). A Transient Rise in Tropical Sea Surface Temperature During the Paleocene-Eocene Thermal Maximum. Science, 302(5650), 1551–1554. doi:10.1126/science.1090110

Zheng, Y.-F. (1993). Calculation of oxygen isotope fractionation in hydroxyl-bearing silicates. Earth and Planetary Science Letters, 120(3-4), 247–263. doi:10.1016/0012-821x(93)90243-3